

University of Alberta

**Natural Zeolite Catalysts for the Integrated Cracking, Waterless
Extraction and Upgrading of Oilsands Bitumen**

by

Abu Saleh Muhammad Junaid

A thesis submitted to the Faculty of Graduate Studies and Research
in partial fulfillment of the requirements for the degree of

Doctor of Philosophy

in

Chemical Engineering

Department of Chemical and Materials Engineering

©Abu Saleh Muhammad Junaid

Spring 2012

Edmonton, Alberta

Permission is hereby granted to the University of Alberta Libraries to reproduce single copies of this thesis and to lend or sell such copies for private, scholarly or scientific research purposes only. Where the thesis is converted to, or otherwise made available in digital form, the University of Alberta will advise potential users of the thesis of these terms.

The author reserves all other publication and other rights in association with the copyright in the thesis and, except as herein before provided, neither the thesis nor any substantial portion thereof may be printed or otherwise reproduced in any material form whatsoever without the author's prior written permission.

To my wonderful wife and family – those who suffered

*And to the memory of my late grandfather Zahurul Haque – I know
you would have been happy*

Abstract

Canadian oilsands bitumen represents one of the largest petroleum reserves in the world, but extraction of that resource raises significant environmental, operational and quality-related challenges. Current extraction processes are water intensive, generating high volume tailings ponds that are challenging to treat. The bitumen has higher concentrations of heteroatoms and heavy metals than those found in typical crude oil, and a large portion of the material consists of high boiling point fractions. Severe upgrading techniques are required to convert this bitumen to synthetic crude oil prior to refining. The multi-step processing operations that address these issues are capital intensive, with substantial operational and maintenance costs.

Inexpensive, globally abundant natural zeolites including chabazites and clinoptilolites offer an alternate approach. These minerals have platy morphology and high external surface areas that can accommodate large molecules such as asphaltenes for cracking. Analytical and surface sensitive techniques show that both raw and ion-exchanged forms of these minerals have higher acid strengths and/or acid site densities than the commercial petroleum cracking catalyst zeolite Y. Interestingly, the addition of small amounts of water creates acid sites on untreated

chabazite and clinoptilolite surfaces by hydrolysis, eliminating the need for ion-exchange to achieve acidification.

Because of these extraordinary features, natural zeolite catalysts can crack oilsands bitumen at temperatures much below typical thermal cracking conditions, lowering viscosities and average molecular weights while adsorbing undesirable heteroatoms (nitrogen, sulfur) and heavy metals (vanadium, nickel). The reactions convert up to ~81% of the heavy residue fraction in a stirred batch system at relatively low severity conditions, and produce very high total liquid yields ($\leq 96\%$), significant amounts of which are residue-free ($\leq 71\%$). High conversion of the asphaltenes results in liquid products that are almost entirely extractable from the sand matrix using light hydrocarbons (pentane and hexane).

Based on these findings, we envision a low severity, integrated extraction and upgrading process for oilsands bitumen that uses self-acidified natural zeolites, is waterless and environmentally friendly, requires fewer steps and improves pipeline transportation. As more energy efficient alternatives, natural zeolites can also be used to upgrade pre-extracted or *in situ* bitumen.

Acknowledgement

The last few years of my life had been anything but dull. I had a bounty of constant stress, anxiety and surprises (both pleasant and not so pleasant!). But now that I look back from the end of the road, I see a very rewarding and educational experience. And I want to take a moment to acknowledge the people who had contributed to making this so.

I will never forget the sunny afternoon I walked into Dr. Steven Kuznicki's office for the first time. Unbeknownst to me, it was only the beginning of a long eventful journey together into the joys (and pains!) of scientific discoveries and endeavors. I am truly grateful to have him not only as my Ph.D. research advisor, but also as my mentor, philosopher and guardian for more than the last four years of my life. There is so much to learn from him, the most valuable of which I found was to approach research with a direct and positive attitude, passion and enthusiasm. I also found this to be true for life outside academia. I consider myself honored and fortunate to receive the mentorship of this great person. He is a true source of inspiration for me.

My sincerest and heartfelt gratitude towards Dr. William McCaffrey, who, despite not being my co-supervisor on paper, had carried on every bit of the responsibility. I am very thankful to have the opportunity to share some of his wealth of wisdom and knowledge in heavy oil processing research. He has always helped me understand the loopholes in my ideas and approaches, and guided me to perfection. I

certainly could not have made it this far without his knowledge and expertise, invaluable suggestions and sound judgment. And for that I remain forever grateful.

Over the course of the last few years I had the opportunity to work with some very bright and enthusiastic minds. I thankfully acknowledge the contributions of Chris Street, Moshfiqur Rahman, Wei Wang and Haiyan Yin, my former colleagues working with me in this project. It was my pleasure to work with Juieta Chowdhury, Paul Swenson, Matt Gersbach, Sarah Zhou and Greg Burland, who had also contributed to different phases and aspects of this project. I appreciate the help, assistance and support I received from Weizhu An and all my other past and present group members. Andree Koenig, Walter Boddez and the members of the machine and instrument shops have provided their valuable expertise, resources and support throughout the entire length of this project.

I thank the Centre for Oilsands Innovation (COSI) at the University of Alberta and Imperial Oil for their financial support for the project and the technical reviews. I would like to gratefully acknowledge the student scholarship supports I have received from the Natural Sciences and Engineering Research Council of Canada, Alberta Innovates-Technology Futures, Prairie Mines and Royalty Inc. and the Faculty of Graduate Studies and Research at the University of Alberta.

I am truly indebted to Dr. Amy Dambrowitz and Albana Zeko for their help, teaching and guidance with the writing of several manuscripts as well as this thesis. Because of you, I believe my writing is now almost readable! It is my pleasure to acknowledge the constant assistance and support of Marion Pritchard, Lily Laser, Heather Green, Jack Gibeau, Tatyana Segin and Brenda Brindza of the Department of Chemical and Materials Engineering. I want to thank the department, my supervisor Dr. Kuznicki, Dr. Hayes, Dr. Wanke, Dr. Mmbaga and all my students in the CHE 345, 445 and 584 (also 594 & 694) courses to provide me the opportunity to teach-it is a role I always love, and it helped me remain enthusiastic throughout my graduate studies at the U of A.

I will never forget the care and affection we received from our friends and neighbors from the Bangladeshi Students' Community in Edmonton and Calgary during my studentship. I would like to particularly acknowledge (in alphabetical order) Asif bhai and Dita, Babu and Lipi, Benzene bhai and Jui, Bishwa and Nancy,

Acknowledgement

Emon bhai and Chaity, Fahim and Shanta, Jony and Mohua, Nafis and Sadia, Pinku bhai, Porag, Rupam and Liza, Shakil bhai and Farhana, and of course Zakaria-I thank you all for the good times and love. I do not have words to express my gratitude towards my family-my mom, dad, Anup, Shumon, Shoumi, Moumi and my aunt. It would not have been possible without your endless love and support. I love you all.

This thesis is a legacy of the sacrifice of my wife Mita, who had placated the pangs, anxieties and stresses of a graduate student with her endless love, care, affection and constant support. I never quite understood how you managed to do that, but I do know that I always had you by my side, when everything else fell apart and broke.

Finally, I am grateful to you Almighty, because you gave me the strength and determination to carry on throughout this very difficult but rewarding phase of my life.

A.S.M. Junaid
Edmonton, September 26, 2011

Table of Contents

CHAPTER 1: INTRODUCTION	1
1.1 Canadian oilsands as a major unconventional resource: Reserves and production	4
1.2 Physical composition and properties of oilsands bitumen	5
1.3 Bitumen production and processing	5
1.3.1 Surface mining	7
1.3.2 Extraction of bitumen by <i>ex situ</i> processes	7
1.3.3 Extraction of bitumen by <i>in situ</i> processes	10
1.3.4 Primary upgrading processes	13
1.3.5 Hydrogen added catalytic mixed primary-secondary upgrading processes	16
1.3.6 Secondary upgrading processes	16
1.4 Challenges with bitumen production	18
1.4.1 High viscosity and density	18
1.4.2 Requirement for upgrading	18
1.4.3 Use of water and generation of tailings ponds	18
1.4.4 Production of greenhouse gas	19
1.4.5 Use of more valuable commodities	19
1.4.6 Complicated and capital-intensive multi-step processing	19
1.5 Natural zeolite cracking for integrated processing of oilsands: A novel approach	20
1.5.1 Background	20
1.5.2 Zeolites as cracking catalysts: Structure and activity	21
1.5.3 Natural zeolites as potential cracking catalyst	24
1.6 Organization of the thesis	28
Bibliography	30

CHAPTER 2: UNIQUE FEATURES OF NATURAL ZEOLITES FOR OILSANDS BITUMEN CRACKING	37
2.1 Introduction	37
2.2 Materials and methods	40
2.2.1 Catalyst preparation	40
2.2.2 Catalyst characterization	40
2.2.3 Si to Al ratio measurement	41
2.2.4 Measurement of strength and density of acid sites	42
2.3 Results	43
2.3.1 Catalyst characterization	43
2.3.2 Si to Al ratio measurement	48
2.3.3 Strength and density of acid sites	48
2.4 Discussion	53
2.4.1 Catalyst characterization	53
2.4.2 Si to Al ratio measurement	54
2.4.3 Strength and density of acid sites	55
2.5 Conclusion	59
Bibliography	60
CHAPTER 3: LIGHT HYDROCARBON EXTRACTION OF NATURAL ZEOLITE-CRACKED OILSANDS BITUMEN	63
3.1 Introduction	63
3.2 Materials and methods	64
3.2.1 Oilsands	64
3.2.2 Catalyst preparation	64
3.2.3 Test Reactions	65
3.2.4 Extraction by organic solvents	65
3.2.5 Characterization of reaction products	65
3.3 Results and discussion	68
3.3.1 Cracking and bitumen recovery	68
3.3.2 Thermogravimetric analysis of liquid products	73
3.3.3 Cracking and acidity	76
3.4 Conclusion	77
Bibliography	78
CHAPTER 4: ACTIVATION OF NATURAL ZEOLITE CATALYST BY WATER ADDITION	79
4.1 Introduction	79
4.2 Materials and methods	83
4.2.1 Materials	83
4.2.2 Dean Stark analysis	83
4.2.3 Test Reactions and gas separation	83
4.2.4 Gas and light fractions separation	84
4.2.5 Extraction of liquids by organic solvents	84
4.2.6 Maltenes, asphaltenes and coke measurement	84

4.2.7	Simulated distillation	85
4.2.8	Mass balance and yield-calculations	85
4.2.9	Average molecular weight (AMW) measurement	86
4.2.10	Viscosity measurement	86
4.2.11	Fourier transform infrared spectroscopy (FTIR) analysis of catalysts	87
4.2.12	Nuclear magnetic resonance (NMR) spectroscopic analysis	87
4.2.13	Energy dispersive X-ray (EDX) analysis	88
4.2.14	Stable isotopic mass spectrophotometric analysis	88
4.3	Results and discussion	89
4.3.1	Characterization of feed	89
4.3.2	Upgrading and product recovery	90
4.3.3	Characterization of product bitumen by ^1H and ^{13}C NMR	95
4.3.4	Proton incorporation from water addition	96
4.3.5	Acid hydroxyl groups on raw NZ surface	98
4.3.6	Carbocationic reactions using water-added NZs	101
4.4	Conclusion	104
	Bibliography	105

CHAPTER 5: ACTIVATED NATURAL ZEOLITE-BASED INTEGRATED EXTRACTION AND LOW SEVERITY UPGRADING

		109
5.1	Introduction	109
5.2	Materials and methods	111
5.2.1	Materials	111
5.2.2	Test reactions	112
5.2.3	Gas analysis and condensate collection	113
5.2.4	Extraction with organic solvents	114
5.2.5	Asphaltenes and coke measurement	114
5.2.6	Simulated distillation	114
5.2.7	Mass balance, liquid yields and residue conversion calculation	115
5.2.8	Viscosity measurement	115
5.2.9	Average molecular weight (AMW) measurement	116
5.2.10	Aromaticity measurement	116
5.2.11	Elemental analysis and heteroatoms measurement	117
5.2.12	Heavy metal contents measurement	117
5.3	Results and discussion	118
5.3.1	Stirred reactions on oilsands	118
5.3.2	NZ catalyzed cracking and recovery	120
5.3.3	Product quality	124
5.3.4	Summary of results	135
5.4	Conclusion	135
	Bibliography	136

CHAPTER 6: ENERGY REQUIREMENTS	139
6.1 Introduction	139
6.2 Methods	141
6.2.1 Assumptions	141
6.2.2 Energy calculations	141
6.2.3 Physical and thermochemical properties	142
6.3 Energy requirements	143
6.4 Conclusion	145
Bibliography	146
CHAPTER 7: UPGRADING OF EXTRACTED BITUMEN AND <i>IN SITU</i> APPLICATION OF NATURAL ZEOLITES	147
7.1 Introduction	147
7.2 Materials and methods	148
7.2.1 Materials	148
7.2.2 Cracking reactions and extraction	148
7.2.3 Viscosity measurements	149
7.3 Results and discussion	149
7.3.1 NZ-cracking for extracted bitumen upgrading	149
7.3.2 Reusability of the catalysts	150
7.3.3 NZ-cracking for prolonged low temperature bitumen upgrading	152
7.4 Conclusion	153
Bibliography	154
CHAPTER 8: CONCLUSIONS	156
8.1 Conclusions from the current study	156
8.1.1 Unique structural and compositional properties of NZs for oilsands bitumen cracking	157
8.1.2 Waterless (light hydrocarbon) extraction of bitumen assisted by NZ-catalyzed cracking	157
8.1.3 Enhanced activity of NZs in the presence of water	157
8.1.4 Potential integrated extraction and low temperature upgrading process using NZ catalysts	158
8.1.5 NZ-based cracking is an energy-intensive process	158
8.1.6 Energy efficient upgrading of extracted bitumen and potential <i>in situ</i> application	159
8.1.7 Reusability and catalyst life	159
8.2 Recommendations and future work	159
8.2.1 Reduction of energy requirements for solid oilsands cracking	159
8.2.2 Increasing the residue-free liquid yields	160
8.2.3 Product homogeneity and process robustness	160
8.2.4 Prolonged low temperature <i>in situ</i> application	160
8.2.5 NZ applications in the extraction of other unconventional resources	161

8.3 Concluding remarks	161
Bibliography	162
APPENDIX A: VAPOR PRESSURE OSMOMETER CALIBRATION AND AVERAGE MOLECULAR WEIGHT MEASUREMENT	163
APPENDIX B: ASTM EQUATION PARAMETERS ESTIMATED BY DATA FITTING	166
APPENDIX C: ESTIMATION OF RELATIVE THERMAL REACTION SEVERITY BY LITERATURE DATA FITTING	168

List of Tables

Table 1-1:	Current proven reserve, and current and estimated future production and consumption of petroleum liquid fuels.	2
Table 1-2:	Reserves and production of Alberta oilsands bitumen as of 2008.	4
Table 2-1:	Basic indicators (Hammett indicators) used for measurement of strength of acid sites in catalyst samples.	42
Table 2-2:	Phase identification of zeolites: commercial zeolite Y (ZY); raw sedimentary calcium chabazite (CC); sodium chabazite (NC); and raw clinoptilolite from Saint Cloud (SC) and Australia (A).	44
Table 2-3:	Surface area and porous structure of the zeolite samples: commercial zeolite Y (ZY); raw sedimentary calcium chabazite (CC); sodium chabazite (NC); and raw clinoptilolite from Saint Cloud (SC) and Australia (A).	46
Table 2-4:	Si/Al ratio of zeolite samples by EDX and ICP analysis: commercial zeolite Y (ZY); sedimentary calcium chabazite (CC); sodium chabazite (NC); and clinoptilolite from Saint Cloud (SC) and Australia (A).	48
Table 2-5:	Strength and site density of the raw and acidified samples determined by acid-base titration: commercial zeolite Y (ZY); calcium chabazite (CC); sodium chabazite (NC); and clinoptilolite from Saint Cloud (SC) and Australia (A).	49

Table 2-6:	Heat of adsorption of the dominant acid sites, and overall site density measured by ammonia TPD for: commercial zeolite Y (ZY); calcium chabazite (CC); sodium chabazite (NC); and clinoptilolites from Saint Cloud (SC) and Australia (A).	51
Table 3-1:	The effect of cracking agents and extraction solvents on liquid hydrocarbon recovery from oilsands samples.	70
Table 3-2(a):	Boiling point distribution of toluene ($\delta=18.3 \text{ MPa}^{0.5}$)-extracted liquid products from thermal and catalytic cracking reactions with zeolite Y (ZY), Na-chabazite (NC), Ca-chabazite (CC), and clinoptilolites from Saint Clouds (SC) and Australia (A).	71
Table 3-2(b):	Boiling point distribution of hexane ($\delta=14.4 \text{ MPa}^{0.5}$)-extracted liquid products from thermal and catalytic cracking reactions with zeolite Y (ZY), Na-chabazite (NC), Ca-chabazite (CC), and clinoptilolites from Saint Clouds (SC) and Australia (A).	72
Table 3-2(c):	Boiling point distribution of pentane ($\delta=14.3 \text{ MPa}^{0.5}$)-extracted liquid products from thermal and catalytic cracking reactions with zeolite Y (ZY), Na-chabazite (NC), Ca-chabazite (CC), and clinoptilolites from Saint Clouds (SC) and Australia (A).	72
Table 4-1:	Assignment of ^1H and ^{13}C NMR bands.	88
Table 4-2:	Characterization of feed oilsands and bitumen.	89
Table 4-3:	Products from thermal and 5% NZ catalyzed reactions with 0% and 3% water addition, presented as percent of feed bitumen present in reactant oilsands.	91
Table 4-4:	Petroleum fractions based on boiling point distribution of toluene-extracted bitumen from thermal and 5% NZ catalyzed reactions with 0% and 3% water addition, as determined by SIMDIST analysis.	92
Table 4-5:	Characterization of toluene-extracted liquid products from 0 and 3 wt.% (of feed oilsands) water-added thermal and 5 wt.% NZ-catalyzed reactions by ^1H and ^{13}C NMR.	95
Table 4-6:	Proton distributions of aliphatic chains in toluene-extracted liquid products from 0 and 3 wt.% (of feed oilsands) water-added thermal and 5 wt.% NZ-catalyzed reactions by ^1H NMR.	96

Table 4-7:	Deuterium incorporation and distribution of toluene-extracted bitumen from 3 wt.% (of feed oilsands) D ₂ O added reacted oilsands, determined by stable isotopic and ² D NMR analyses.	97
Table 4-8:	Atomic composition of the raw and protonated forms of the SC and CC catalysts determined EDX analysis.	99
Table 5-1:	Composition of untreated feed oilsands and extracted bitumen.	112
Table 6-1:	Industrial and proposed process conditions for oilsands bitumen extraction and upgrading mass and energy balance calculations.	141
Table 6-2:	Physical and thermochemical properties used for energy balance calculations for industrial and proposed oilsands bitumen extraction and upgrading processes.	142
Table 6-3:	Mass and energy requirements for the industrial and proposed processes for oilsands bitumen extraction and upgrading, based on 1 kg of liquid product.	143
Table 6-4:	Mass and energy requirements for the industrial and proposed processes for extracted bitumen upgrading based on 1 kg of liquid product.	145
Table B-1:	ASTM equation parameters estimated for toluene-extracted liquid products from 3 wt.% water-added 1 h oilsands reactions.	166
Table B-2:	ASTM equation parameters estimated for liquid products from 10 wt.% water-added 300 °C toluene-extracted bitumen reactions.	167
Table B-3:	ASTM equation parameters estimated for liquid products from 10 wt.% water-added 300 °C toluene-extracted bitumen reactions for 24 h, conducted to test the reusability of the catalysts.	167
Table C-1:	Estimation of relative reaction severity from literature data fitting.	169

List of Figures

Figure 1-1:	Distribution of total world oil reserve.	3
Figure 1-2:	A generalized oilsands processing scheme using water-based extraction of bitumen.	6
Figure 1-3:	Flow diagram for oilsands bitumen extraction by a typical CHWE process: (a) ore preparation and slurry conditioning; (b) extraction and tailings facilities.	8
Figure 1-4:	Schematic diagram of a SAGD process: (a) horizontal well pair; and (b) cross-sectional view of the steam chamber.	11
Figure 1-5:	Schematic diagram of a typical delayed coking process.	14
Figure 1-6:	A schematic diagram of a fluid coking process.	15
Figure 1-7:	A schematic diagram of a hydrotreating process.	17
Figure 1-8:	Frameworks of faujasite: (a) 12-membered ring viewed along (111) direction; (b) the β -cage; and (c) the faujasite structure.	21
Figure 1-9:	Framework and structure of clinoptilolite and chabazite: (a) clinoptilolite framework viewed along [001]; (b) 8 and 10 membered rings of clinoptilolite viewed along [001]; (c) chabazite framework viewed normal to [001]; and (d) 8-ring of chabazite viewed normal to [001].	26
Figure 1-10:	Conceptual representation of NZ-based integrated extraction and upgrading of oilsands bitumen.	27

Figure 2-1:	X-Ray powder diffraction pattern of the zeolite samples: commercial zeolite Y (ZY); raw sedimentary calcium chabazite (CC); sodium chabazite (NC); and raw clinoptilolites from Saint Cloud (SC) and Australia (A).	44
Figure 2-2:	Scanning electron microscopy images of the zeolite samples: commercial zeolite Y (ZY); raw sedimentary calcium chabazite (CC); sodium chabazite (NC); and raw clinoptilolite from Saint Cloud (SC) and Australia (A).	45
Figure 2-3:	Pore size distribution of the zeolite samples determined by BJH method: commercial zeolite Y (ZY); raw sedimentary calcium chabazite (CC); sodium chabazite (NC); and raw clinoptilolite from Saint Cloud (SC) and Australia (A).	47
Figure 2-4:	Ammonia TPD curves of the ammonium-exchanged zeolites conducted at a ramp rate of 15 °C min ⁻¹ : commercial zeolite Y (ZY); calcium chabazite (CC); sodium chabazite (NC); and clinoptilolite from Saint Cloud (SC) and Australia (A).	50
Figure 2-5:	Ammonia TPD curves at a ramp rate of 15 °C min ⁻¹ for raw sedimentary calcium chabazite (CC); and raw clinoptilolite from Saint Cloud (SC), compared to commercial zeolite Y (ZY).	51
Figure 2-6:	Representative composite ammonia TPD curves of the samples: commercial zeolite Y (ZY); raw sedimentary calcium chabazite (CC); and ammonium-exchanged clinoptilolite from Saint Cloud (SC).	52
Figure 2-7:	Heat of adsorption estimation for the dominant sites using Polyani-Wigner equation for commercial zeolite Y (ZY); raw sedimentary and ammonium-exchanged calcium chabazite (CC); ammonium-exchanged sodium chabazite (NC); and raw clinoptilolite from Saint Cloud (SC) and Australia (A).	53
Figure 2-8:	Effect of ammonium-exchange on the acid sites of chabazites (CC and NC) and clinoptillite (SC) demonstrated by ammonia TPD (normalized by sample weight).	58
Figure 3-1:	A photographic representation of the reaction and extraction experiments.	66
Figure 3-2:	A representative time-temperature plot for the TGA experiments.	67

Figure 3-3:	Conversion of boiling points under vacuum to effective atmospheric boiling temperatures for TGA of liquid hydrocarbon samples (—), and the difference between the effective and vacuum temperatures (---).	67
Figure 3-4:	Oilsand samples after extraction with pentane: raw (left); thermally cracked (middle) and cracked using clinoptilolite (right).	69
Figure 3-5:	Effect of natural zeolite cracking on product quality: boiling point distribution of pentane-extracted liquid products from unreacted raw oilsands (●), and thermally cracked (Δ), zeolite Y (ZY) cracked (○) and Australian clinoptilolite (A) cracked (□) oilsands as determined by thermogravimetric analysis.	74
Figure 3-6:	The effect of selected extraction solvents (toluene (no symbol), hexane (×), and pentane (*)) on the distribution of boiling points in extracted samples as determined by thermogravimetric analysis.	75
Figure 4-1:	Composition of gaseous products from 0 and 3 wt.% (based on feed oilsands) water added thermal and NZ-catalyzed reactions.	92
Figure 4-2:	Average molecular weight (AMW) of liquid products from 0 and 3 wt.% (of feed oilsands) water-added thermal and 5 wt.% NZ-catalyzed cracking of oilsands, determined by vapor pressure osmometry.	94
Figure 4-3:	Viscosity of the liquid products from 0 and 3 wt.% (of feed oilsands) water-added thermal and 5 wt.% NZ-catalyzed cracking of oilsands, measured at 50 °C.	94
Figure 4-4:	High-resolution ²⁹ Si NMR of (a) uncalcined SC (b) calcined SC (c) uncalcined CC and (d) calcined CC catalyst.	99
Figure 4-5:	FTIR analysis of raw, ammonium-exchanged (NH ₄ ⁺ -form), and ammonium-exchanged and calcined (H ⁺ -form) SC (top) and CC (bottom) catalysts.	100
Figure 5-1:	Schematic diagram of the experimental setup for oilsands reaction, product separation and extraction.	113
Figure 5-2:	Typical wall and centerline temperature profiles for the thermal reactions conducted at different severities.	119
Figure 5-3:	Residue free liquid yield from thermal and NZ catalyzed reactions.	121

Figure 5-4:	Gas make from thermal and NZ catalyzed reactions.	121
Figure 5-5:	Coke make from thermal and NZ catalyzed reactions.	122
Figure 5-6:	Total liquid yield from thermal and NZ catalyzed reactions.	122
Figure 5-7:	Composition of gases produced from thermal and NZ catalyzed reactions.	123
Figure 5-8:	Sample boiling point distribution curves of toluene-extracted liquid products from lower severity (top) and higher severity (bottom) reactions compared to raw oilsands bitumen.	125
Figure 5-9:	C ₅ -asphaltenes yield from thermal and NZ catalyzed reactions.	126
Figure 5-10:	Average molecular weight of toluene-extracted liquid products from thermal and catalytic reactions as a function of residue conversion.	127
Figure 5-11:	Viscosity of toluene-extracted liquid products from thermal and catalytic reactions as a function of residue conversion, measured at 50 °C.	129
Figure 5-12:	Effect of shear rate on the viscosities of liquid products. Three representative liquid samples from reactions conducted at different conditions were subjected to varying shear rates. The viscosity values remained unchanged.	129
Figure 5-13:	Aromaticity of liquid products from thermal and NZ catalyzed reactions as a function of residue conversion (left) and H/C ratio (right).	130
Figure 5-14:	Sulfur concentration in liquid products from thermal and NZ catalyzed reactions.	131
Figure 5-15:	Nitrogen concentration in liquid products from thermal and NZ catalyzed reactions.	131
Figure 5-16:	Vanadium concentration in liquid products from thermal and NZ catalyzed reactions as determined by INAA.	133
Figure 5-17:	Vanadium concentration in liquid products from thermal and NZ catalyzed reactions as determined by ICP-MS analysis.	133

Figure 5-18:	Nickel concentration in liquid products from thermal and NZ catalyzed reactions as determined by ICP-MS analysis.	134
Figure 6-1:	Process flow diagram for the typical industrial process used for the energy balance calculations. The process consists of a Clark hot water extraction (CHWE), paraffinic froth treatment (PFT) and primary upgrading (PU) unit.	140
Figure 6-2:	The flow diagram for the proposed NZ-based integrated extraction-upgrading process for oilsands bitumen.	140
Figure 7-1:	Viscosity of liquid products following thermal or NZ catalyzed cracking of industrially-extracted partially deasphalted Athabasca bitumen; values reported at 50 °C.	150
Figure 7-2:	Reusability of NZ catalysts measured with respect to viscosity reduction of the liquid products. The recovered catalysts from the first cycle were reused in the second of cracking reactions.	151
Figure 7-3:	Viscosity reduction of liquid products by low temperature prolonged catalytic cracking of toluene-extracted Athabasca bitumen; values reported at 50 °C.	152
Figure A-1:	Calibration of Knauer K-7000 vapor pressure osmometer and determination of the calibration constant, K_C .	164
Figure A-2:	Determination of the measurement constant, K_M , for a sample of unknown AMW.	164
Figure C-1:	Fitting of literature data on thermal reaction severity as a function of residue conversion (Athabasca residue feed).	168

List of Nomenclature

ABBREVIATIONS

A	Clinoptilolite procured from Australia
AMW	Average molecular weight
ASTM	American society for testing and materials
BET	Brunauer, Emmett and Teller method for surface area measurement
BJH	Barrett–Joyner–Halenda method for pore size distribution
CC	Ca-chabazite procured from Bowie deposit in Arizona
CHWE	Clark hot water extraction process
CP	Cross polarization
CSS	Cyclic steam stimulation
D	Distillate oil
DFT	Density functional theory
DRU	Diluent recovery unit
EDX	Energy dispersive x-ray analysis
FC	Floatation cells
FCC	Fluid catalytic cracking
FID	Flame ionization detector
FTIR	Fourier transform infrared spectroscopy
G	Gas oil

GC	Gas chromatograph
GHG	Greenhouse gas
HTSD	High temperature simulated distillation
ICP-AES	Inductively coupled plasma atomic emission spectroscopy
ICP-MS	Inductively coupled plasma mass spectrophotometry
INAA	Instrumental neutron activation analysis
IR	Infrared spectroscopy
K	Kerosene
M	Metal
MAS	Magic angle spinning
N	Naphtha
NC	Na-chabazite procured from Bowie deposit Arizona
NMR	Nuclear magnetic resonance spectroscopy
NZ	Natural zeolite
PDF	Powder diffraction file
PFT	Paraffinic froth treatment
PGT	Princeton Gamma Tech
PSC	Primary separation cells
PSD	Pore size distribution
PSV	Primary separation vessels
PU	Primary upgrading
R	Gas constant; and residuum
RC	Residue conversion
RS	Reaction severity
RSS	Relative reaction severity
SAGD	Steam assisted gravity drainage
SARA	Saturated, aromatics, resins and asphaltenes
SC	Clinoptilolite sample procured from Saint Clouds deposit in New Mexico
SCO	Synthetic crude oil
SD	Standard deviation
SEM	Scanning electron microscopy
SIMS	Stable isotope mass spectrometry
Sep Cell	Separation cell

SRU	Solvent recovery unit
TCD	Thermal conductivity detector
TGA	Thermogravimetric analysis
TMS	Tetramethylsilane
TOR	Tails oil recovery
TPD	Temperature programmed desorption
TSRU	Tailings solvent recovery unit
VAPEX	Vapor extraction process
XRD	X-ray diffraction
ZY	Zeolite Y

ENGLISH SYMBOLS

A	Pre-exponential factor of desorption
a_1 and a_2	ASTM equation constants for temperature dependent viscosity
[B]	Concentration of neutral base (au)
[BH ⁺]	Concentration of conjugate acid (au)
C	Concentration (mole kg ⁻¹ or g kg ⁻¹)
C _{al}	Aliphatic carbon (%)
C _{ar}	Aromatic carbon (%)
C _p	Heat capacity at constant pressure (J kg ⁻¹ K ⁻¹ or J mol ⁻¹ K ⁻¹)
Da	Damköhler number
D _{al}	Aliphatic deuterium (%)
D _{ar}	Aromatic deuterium (%)
D _α	Deuterium attached to the carbon nearest to an aromatic structure (%)
D _β	Deuterium attached to the carbon second nearest to an aromatic structure (%)
D _γ	Deuterium attached to the carbon third nearest to an aromatic structure (%)
d	Spacing between parallel planes in a crystal (Å)
d _p	Pore size (Å)
E	Energy (J or kJ)
E _d	Heat of desorption (kJ mol ⁻¹)

H_0	Hammett and Deyrup's acidity function
H_{al}	Aliphatic hydrogen (%)
H_{ar}	Aromatic hydrogen (%)
H_v	Heat of vaporization (kJ mol^{-1})
H_α	Hydrogen attached to the carbon nearest to an aromatic structure (%)
H_β	Hydrogen attached to the carbon second nearest to an aromatic structure (%)
H_γ	Hydrogen attached to the carbon third nearest to an aromatic structure (%)
K_C	Calibration constant of average molecular weight measurement
K_M	Constant of measurement of a sample with unknown average molecular weight
k	Reaction rate constant
M_C	Mass of coke produced from the reaction (g)
M_G	Mass of gaseous products (g)
M_i	Mass of product component 'i' (g)
M_{TL}	Mass of total liquid products (g)
M_{RB}	Mass of residue in unreacted bitumen (g)
M_{RFL}	Mass of residue free liquid product (g)
M_{RP}	Mass of residue in liquid product (g)
MV	Measurement value for average molecular weight (kg mol^{-1} or kg g^{-1})
m	Mass (g or kg)
pK_a	Logarithmic constant for acid dissociation
pK_{BH^+}	Logarithmic constant for dissociation of conjugate acid
P/P_0	Amount adsorbed as a fraction of maximum pressure
T	Temperature ($^{\circ}\text{C}$ or K)
T_b	Boiling point temperature ($^{\circ}\text{C}$ or K)
T_{max}	Peak temperature of desorption ($^{\circ}\text{C}$ or K)
t	Time (s)

GREEK SYMBOLS

β	Heating rate ($^{\circ}\text{C min}^{-1}$)
δ	Hildebrand solubility parameter ($\text{MPa}^{0.5}$)
θ	Scattering angle ($^{\circ}$)
λ	Wave length (\AA)
μ	Viscosity (cP)
ρ	Density (mol L^{-1})

Chapter 1

Introduction

As world's conventional fossil fuel reserves near depletion, harvesting unconventional energy resources such as oilsands (also known as tar sands), shale oil and extra heavy oil is increasingly gaining importance. The world's current total petroleum resources reserve is approximately 9-13 trillion bbl [1], out of which only 1.47 trillion bbl is considered to be proven reserve [2], that is, recoverable using current technologies. The proven reserve, the majority of which is conventional crude oil, is expected to sustain up to the next forty years at the current level of production [3,4].

The global demand for energy, on the other hand, continues to rise steeply. According to the International Energy Outlook 2010 report, the world energy consumption is projected to increase by 49%, or 1.4% per year from 739 quadrillion Btu in 2007 to 739 quadrillion Btu in 2035 [5]. Fossil fuels will continue to supply most of these demands [5]. Despite the massive investment and rapid growth (annually 19-27% on average) in the wind and solar power capacities during 2005-2009, they still comprise a small fraction of the world's total energy supply. As a matter of fact, renewable energy in total currently supplies only 19% of the global

consumption including the majority (~13%) from traditional biomass, the use of which is either declining or stagnant [6]. It is therefore evident that world's fossil fuel consumption will continue to rise in the foreseeable future. The use of liquids and other petroleum fuels is projected to grow from 86.1 million bbl day⁻¹ in 2007 to 110.6 million bbl day⁻¹ in 2035 [5]. The world and North American proven oil reserve, and current and estimated production and consumption are reported in Table 1-1.

Table 1-1: Current proven reserve, and current and estimated future production and consumption of petroleum liquid fuels.

	Estimated proven oil reserve as of Jan. 1, 2011 ^a (trillion bbl)	Oil production ^a (million bbl day ⁻¹)		Liquids and other petroleum fuel consumption ^b (million bbl day ⁻¹)	
		Actual in 2009	Estimated for 2010	Actual in 2007	Predicted for 2035
North America	0.21	10.7	11.0	25	27
Total World	1.47	70.9	72.1	86.1	110.6

a From reference [2]

b From references [5,7]

To accommodate with the growing demand, petroleum production is increasing rapidly. The oil production in North America and Asia were projected to climb 2.4% and 4.0% respectively in 2010 from 2009 averages [8]. Between 2007 and 2035, liquid petroleum production from both conventional and unconventional resources is projected to increase by a total of 25.8 million bbl day⁻¹ [5]. Considering the fact that almost all of the world's easily harvestable low production cost crude oil resources had been discovered [9,10], a worldwide energy crisis is imminent before we are technologically sufficiently advanced to meet the global demands from the renewable sources.

Unconventional fossil fuels comprise 70% of the total world's estimated oil reserves [1]. Detailed distribution of the reserves is presented in Figure 1-1. However, because of the difficulty and cost associated with recovery, most of these

deposits are not counted within the proven reserve estimate. Due to the rise in oil price from a number of factors, exploring unconventional resources is becoming economically competitive using current technology [7]. With an average annual growth of 4.9%, the world production of unconventional liquid fuels is projected to increase from only 3.4 million bbl day⁻¹ in 2007 to 12.9 million bbl day⁻¹ in 2035, accounting for 12% of world's total liquid fuel supply [7]. With conventional crude oil depletion, and geopolitical and other “above ground” constraints with many conventional resources [7], exploration of unconventional resources is the subject of increasing attention and research. With better technology and harvesting methods, it is possible to overcome the environmental and economic challenges associated with the development, exploration and recovery of these resources. Consequently, unconventional deposits can be developed as the world's reliable energy resources for the next several decades until sufficient advancements in the capacities of renewable resources are achieved.

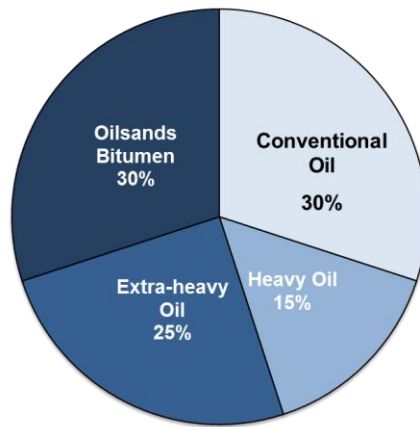


Figure 1-1: Distribution of total world oil reserve [1].

Among the unconventional resources, Venezuela's Orinoco belt contains most of the heavy and extra-heavy oil reserve in the world [11]. Despite the fact that these are less degraded forms of crude oil and can be harnessed more easily by conventional extraction methods compared to oilsands bitumen, lack of access to first-world capital and technological prowess, absence of environmental controls, and political unrest impede their development as constant and reliable sources of

energy [7,12]. On the other hand, the great majority of the oilsands bitumen reserves are located in the Athabasca, Cold Lake and Peace River areas in northern Alberta in Canada [13]. Other reserves include deposits in the province of Saskatchewan in Canada, the state of Utah in the United States [14], Russia [15], China [16], Africa [17], Indonesia [15] and various countries in the Middle East [15,18].

1.1 CANADIAN OILSANDS AS A MAJOR UNCONVENTIONAL RESOURCE: RESERVES AND PRODUCTION

Canadian (Alberta) oilsands contain approximately 81% of the world’s total bitumen reserves [11]. Out of a total estimated deposit of 1.7 trillion bbl, approximately 170 billion bbl can be recovered using current technology [13,19-21]. This makes it the second largest oil reserve in the world after Saudi Arabia. Detailed reserves and production data are presented in Table 1-2 [19].

Table 1-2: Reserves and production of Alberta oilsands bitumen as of 2008.^a

	Crude bitumen reserve (billion bbl)
Ultimate in-place volume	2,500
Initial in-place volume	1,731
Initial established reserves	177
Cumulative production volume	6.4
Remaining established reserves in 2008	170
Annual production in 2008	0.477
Ultimate potential recoverable reserve	315

^a From reference [19]

Currently, Albertan oilsands are being exploited as a major energy source [22-24] and feedstock for refineries [22,23,25]. Despite the technical and environmental challenges associated with exploration and transportation, oilsands bitumen is increasingly gaining interest as a reliable source of energy, especially in North America. According to International Energy Outlook 2010, given the high oil

prices, the exploration and production of Canadian bitumen will increase significantly in the future [7]. In 2009, crude bitumen production from oilsands was 1.5 million bbl day⁻¹ and with the steep increase in demand, it is projected to exceed 3.2 million bbl day⁻¹ by 2019 [13].

Based on the preceding discussion, it is evident that the vast energy resources in oilsands bitumen reserves have the potential to play a pivotal role in shaping the future of energy in North America. The following sections of this chapter will briefly discuss the properties, current extraction and upgrading methods, problems and environmental concerns related to the exploration of this important resource.

1.2 PHYSICAL COMPOSITION AND PROPERTIES OF OILSANDS BITUMEN

Oilsands, also known as tar sands and bituminous sands, are naturally occurring mixtures of sand, clay or other minerals, water and bitumen [13]. The typical composition of the Athabasca deposit in Alberta is 6–14 wt.% bitumen and 80–85 wt.% mineral solids, balanced by water [26]. The sand matrix is impregnated with the highly viscous high molar mass bitumen [13] that can be recovered and upgraded for use as petroleum. Depending on the bitumen content, the ores are graded as “poor” or “low-grade” (<6-8 wt.%), “average” or “medium-grade” (8-12 wt.%) and “rich” or “high-grade” (>12 wt.%) [27,28]. The water content in the ores varies between 1-5 wt.%.

The mineral composition of the sand is mainly quartz (>90%) with minor amounts of potash, feldspar, chert and muscovite [29,30]. Mineral solids in the oilsands that are <44 µm in size are known as “fines”, and are typically found in low grade ores. Clay minerals, dominantly kaolinite, illite and some montmorillonite [26] only appear in the fines fraction.

1.3 BITUMEN PRODUCTION AND PROCESSING

Oilsands bitumen production is a multi-step complex process which involves substantial capital and operational costs and problems. In the first major step, known as extraction, the bitumen is liberated and separated from the sand matrix by the use of water and/or other chemicals, thermal treatment and/or mechanical shear [28].

This is common for both *ex situ* and *in situ* operations for bitumen production. The bitumen slurry is then diluted with solvents to facilitate pipeline transportation, and sent to treatment and solvent recovery units. The heavy fractions of the separated bitumen are thermally or catalytically cracked (with or without hydrogen) into smaller fragments in primary upgrading units. Finally the bitumen is further upgraded to synthetic crude oil (SCO) in secondary upgraders by removing undesirable heteroatoms (N, S) and heavy metals (V, Ni etc.) prior to transportation to the refineries for typical crude oil fractionation. A generalized schematic diagram for an oilsands operation using water-based extraction is presented in Figure 1-2 [31].

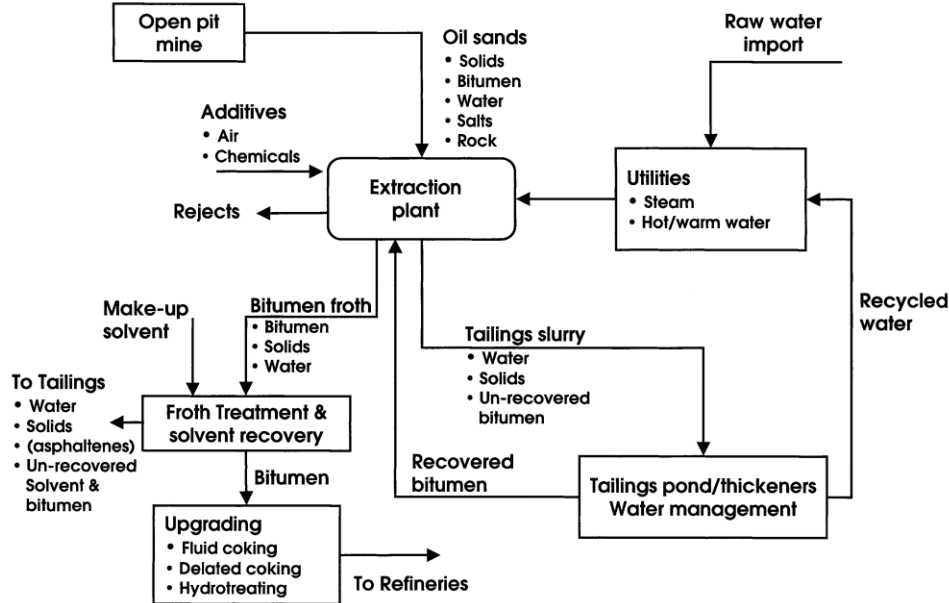


Figure 1-2: A generalized oilsands processing scheme using water-based extraction of bitumen [31]. Reused with permission from John Wiley and Sons.

The following subsections discuss the main steps and processes involved in oilsands bitumen production.

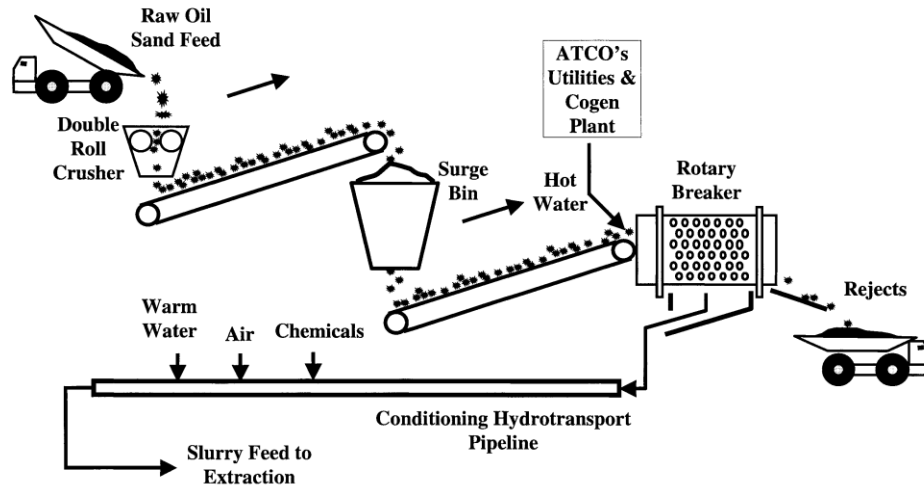
1.3.1 Surface mining

In ex-situ processes oilsands ores are pit mined [28]. The ore body (20-90 m) is excavated following removal of any overburden materials (up to 30 m in thickness). From an economic viewpoint, the stripping ratio, defined as ratio of the volumes of overburden to oilsands, needs to be $\ll 2$ (typical values between 0.36-1.36) for a viable mining operation. In the earlier operations, the ore body was mined by draglines and bucketwheel excavators with conveyer belts to carry them to the extraction facilities [32]. However, in the last decade or so, as the minable area has shifted to distant locations, more energy efficient truck and shovel have replaced these devices [28]. About 12,600 kg of oilsands need to be pit mined to produce 1 m³ of upgraded bitumen [28].

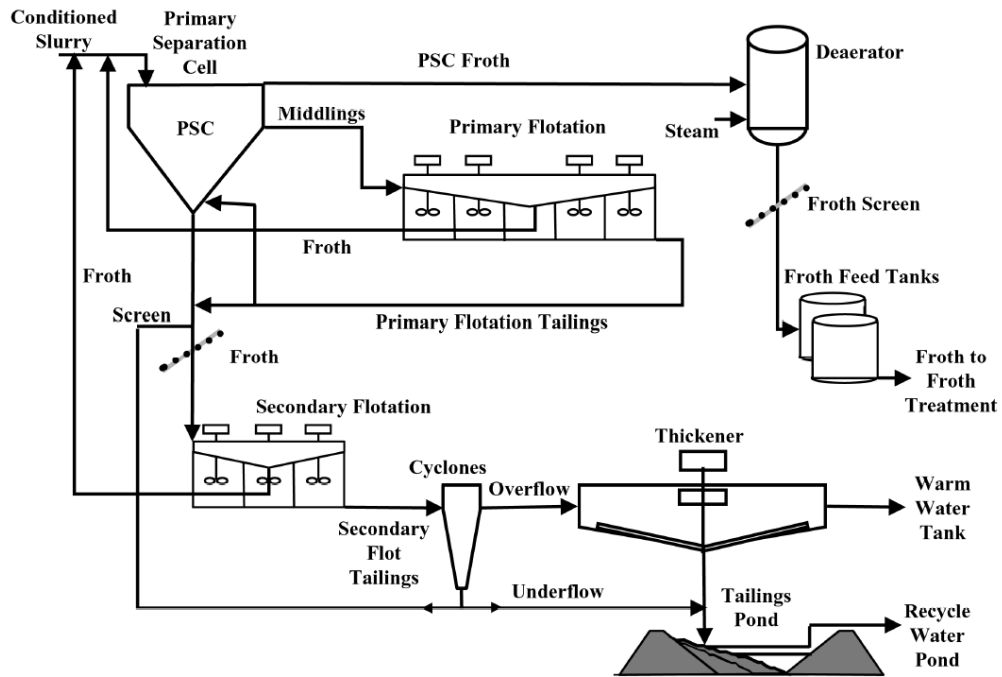
1.3.2 Extraction of bitumen by *ex situ* processes

Bitumen extraction in ex-situ processes is largely dominated by the Clark hot water extraction process (CHWE) or its variations, based on the concepts developed by Karl Clark [33-36]. The process requires moderate operating temperature (35-80 °C), caustic addition, aeration and a significant number of steps. Bitumen recovery from surface mined water-based processes is quite high (~90 wt.% of total bitumen content) [28]. Flow diagrams for a typical CHWE process for bitumen extraction and tailings is presented in Figure 1-3 (a) and (b) [31].

The surface mined oilsands ores are crushed and mixed with process water in mixing boxes, double roll crushers, stirred tanks, cyclo-feeders or rotary breakers [28]. For distant mining locations, as in Syncrude's Aurora mine, Suncor's Steepbank mine or Albion Sand's Muskeg River mine, the slurry is hydrotransported by pipelines [28]. Bitumen liberation from sand grains begins during contact with water at 35-80 °C, caustic and air in the rotary drums/breakers (tumblers) and/or hydrotransport pipelines. Caustic addition neutralizes the organic acids in bitumen to produce surfactants which lowers the bitumen-water interfacial tension, thereby allowing bitumen film to pin, rupture and recede easily from the grains [28]. Due to agitation and thermal energy the ablated layers of oilsands lumps are sheared off, and bitumen starts receding from the sand grains, forming small droplets. Air entrainment on the other hand, initiates air attachment to the droplets.



(a)



(b)

Figure 1-3: Flow diagram for oilsands bitumen extraction by a typical CHWE process: (a) ore preparation and slurry conditioning; (b) extraction and tailings facilities [31]. Reused with permission from John Wiley and Sons.

Large gravity separation vessels, known as primary separation vessels (PSV) primary separation cells (PSC), or, simply, separation cells (Sep Cells), are used to separate the liberated bitumen aggregates from the water-solids slurry [28]. The primary froth from these vessels, containing most of the bitumen, is sent to froth treatment plants. The middlings and/or the bottom tailings streams are subjected to further recovery of small bitumen aggregates (usually un-aerated) by additional separation units as secondary gravity separation vessels, primary and/or secondary floatation cells (use further aeration), cyclo-separators (Syncrude) or hydrocyclones. The froth from these units is recycled with the feed to PSV or PSC. The additional units as cyclo-separators are also known as tails oil recovery (TOR) units.

The tailings (bottoms) from the gravity separation vessels and floatation cells are combined and pumped to tailings ponds (Syncrude and Suncor) [28]. Albian sands, on the other hand, has a warm water reclamation process for recycling that uses large thickening units prior to discarding to tailings. While the coarser particles in the ponds settle fairly quickly, fines settling can take many years, obstructing the increase in the depth of the recyclable top free water zone. The mature fine tailings, a term used for the fine solids as they reach 30 wt.% concentration in the suspension over 2-3 years, are typically treated with gypsum for consolidation together with the coarse solids. This process is known as the composite tailings process [28].

Bitumen froth from the separation vessels and the floatation cells is de-aerated in de-aeration towers by a counter-current flow of steam, and then sent to froth treatment facilities to remove most of the mineral solids and water [28]. Froth treatment processes are naphtha- (Syncrude and Suncor) or paraffin-based (Albian Sands). The froth, with reduced viscosity from diluent addition, is removed from the solids and water by a set of inclined plate settlers, centrifuges and cyclones (Syncrude and Suncor). The naphtha is recovered in a diluent recovery unit (DRU), and the free bitumen stream is sent for upgrading. The paraffinic froth treatment (PFT) process, on the other hand, typically uses hexane instead of naphtha and leads to substantial asphaltene precipitation (8-10 wt.% of the total feed) [28]. The precipitated asphaltene actually aid in the demulsification of the water droplets and fine solids as flocculants. A multi-stage mixer/settler device is used instead of centrifuges to separate the different phases prior to recovering the paraffin in a solvent recovery unit (SRU) by distillation. The tailings from the last stage are

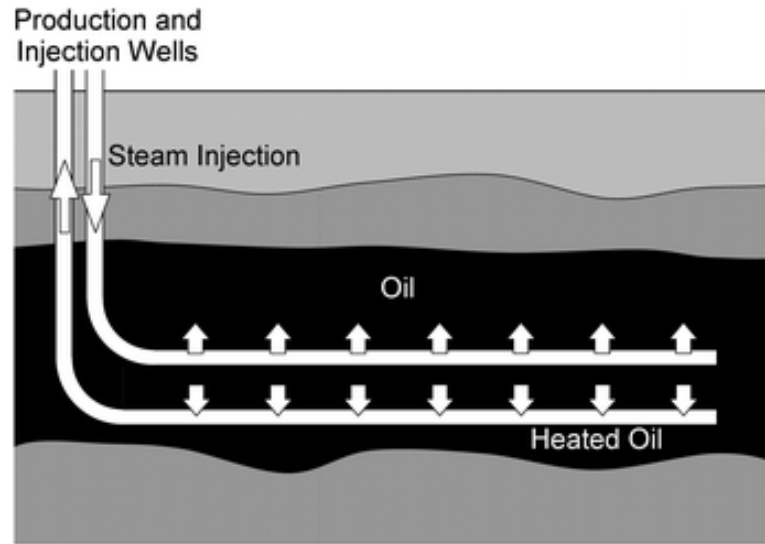
stripped off any remaining solvent in a tailings solvent recovery unit (TSRU), and sent for upgrading. The PFT process produces much cleaner bitumen with very small amounts of solids and water compared to the naphtha-based process. However, the solvent vapor pressure and loss during the processing are significant operating issues [28].

1.3.3 Extraction of bitumen by *in situ* processes

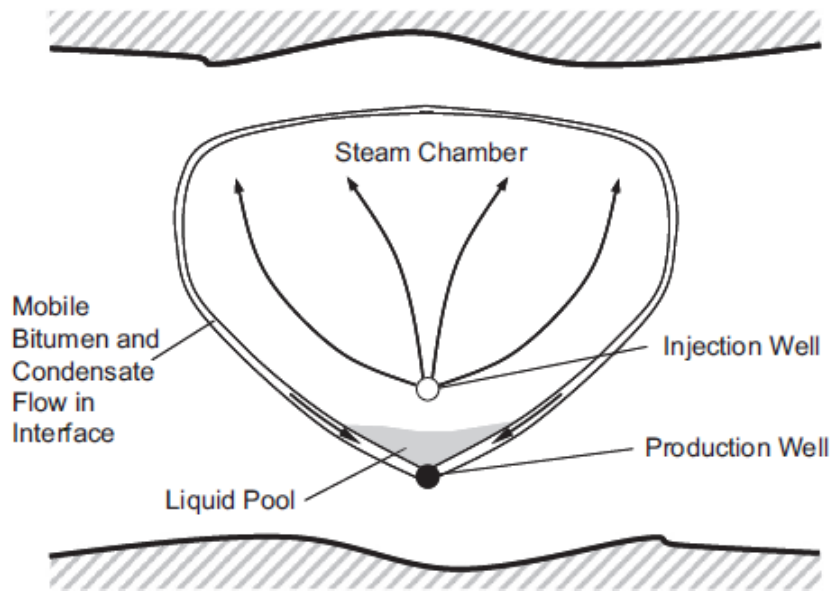
While surface mining is currently the dominant method of bitumen extraction, only 15% of the resource is buried at the shallow depths accessible to this harvesting technique [37]. The rest of the resource is located deeper, requiring different technologies. By the end of 2008, only 34.5 billion bbl of the remaining established reserve were available for surface mining as compared to the 135.7 billion bbl available for *in situ* extraction [19]. This vast amount and the benefits of reduced water consumption and environmental impacts are increasing the importance of *in situ* techniques. Some of these techniques are still under development. Among the available *in situ* methods, cyclic steam stimulation (CSS), steam assisted gravity drainage (SAGD), vapor extraction process (VAPEX) or hybrid processes are the most prominent.

The first commercial *in situ* initiative was undertaken by Imperial Oil at the Cold Lake lease [28]. This CSS or “huff-and-puff” technique required steam injection through vertical wells for several months, followed by soaking for several weeks. The wells then enter production as the heated bitumen is pumped to the surface until no more bitumen is available. This cycle is repeated until recovery of all extractable bitumen.

SAGD, a process invented by Dr. Roger Butler and his colleagues at Imperial Oil in the late 1970s [38], is probably the most widely employed *in situ* technique, and has opened a massive new frontier in deep-lying bitumen resources [37]. This method uses horizontal wells that can reside within the deposits over several km, tapping a much greater portion of the deposit compared to the vertical well systems [28]. The system consists of a pair of parallel horizontal wells drilled one above the other at a separation distance of 5-10 m [39]. The typical length of the wells is 500-1000 m. Schematic diagrams of a typical SAGD process are presented in Figure 1-4 [39,40].



(a)



(b)

Figure 1-4: Schematic diagram of a SAGD process: (a) horizontal well pair [40]; and (b) cross-sectional view of the steam chamber [39]. Reused with permission from (a) the Royal Society of Chemistry; and (b) Elsevier.

The top well of the setup is the injection well, used to input steam into the steam or depletion chamber. The lower well, also known as the producer well, is drilled about 1-2 m above the formation base [41]. The steam releases latent heat at the edge of the depletion chamber, which reduces the viscosity of bitumen in the oilsands, making it mobile and allowing it to flow under the effect of gravity towards the producer well [39]. Several sets of well pairs are drilled for large scale production, approximately 100-150 m apart [28]. The maximum steam pressure must be kept well below the fracture pressure of the formation.

Production rate from SAGD is usually about 15 times higher than CSS processes, but it can only be considered to be a viable process for deposits with overburden >30 m, formation thickness >15 m with a bitumen content >6 wt.% [28]. The recovery of bitumen is much lower than water-based *ex situ* extraction processes: about 60-77 wt.% of the *in situ* bitumen when a steam to oil ratio of ~2.5 is maintained. The production life of the well pairs can be up to 15 years.

Because of the high thermal energy requirement of the SAGD process, VAPEX introduced the use of light hydrocarbons such as propane, instead of steam, to reduce bitumen viscosity [28]. The process focuses on creating a chamber analogous to the steam chamber in the SAGD process by maintaining the operating pressure at the dew point pressure of the hydrocarbon [28]. The hydrocarbon imparts a solvent effect to reduce the viscosity of bitumen. However, because the method uses a high value commodity to recover a less valuable commodity, it is restricted to cases where almost all the solvent is recoverable. It has been reported that hybrid *in situ* processes, involving simultaneous injection of steam and light hydrocarbons are currently under development although the details remain highly proprietary [28].

The bitumen produced by *in situ* processes is subjected to bitumen de-aeration, emulsion formation, aggregation and all of the later features of surface mining processes [28]. Therefore *in situ* operations require a number of processing units, as well as significant number of units for gas-oil, gas-steam, steam-oil separation and water treatment prior to upgrading of produced bitumen. These processes require water in form of steam, which requires substantial energy. In some cases valuable light hydrocarbons are required for extraction. The *in situ* processes

also have the disadvantages of heat loss from the overburden, solvent loss, higher production time and lower recovery.

1.3.4 Primary upgrading processes

Upgrading of bitumen or heavy oil is a subset of refining technology [42]. The processing steps in upgrading are adapted from refining, the only difference being the fact that in refining highly purified streams meeting the market specifications are produced, whereas bitumen/heavy oil upgrading generates an intermediate stream requiring further refining. Upgrading operations are divided into “primary” and “secondary” operations.

In primary upgrading, the heavy residue fraction in bitumen/heavy oil is converted to smaller more distillable components by significant breakage of carbon-carbon bonds [43]. Primary upgrading processes can be based on thermal cracking, coking or hydroconversion [42]. Following a separation process, typically consisting of desalting, deasphalting and distillation, the bitumen from the extraction facilities is sent to the primary upgrader [42].

Thermal visbreaking is a relatively mild (475-500 °C, 0.5-7 Mpa) low cost primary upgrading process that focuses on reducing the viscosity by removing the side chains from the high molecular weight compounds in bitumen without significant conversion to distillates [42,44]. The process is simple; the reaction takes place in furnace tubes, followed by a quenching step with recycled oil and a fractionation unit for product separation. Although relatively simple and less severe, the application of the process is limited by low conversion rates and several operational issues. The products from straight thermal processing contain olefins, which, in turn, form unstable compounds [42,45] that undergo polymerization to generate tars and gums [42]. Substantial coke formation also occurs due to polymerization and condensation reactions [24]. The heavy fraction may form solids or sediments, limiting the range of conversion as well as causing operational problems [42]. Hydrogen addition to visbreaking, a process known as hydrovisbreaking, generally improves the product quality but is expensive [42].

Delayed coking is a widely employed and effective severe thermal technique (450–470 °C) for primary upgrading processes, particularly for heavy residues [42,46].

This semi-batch process employs insulated coke drums where the preheated (480-515 °C) feed is maintained at ~415-465 °C and 0.1- 0.4 MPa [46] to accumulate coke enriched with nitrogen, sulfur and metals, thereby producing distillates and gas products with lower concentrations of these elements [42]. A schematic diagram of the delayed coking process is presented in Figure 1-5 [46]. The gas, naphtha and distillate fractions are separated in a fractionator unit and the unconverted residue is recycled to the coke drum along with the fresh feed [46]. Coke is accumulated in the coke drum for prolonged periods of time (~24 hours), hence the process name. Despite the higher conversion and better quality of products, delayed coking has several operational disadvantages. First, it requires long down time to remove the accumulated coke from the drum (a typical cycle is ~48 h), necessitating multiple units and manual operation [43]. In addition drum sizes and throughputs are limited by the thermal stresses of heating and cooling cycles [42]. Other operational issues include foaming in the drums and coking in the tubes of the coker heaters. Delayed cokers also reject a substantial fraction of the carbon by coking: ~25% according to Suncor design data although figures based on actual operation are higher [42].

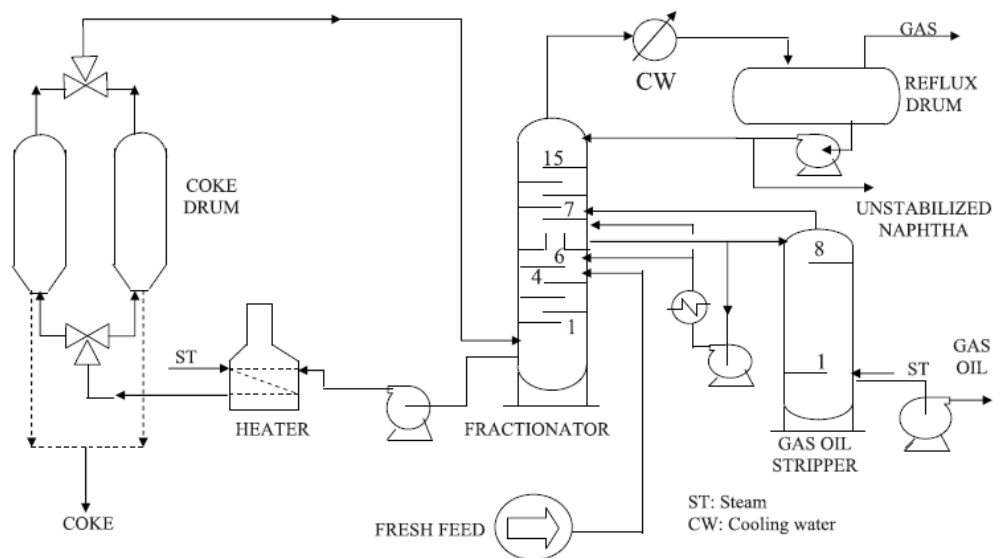


Figure 1-5: Schematic diagram of a typical delayed coking process [46].
Reused with permission from John Wiley and Sons.

Fluid coking, a continuous thermal technique, can handle larger volumes of residue [43]. A schematic diagram of the process is presented in Figure 1-6 [47]. The feed is sprayed over a fluidized bed of coke particles to start the coking process. The vapor, generated from cracking at about 510-550 °C, rises to the top of the reactor and is separated and quenched. The coke is stripped with steam to remove liquids, and is partially burned prior to recirculation to the coker unit. The process produces slightly less coke and lower quality products than delayed coking [42]. It also has some operational disadvantages, however, such as accumulation of coke inside the units and production of sulfur from the reaction burner. An alternate approach uses a coke gasifier to convert the carbonaceous materials to hydrogen and hydrogen sulfide containing gas streams, but requires additional large reactors for conversion, and scrubber units for separation of sulfur gases [42]. The Felixcoking process at Exxon employs this method [48].

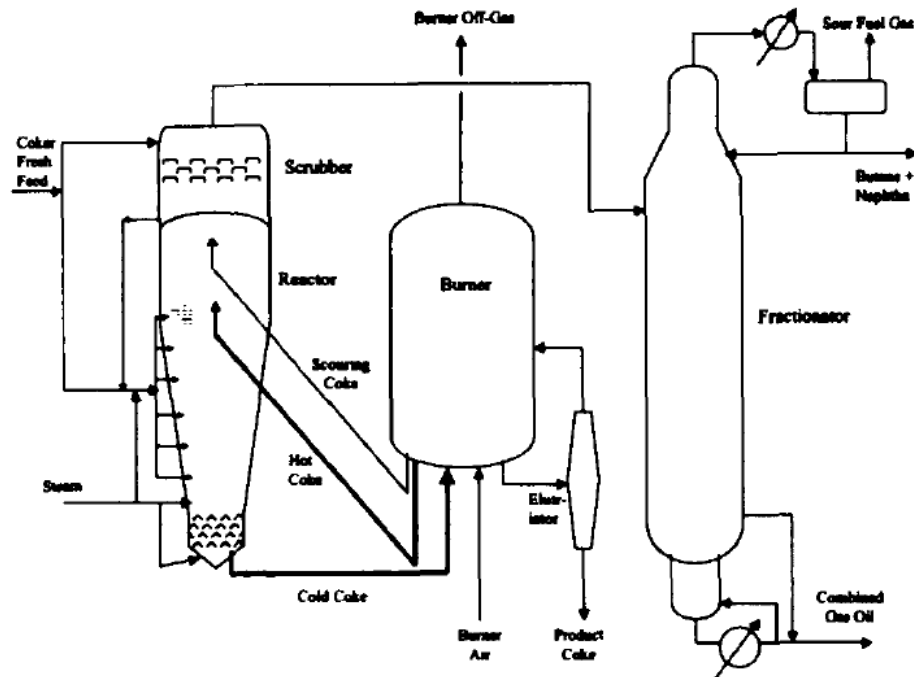


Figure 1-6: A schematic diagram of a fluid coking process [47]. Reused with permission from John Wiley and Sons.

1.3.5 Hydrogen added catalytic mixed primary-secondary upgrading processes

With the addition of hydrogen and catalysts, both conversion and product quality can be significantly improved. This, however, increases the processing cost substantially. The process, known as hydroconversion, may incorporate breakage of chemical bonds at temperatures over 410 °C and simultaneous coking suppression with hydrogen [42]. Lower temperature processes are used for secondary upgrading, typically known as hydrotreating. Sometimes a high pressure hydrocracking process is used with a bifunctional catalyst to provide both hydrogenation and acidic reactions, and accomplishes both residue conversion and secondary upgrading. Since both primary and secondary reactions occur in these methods it is difficult to classify them as one over the other.

Ebullated bed processes as LC-Fining and H-Oil use alumina supported transition metal sulfide catalysts suspended in hydrogen fluidized beds to treat residues [42]. Fluidization prevents plugging by solids. Typical operating conditions are 420-450 °C and 10-15 MPa hydrogen pressure. These processes require addition of fresh catalysts and removal of spent catalysts on a regular basis, and have low to moderate conversion of residues. With addition of secondary reactors, recycling and treatment of unconverted feed, the conversion can be somewhat increased [42].

Additive or slurry-based processes such as CANMET or ENI Slurry Technology add finely ground solids or soluble compounds to the feeds that are carried through the reactor for conversion of the feed [42]. These processes mainly focus on hydroconversion of residue, while bulk of the secondary upgrading is achieved in a follow-up hydrotreating unit. Typical catalysts are iron or organometallic compounds, and operating conditions are 420-490 °C and 6-25 MPa. The recovery of catalysts can be impractical, and the additive may remain within the slurry requiring further processing and/or separation [42], reducing the practicality of these approaches.

1.3.6 Secondary upgrading processes

Secondary upgrading involves removal of heteroatoms such as sulfur, nitrogen and heavy metals, typically by catalytic hydrogenation processes referred to

as hydrotreating. The upgrading results in the hydrogenation of aromatics and olefins, while seeking to suppress coking. As discussed earlier, secondary upgrading may occur in some of the hydrogen addition mixed upgrading processes. Hydrotreating differs from hydroconversion in that it is intended to selectively remove heteroatoms from the feed, rather than cracking hydrocarbon molecules [42].

A typical hydrotreating process consists of one or more fixed bed reactors. A schematic diagram of the process is presented in Figure 1-7 [49]. The feed is preheated and passed through the reactor with the hydrogen stream maintained in excess of stoichiometric quantity to limit the accumulation of hydrogen sulfide. The usual catalysts used for the process are cobalt or nickel promoted molybdenum sulfides on gamma alumina supports. Despite the simplicity of scale-up and operation, the mineral solids in the residue feed accumulate and deactivate the catalysts rapidly [42].

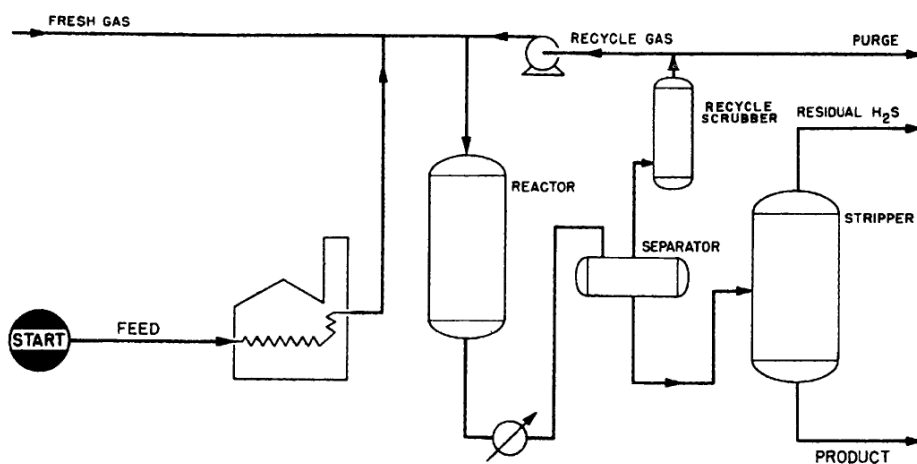


Figure 1-7: A schematic diagram of a hydrotreating process [49]. Reused with permission from Elsevier.

1.4 CHALLENGES WITH BITUMEN PRODUCTION

Bitumen production has unique operational, environmental and product quality related issues. They are discussed in the following subsections.

1.4.1 High viscosity and density

The extracted bitumen is too viscous ($5-7 \times 10^9 \text{ m}^2 \text{ s}^{-1}$ at $40 \text{ }^\circ\text{C}$) [43] for pipeline transportation to upgrading/refining facilities because of the large heavy hydrocarbon fractions [23-25,50], and requires the addition of naphtha, gas condensates, or other diluents to meet pipeline specifications ($19 \text{ }^\circ\text{API}$ and 350 cSt at $8 \text{ }^\circ\text{C}$ within pipelines) [25,50]. This increases both capital and operating costs for production.

1.4.2 Requirement for upgrading

Oilsands bitumen has high asphaltene and polar resin contents and a correspondingly high boiling point distribution. It also has high heteroatom ($0.4-0.5 \text{ wt.}\% \text{ N}$, $4.4-4.9 \text{ wt.}\% \text{ S}$) [43] and heavy metals ($130-200 \text{ ppm Ni}$, $190-490 \text{ ppm V}$ and others) [42] contents, and a low H/C ratio (~ 1.50) [42] all of which necessitate extensive treatment [23-25] by upgrading facilities prior to sending to refineries for conversion to transportation fuels.

1.4.3 Use of water and generation of tailings ponds

Oilsands extraction methods consume multiple barrels of fresh water to produce a single barrel of oil. The processes generate high volume of chemical waste water in tailings ponds that is difficult to treat prior to reuse or reclaim [51]. In mining operations, $7.5-10 \text{ bbl}$ of water is used per bbl of SCO produced [13]. With recycle rates of $40-70\%$ this is $3-4.5 \text{ bbl}$ of fresh make up water. For *in situ* operations the total and fresh water requirements for per bbl of SCO are $2.5-4 \text{ bbl}$ and 0.5 bbl respectively, with recycle rates of $70-90\%$ [13]. Long term use of hot water extraction for high output oil production raises concerns about both water management and environmental impacts in the Athabasca River basin [52].

Besides high consumption, water management and tailings generation represent real environmental issues [28]. The net increase in the volume of fine

tailings is about 0.1 m³ per ton of processed oilsands. These tailings have to be contained in massive ponds that also host the residual bitumen and chemicals (caustic, surfactants, flocculants etc.) from processing. This has now become a global environmental concern related to oilsands processing. The fine tailings in these ponds settle at a very slow rate, leaving only a small fraction of free water at the surface available for recycling.

1.4.4 Production of greenhouse gas

Oilsands processing involves substantial amount of greenhouse gas (GHG) production. In 2008, the total amount of GHG production from Alberta oilsands processing was 110.9 Mton [13]. This may further increase with the anticipated steep rise in oilsands bitumen production.

1.4.5 Use of more valuable commodities

Currently, some primary and all secondary upgrading operations use hydrogen, an expensive commodity that is typically generated from natural gas, which itself is a much cleaner source of energy. Moreover, transportation, froth treatment and solvent based *in situ* extraction processes use light hydrocarbons, the economics of which will only be justified if there is little or no loss.

1.4.6 Complicated and capital-intensive multi-step processing

Based on the previous discussion on extraction and upgrading techniques, it is evident that oilsands processing requires complex multi-step processing. The operation and maintenance of these processes involve significant problems, limitations and complexity. The large number of distinct steps in separate extraction and upgrading processes also make bitumen processing highly capital-intensive.

There is currently no single technique for oilsands processing that can address the environmental concerns related to processing while maintaining high recovery and low capital and operating costs. An integrated extraction and upgrading approach may help minimize these costs as well as operational problems by reducing the number of steps involved in the processing.

1.5 NATURAL ZEOLITE CRACKING FOR INTEGRATED PROCESSING OF OILSANDS: A NOVEL APPROACH

1.5.1 Background

Natural and synthetic clay minerals have been long used for catalytic cracking of heavy petroleum feedstock [53]. In the early 1930s scientists at the Universal Oil Products Company observed the activity of natural clays for catalytic cracking of gas oils, and made attempt to modify their properties to develop them as effective high temperature solid acid catalysts [54]. During the early stages of development intensive research on halloysites from Utah, kaolinites from Georgia, and bentonites containing calcium montmorillonite from Arizona and Mississippi were jointly spearheaded by the Houdry Process Corporation and Filtrol Corporation [55]. The first cracking catalyst used for cracking of heavy petroleum fractions was an acidified form of montmorillonite, a hydrated aluminum silicate with some magnesia [53]. Following the production of the first synthetic silica-alumina catalyst by Houdry Process Corporation in 1940, the natural clays started being replaced. These were amorphous alumina-silica catalysts with higher thermal stability and mechanical strength. However, due to the higher cost of these catalysts, clay materials continued being used as petroleum cracking agents. A semi-synthetic class of catalysts emerged in 1957, introducing clay materials such as kaolinite in the synthetic silica-alumina [55]. Until the 1990s, some of the state of the art cracking catalysts used in petroleum processing were either acid-leached and/or untreated kaolin-derived, and/or silica fume derived zeolites, caustic-treated calcined kaolin, or semi-synthetic kaolin-based matrices in combination with zeolites [55].

The introduction of synthetic zeolites in the early 1960s revolutionized the petroleum processing industries [56]. In fact, introduction of synthetic faujasites (X and Y) in industrial refining of heavy petroleum distillates, one of the most important chemical processes in the world, was a landmark event [57]. The new zeolite catalysts were orders of magnitude more active than the amorphous alumina-silica catalysts and provided much higher yields of gasoline. To date, synthetic zeolite Y (ZY) is the most widely used cracking catalyst for refining of heavy petroleum feedstocks, typically employed in fluid catalytic cracking (FCC) processes.

1.5.2 Zeolites as cracking catalysts: Structure and activity

Typically zeolites are crystalline aluminosilicates with well-defined structures, widely used for adsorption and molecular sieving [58]. The structures of zeolites are built based on a truncated octahedron as the framework-forming unit, where the corners of the octahedron are occupied alternately by SiO_4 , and AlO_4 tetrahedra, the primary building units [58]. This fundamental aluminosilicate skeleton, composed of four-membered and six-membered rings, is denoted as a sodalite cage or a β -cage. The structure of a faujasite zeolite as ZY is constructed from this polyhedron. The 12-membered ring (pore diameter of $\sim 7.4\text{\AA}$) and the frameworks of the β -cage and the faujasite structure are presented in Figure 1-8 [59].

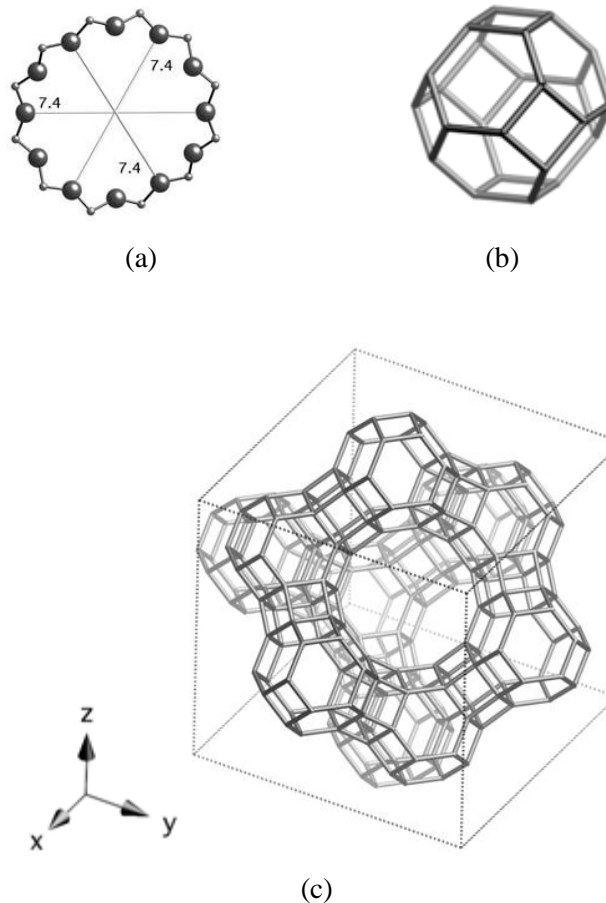
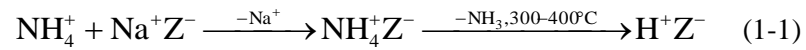


Figure 1-8: Frameworks of faujasite: (a) 12-membered ring viewed along (111) direction; (b) the β -cage; and (c) the faujasite structure [59].

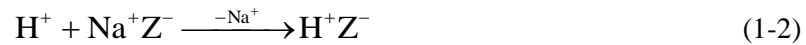
Zeolites catalyze cracking reactions as solid acids [53,57]. The isomorphous replacement of Si^{4+} by Al^{3+} within the zeolite structure produces a net negative charge in the lattice [60]. In order to be electrically neutral, the negative charges on aluminum anions in the zeolite structure are balanced by cations [53,60]. For any industrial cracking application, these cations are replaced with protons to form Brønsted acid sites on the zeolite surface by any of the following four schemes [57]:

- i) Aqueous ion-exchange with ammonium salt followed by thermal decomposition of the ammonium ions:



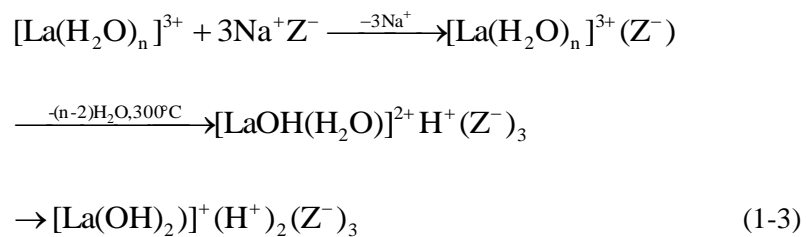
Here, Z denotes the zeolite framework. This is the most widely used method for acidifying zeolites.

- ii) Direct ion-exchange with mineral acids:

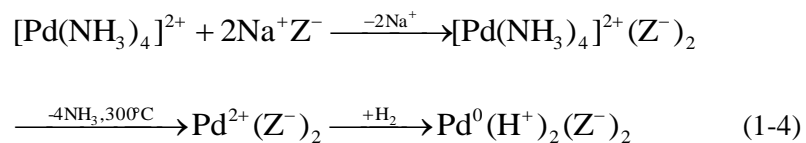


This method can result in framework dealumination.

- iii) Aqueous ion-exchange with a multivalent metal (alkaline or rare earth) cation followed by thermal dehydration (Hirschler-Plank Scheme):

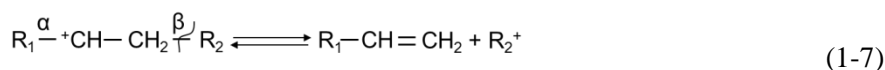
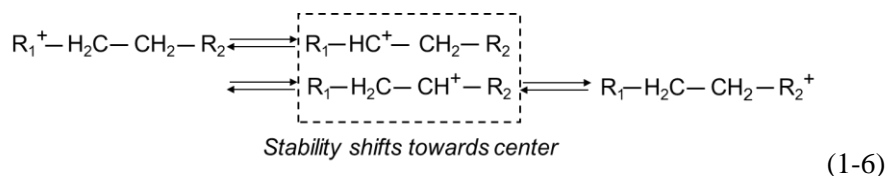
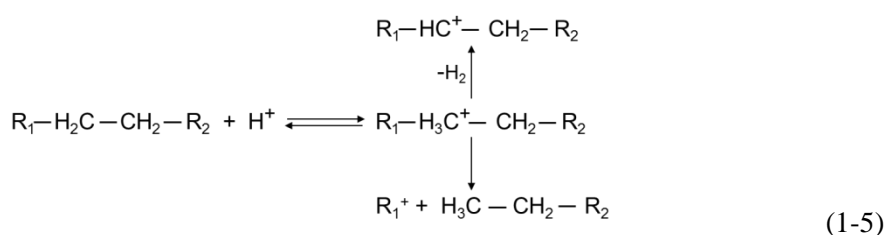


- iv) Reducing metals nobler than hydrogen by molecular hydrogen:



The nature of the generated acid sites is the same, regardless of the method. These Brønsted acid sites may degrade to Lewis acid sites by dehydroxylation. The nature of the Lewis sites is less clear, but under certain circumstances they may enhance the strength of the Brønsted acid sites, and impart an indirect influence on the acidity of the catalysts [57].

Catalytic cracking reactions are carbocationic, unlike thermal cracking which are free-radical based [53,61]. Usually addition of a proton (H^+) from a Brønsted center or abstraction of hydride ion (H^-) by a Lewis site creates a carbocation from a petroleum molecule, which then undergoes skeletal isomerization (methyl shift) or charge isomerization (hydride shift) or hydride ion transfer to obtain a stable formation [61]. In the cracking step, the carbon-carbon bond at the β -position to the electron deficient carbon atom, which is weaker than the bond at any at the α -position, is broken to produce an olefin and another carbocation, as long as the smallest fragment contains at least three carbon atoms. The carbocations generated from the scission participate in further β -scission as long as the conditions are satisfied. Finally, progressive blocking of the acid sites by strong adsorption of high molecular mass ions, generally produced by polymerization, cyclization, dehydrogenation or condensation reactions, terminates the reaction [61]. The mechanism of cracking of a saturated hydrocarbon molecule undergoing charge isomerization is illustrated by Equations 1-5 to 1-7. Here R_1 and R_2 are alkyl groups.



The extent of catalytic cracking are, however, dependent on the structural and acidic characteristics of the catalyst, which will be discussed in greater details in the following chapter.

1.5.3 Natural zeolites as potential cracking catalysts

In the oilsands industry, zeolites are used as cracking catalysts in the refining of SCO produced from upgraded raw bitumen. As discussed in the previous sections, oilsands bitumen is extremely rich in heavy residual materials, heteroatoms, and heavy metals. Direct use of expensive commercial ZY for cracking of such feedstock will lead to rapid deactivation and/or poisoning of the catalysts, and therefore cause operational problems and substantial increase in production costs. Similarly, the use of the ZY in the pre-extraction phase is essentially unrealistic, considering the amounts required for processing and the high cost of the catalyst. The use of zeolites in oilsands bitumen cracking and upgrading will only be attractive if a more economical, but still effective, approach can be developed.

While synthetic zeolites have been widely employed as commercial petroleum cracking agents, natural zeolites (NZ) have not because of impure phases and variation in chemical composition [57]. In certain cases, however, ion-exchanged/modified natural zeolites and composite clays were used as petroleum cracking catalysts. Composite catalysts of NZs and clays have been found to be capable of cracking vacuum distilled feeds, fuel oil and heavy residue into lighter fractions [62,63]. One study has demonstrated that a composite catalyst of rare-earth exchanged NZ effectively breaks down heavy oil to produce high amounts of liquid products, isoparaffin, and low-olefin hydrocarbons [64]. Ion-exchanged and unexchanged forms of clinoptilolites and phillipsites have also been shown to catalytically crack petroleum residue [65].

Use of natural minerals for oilsands bitumen cracking is a novel approach. Interestingly, a previous study found that if a portion of the native inorganic solids from the parent oilsands is returned to the extracted bitumen prior to thermal treatment at temperatures around 525 °C, a lower boiling point, less viscous product is obtained from thermal visbreaking, which indicated the catalytic activity of the clay within oilsands itself on bitumen [66]. Taking into account that such activity had been observed for other naturally occurring aluminosilicate minerals, a study in our

lab found that upgraded and acidified Ca-chabazites procured from Bowie, Arizona could crack the heavy components of bitumen within the oilsands to lighter and less viscous toluene-extractable fractions in micro-batch reactor systems [67]. This work was done on pit-mined, unextracted oilsands. However, since authorities predict a multiple-fold increase in crude bitumen production in Alberta any practical in-field upgrading would need to scale-up proportionately and employ properly engineered practical and economic technology. In order to develop a practical, low cost, high-throughput process, the catalytic potential of more abundant and untreated natural minerals must be investigated in realistically engineered systems.

Natural clinoptilolites and chabazites have similar chemical properties and can be considered as excellent candidate catalysts. Clinoptilolites are the most abundant, inexpensive NZ found in multiple global deposits [60,68,69]. Clinoptilolite has the chemical formula of $\text{Na}_{0.1}\text{K}_{8.57}\text{Ba}_{0.04}(\text{Al}_{9.31}\text{Si}_{26.83}\text{O}_{72})\cdot 19.56\text{H}_2\text{O}$ [70]. However, the chemical composition varies in different deposits and even within single deposits. The empirical formula for the raw clinoptilolite as obtained from the Saint Cloud's deposit is $(\text{K,Ca,Mg})_{20}\text{-Al}_2\text{O}_3\text{-10SiO}_2\cdot 6\text{H}_2\text{O}$. The characteristic tabular morphology of the clinoptilolite shows an open reticular structure of easy access, formed by open channels of eight (3.6 and 4.6 Å opening) and ten (3.1 and 7.5 Å opening) open membered rings [71] as shown in Figure 1-9 [59]. Chabazite, on the other hand, is built of double six-membered rings forming one cage per unit cell; each cage has six octagonal, two hexagonal and twelve quadrilateral faces, and is connected to six neighboring cages by eight-membered rings [72], also shown in Figure 1-9. Typical chemical formula for chabazite is $\text{Ca}^{2+}_6(\text{Al}_{12}\text{Si}_{24}\text{O}_{72})\cdot 40\text{H}_2\text{O}$ [59].

Both clinoptilolite and chabazite have high exchange capacities [69,73,74] that can be utilized to generate large number of acid sites on the surface to participate in acid catalytic cracking. These minerals are extremely strong adsorbents, found to effectively remove heavy metal cations from waste streams [60,68,69,73,75-78]. Therefore, their acidic, ion-exchange and adsorptive properties can be employed for an additional potential benefit related to oilsands bitumen processing: to remove basic nitrogenous compounds, sulfur and heavy metals to produce cleaner high quality upgraded bitumen.

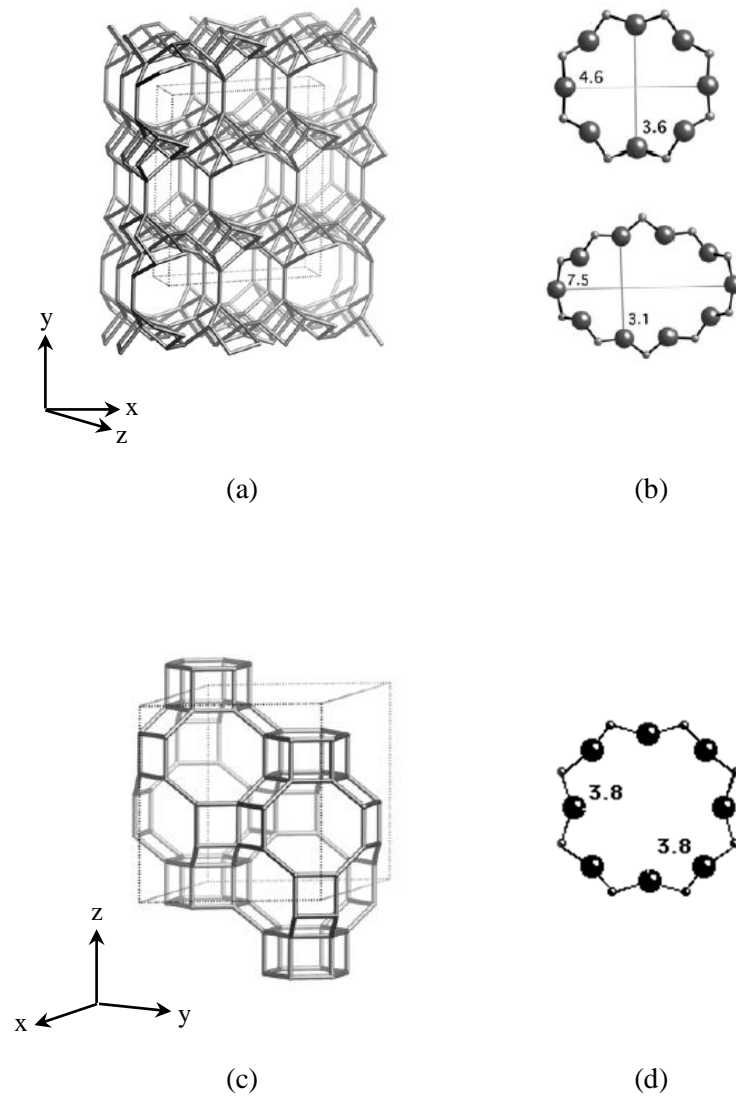


Figure 1-9: Framework and structure of clinoptilolite and chabazite: (a) clinoptilolite framework viewed along [001]; (b) 8 and 10 membered rings of clinoptilolite viewed along [001]; (c) chabazite framework viewed normal to [001]; and (d) 8-ring of chabazite viewed normal to [001] [59].

This study investigates the potential to develop an integrated extraction-upgrading process for oilsands bitumen using natural clinoptililite and chabazite catalysts. The NZ-catalyzed cracking reactions are designed to break down the heavy molecules in bitumen into lighter, less viscous components at temperatures much below than that required for thermal visbreaking. The resultant products will be readily extractable by light hydrocarbons such as pentane or hexane. The spent catalysts will retain the heteroatoms (sulfur, nitrogen) and heavy metals, leaving a cleaner product that requires less downstream processing. The idea is summarized in Figure 1-10 [79]. This will eliminate the need to use water for extraction, and help develop a more environmentally friendly, tailings-free process. Since this process will integrate extraction and upgrading to a significant extent, fewer processing steps will be required, reducing total operating and capital costs. This novel approach could improve the long-term economics of oilsands extraction, which is the ultimate objective of this project.

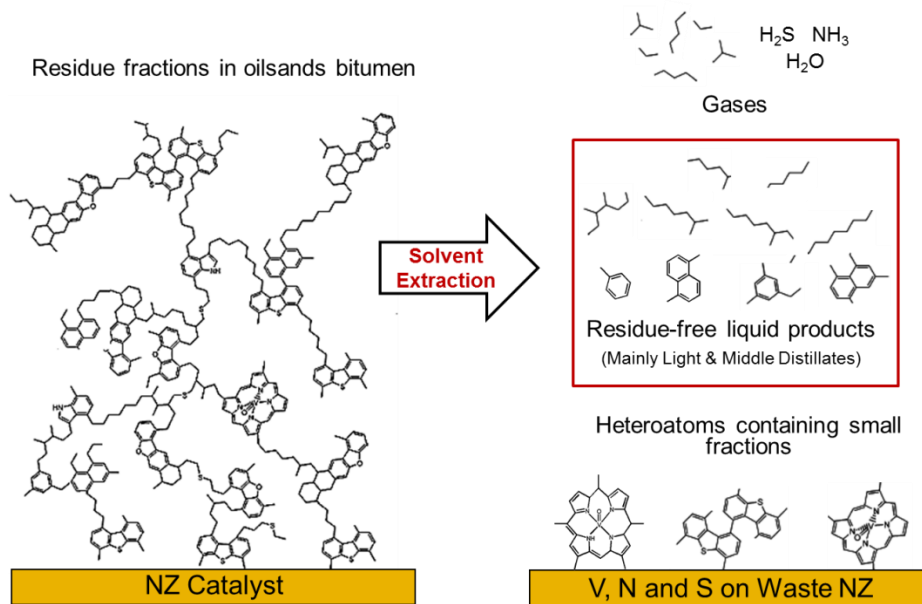


Figure 1-10: Conceptual representation of NZ-based integrated extraction and upgrading of oilsands bitumen. Partly adopted from Junaid et al. 2011 [79], and reused with permission from Elsevier.

1.6 ORGANIZATION OF THE THESIS

This study is organized in the following manner:

Chapter 1 provides a background on current oilsands processing techniques and issues. It also introduces the concept and potential of a NZ-based effective, economic and environmentally friendly integrated extraction and upgrading process for oilsands.

Chapter 2 presents an investigation of the unique structural, compositional and acidic properties of raw and ion-exchanged natural clinoptilolites and chabazites to test their feasibility for cracking of heavy hydrocarbon fractions using a series of characterization and surface sensitive techniques [80]. The properties of the NZs are compared with the baseline properties of the commercial petroleum cracking catalyst, ZY.

Chapter 3 presents a proof-of-concept study on the efficacy of waterless light hydrocarbon extraction of liquid products following ion-exchanged NZ-cracking of Athabasca oilsands. Using ammonium-exchanged, acidified clinoptilolites and chabazites, oilsands bitumen samples are cracked into lighter fragments in unstirred microbatch reactors and are extracted by pentane or hexane [81]. The recovery and boiling point distribution of the products are compared to those from thermal and ZY catalyzed reactions.

Chapter 4 showcases the development of an alternate method for acid site generation on an untreated and unexchanged NZ surface by hydrolysis [82]. This essentially eliminates the ion-exchange step, and provides a less complicated and low cost method for catalyst activation. A series of measurements and surface sensitive techniques have been employed to determine the underlying mechanism of the process.

Chapter 5 presents the development of a scaled-up engineered process for solid oilsands cracking with reduced loadings of hydrolyzed and self-acidified NZ-catalysts in a more realistic environment [79]. The performance of the process is measured with respect to the total and residue-free oil recovery and product quality (boiling point distribution, viscosity, average molecular weight, aromaticity, heteroatoms and heavy metals contents etc.).

Chapter 6 estimates the comparative energy consumption of the proposed NZ-based process with respect to conventional extraction and upgrading operations.

Chapter 7 presents an alternate application of the catalysts on pre-extracted oilsands bitumen solely for the purpose of a more energy efficient low temperature upgrading. The reusability and potential *in situ* application of the catalysts are also evaluated.

Finally, Chapter 8 draws conclusions from the findings and proposes future work.

BIBLIOGRAPHY

- [1] Alboudwarej H, Felix J, Taylor S, Badry R, Bremner C, Brough B et al. Highlighting heavy oil. Oilfield Review [Internet]. 2006 summer [cited 2011 May 27]; 18(2): 34-53. Available from: http://www.slb.com/~media/Files/resources/oilfield_review/ors06/sum06/heavy_oil.ashx
- [2] Worldwide look at reserves and production. Oil Gas J. 2010; 108(46): 48-9.
- [3] Bahorich M. End of oil? No, it's a new day dawning. Oil Gas J. 2006; 104(31): 30-4.
- [4] Historical world reserves-to-production ratio of oil, 1980 to present [Internet]. ChartsBin – [cited 2011 May 26]. Available from: <http://chartsbin.com/view/t3t>
- [5] Doman LE. World energy demand and economic outlook. In: International Energy Outlook 2010 [Internet]. Washington (DC): United States Energy Information Administration, Office of the Integrated Analysis and Forecasting; 2010 Jul. [cited 2011 May 27]. Report No. DOE/EIA-0484(2010). Sponsored by the United States Department of Energy. Available from: [www.eia.gov/oiaf/ieo/pdf/0484\(2010\).pdf](http://www.eia.gov/oiaf/ieo/pdf/0484(2010).pdf).
- [6] Sawin JL, Martinot E, Sonntag-O'Brien V, McCrone A, Roussell J, Barnes D, Flavin C. Renewables 2010 global status report [Internet]. Paris: Renewable Energy Policy Network for the 21st Century; 2010 Sep. [cited 2011 May 27]. 40 p. Available from: http://www.ren21.net/Portals/97/documents/GSR/REN21_GSR_2010_full_revised%20Sept2010.pdf
- [7] Mayne LD, Yucel EM. Liquid fuels. In: International Energy Outlook 2010 [Internet]. Washington (DC): United States Energy Information Administration, Office of the Integrated Analysis and Forecasting; 2010 Jul. [cited 2011 May 27]. Report No. DOE/EIA-0484(2010). Sponsored by the United States Department of Energy. Available from: [www.eia.gov/oiaf/ieo/pdf/0484\(2010\).pdf](http://www.eia.gov/oiaf/ieo/pdf/0484(2010).pdf).
- [8] Radler M. Total reserves, production climb on mixed results. Oil Gas J. 2010; 108(46): 46-7.
- [9] Donnelly J. Price rise and new deep-water technology opened up offshore drilling. The Boston Globe [Internet]. 2005 Dec 11 [cited 2011 May 30]. Available from: http://www.boston.com/news/world/articles/2005/12/11/price_rise_and_new_deep_water_technology_opened_up_offshore_drilling/
- [10] Wheatcroft P. The next crisis: Prepare for peak oil. 2011 Feb 11 [cited 2011 May 30]. Available from: <http://online.wsj.com/article/SB10001424052748704140104575057260398292350.html>

- [11] Meyer RF, Attanasi ED. Heavy oil and natural bitumen--strategic petroleum resources [Internet]. Reston (VA): United States Geological Survey; 2003 Aug. [cited 2011 May 31]. Fact Sheet No. 70-03. Sponsored by the United States Department of the Interior. Available online: <http://pubs.usgs.gov/fs/fs070-03/fs070-03.html>
- [12] Sweeney D. The heavy oil issue [Internet]. Santa Barbara: Dan Sweeney. 2007 Mar - [cited 2011 May 31]. Available from: <http://www.alternatefuelsworld.com/heavyoil.html>
- [13] Government of Alberta, Energy [Internet]. Edmonton: Government of Alberta; [cited 2011 May 12]. Available from: <http://www.energy.alberta.ca/OilSands/791.asp>
- [14] Subramanian M, Hanson FV. Supercritical fluid extraction of bitumens from Utah oil sands. *Fuel Process Technol* 1998; 55: 35-53.
- [15] Ma Y, Li SY. Study of characteristics and kinetics of oil sand pyrolysis. *Energy Fuel* 2010; 24: 1844-7.
- [16] Li SY, Wang JQ, Tan HP, Wu ZL. Study of extraction and Pyrolysis of Chinese oil sands. *Fuel* 1995; 74: 1191-3.
- [17] Sonibare O, Egashira R, Adedosu TA. Thermo-oxidative reactions of Nigerian oil sand bitumen. *Thermochim Acta* 2003; 495: 195-205.
- [18] Khraisha YH. Study of extraction and pyrolysis of Jordan tar sand. *Int J Energy Res* 1999; 23: 833-9.
- [19] Burrowes A, Marsh R, Evans C, Teare M, Ramos S, Rahnama F, Kirsch M, Philp L, Stenson J, Yemane M, Van Horne J, Fong J, Sankey G, Harrison P. Alberta's Energy Reserves 2008 and Supply/Demand Outlook 2009-2018 [Internet]. Hill, C, Crowfoot C, MacGillivray J, Rahnama F, editors; Giles, D, Van Horne J, Ashrafi B, data; Stonkus O, Willett T, Hamza S, Tran B, Wagner J, Logan K, de Grace R, production; Sheremata D, communications advisor; Crowfoot C, coordinator. Calgary (AB): Energy Resources Conservation Board; 2009 Jun. [cited 2011 May 31] 220 p. Report No. ST98-2009. Available from: <http://www.ercb.ca/docs/products/STs/st98-2009.pdf>
- [20] Ding F, Ng SH, Xu C, Yui S. Reduction of light oil catalytic cracking of bitumen-derived crude HGOs through catalytic selection. *Fuel Process Technol* 2007; 88: 833-45.
- [21] Ng S, Zhu Y, Humphries A, Zheng L, Ding F, Gentzis T, et al. FCC study of Canadian oil-sands derived vacuum gas oils: 1. Feed and catalyst effects on yield structure. *Energy Fuels* 2002; 16: 1196-1208.
- [22] Dutta RP, McCaffrey WC, Gray M, Muehlenbachs, K. Use of ¹³C tracers to determine mass-transfer limitations on thermal cracking of thin films of bitumen. *Energy Fuels* 2001; 15: 1087-93.

- [23] Yufeng Y, Shuyuan L, Fuchen D, Hang Y. Change of asphaltene and resin properties after catalytic aquathermolysis. *Pet Sci* 2009; 6: 194-200.
- [24] Shen Z, Cao Z, Zhu X, Li X. Visbreaking of Chinese oilsands bitumen. *Pet Sci Technol* 2008; 26: 1676-83.
- [25] Ha HZ, Koppel P. Accurately predict viscosity of syncrude blends: An evaluation for mixing rules uncovers potential errors in fluid transportation of bitumen-based feeds. *Hydrocarb Process* 2008; 87: 87-92.
- [26] Liu J, Xu Z, Masliyah J. Role of fine clays in bitumen extraction from oil sands. *AIChE J* 2004; 50: 1917-27.
- [27] The Oil Sands Story [Internet]. The Oil Sands Discovery Centre – [cited 2011 Jun 14]. Available from:
http://www.oilsandsdiscovery.com/oil_sands_story/pdfs/oilsands.pdf
- [28] Masliyah J. Fundamentals of oilsands extraction (ChE 534 Course Materials). Edmonton (AB): University of Alberta; 2011.
- [29] Carrigy MA, Kramers JW, editors. Guide to the Athabasca Oil Sands Area. Alberta Geological Survey Information Series No. 65. Edmonton: Alberta Research Council; 1973.
- [30] Boon JA. Fluid-rock interactions during steam injections. In: Redord DA, Winestock AG, editors. The Oil Sands of Canada-Venezuela 1977. Proceedings of the Canada-Venezuela Oil Sands Symposium; 1977 May 30- Jun 4; Edmonton, Canada. Montreal: Canadian Institute of Mining and Metallurgy; 1977. p. 133-8.
- [31] Masliyah J, Zhou Z, Xu Z, Czarnecki J, Hamza H. Understanding water-based bitumen extraction from Athabasca oil sands. *Can J Chem Eng*; 2004: 82, 628-54.
- [32] Fair AE, Hill WA, Payne FR, Bruce B. Economic comparison of oil sands surface mining technologies. Oil Sands-Our Petroleum Future Conference; 1993 Apr 4-7; Edmonton, Canada.
- [33] Clark KA. Hot water separation of bitumen from Alberta bituminous sand. *Ind Eng Chem* 1932; 24: 1410-6.
- [34] Clark KA. Hot-water separation of Alberta bituminous sand. *Trans Can Inst Min Metall* 1944; 47: 257-74.
- [35] Clark KA. The hot water washing method for recovering of oil from the Alberta tar sands. *Can Oil Gas Ind* 1950; 3: 46-50.
- [36] Camp FW. The tar sands of Alberta, Canada. 3rd ed. Denver: Cameron Engineers Inc.; 1978.

- [37] Morgan G. An energy renaissance in oil sands development. *World Energy* 2001; 4: 46-53.
- [38] Butler RM. SAGD comes of age. *J Can Pet Tech* 1998; 37: 9-12.
- [39] Dharmeshkumar RG, Gates ID. Stability of the edge of a SAGD steam chamber in a bitumen reservoir. *Chem Eng Sci* 2011; 66: 1802–9.
- [40] Shah A, Fishwick R, Wood J, Leeke G, Rigby S, Greaves M. A review of novel techniques for heavy oil and bitumen extraction and upgrading. *Enrgy Environ Sci* 2010; 3: 700-714.
- [41] O'Rourke JC, Begley AG, Boyle HA, Yee CT, Chambers JI, Luhning RW. UTF project status update, May 1997. *J Can Pet Tech* 1999; 38: 44-53.
- [42] Gray MR. Hydrocarbon fluid properties & processing (ChE 522 Course Materials). Edmonton (AB): University of Alberta; 2008.
- [43] Gray MR. Upgrading petroleum residues and heavy oils. New York: Marcel Dekkar, Inc.; 1994.
- [44] Hatch LF. A chemical view of refining. *Hydrocarb Process* 1969; 48: 77-88.
- [45] Casalini A, Mascherpa A, Vecchi C. Modifications induced by visbreaking on composition and structure of atmospheric residues. *Fuel Sci Technol Inter* 1990; 8: 427-45.
- [46] Sawarkar AN, Pandit AB, Samant SD, Joshi JB. Petroleum Residue Upgrading Via Delayed Coking: A Review. *Can J Chem Eng* 2007; 85: 1-24.
- [47] Gray MR. Fundamentals of bitumen coking processes analogous to granulations: a critical review. *Can J Chem Eng* 2002; 80: 393-401.
- [48] Cartlidge CR, Dukhedin-Lalla L, Rahimi P, Shaw JM. Preliminary phase diagrams for ABVB+n-dodecane+hydrogen. *Fluid Phase Equilib* 1996; 117: 257-264.
- [49] Cheremisinoff NP. Pressure safety design practices for refinery and chemical operations. Westwood (NJ): Noyes Publications; 1998.
- [50] Chrones J, Germain RR. Bitumen and heavy oil upgrading in Canada. *Pet Sci Technol* 1989; 7: 783-821.
- [51] Mossop GD. Geology of the Athabasca oil sands. *Science* 1980; 207: 145-52.
- [52] National Energy Board (CA). Canada's oil sands-opportunities and challenges to 2015: an update [Internet]. Calgary (AB): National Energy Board (CA); 2006 [cited 2011 Jul 3]. 71 p, Available from: <http://www.neb.gc.ca/clf-nsi/mrgrnfmtn/nrgyrprt/lsnd/lsnd-eng.html>. Retrieved on 2007-08-14.

- [53] DECROOCQ D. Catalytic cracking of heavy petroleum fractions. Houston: Gulf Publishing Company; 1984.
- [54] Thomas CL. A history of early catalytic cracking research at Universal Oil Products Company. In: Davis BH, Hettinger WP, editors. Heterogeneous catalysis: selected American histories. ACS Symposium Series 222. Washington DC: American Chemical Society; 1982. p. 241-5.
- [55] Hettinger WP Jr. Contribution to catalytic cracking in the petroleum industry. *Appl Clay Sci* 1991; 5: 445-68.
- [56] Tonetto G, Atias J., de Lasa H. FCC Catalysts with different crystalline sizes: acidity, structural properties and reactivity. *Appl Catal A* 2004; 270: 9-25.
- [57] Weitkamp J. Zeolites and catalysis. *Solid State Ionics* 2000; 131: 175-88.
- [58] Schwochow F, Puppe L. Zeolites-their synthesis, structure, and applications. *Angew Chem Internat Edit* 1975; 14: 620-8.
- [59] Database of Zeolite Structures [Internet]. Zurich (CH): International Zeolite Association. C2008 - [cited 2011 Jul 10]. Available from: <http://www.iza-structure.org/databases>
- [60] Erdem E, Karapinar N, Donat R. The removal of heavy metal cations by natural zeolites. *J Colloid Interface Sci* 2004; 280: 309-14.
- [61] Raseev S. Thermal and catalytic processes in petroleum refining. New York: Marcel Dekkar, Inc.; 2003.
- [62] Ibrasheva RH, Zhubanov KA. Catalytic cracking of heavy oil fractions over natural zeolite contained composites. *Stud Surf Sci Catal* 2000; 130: 2447-52.
- [63] Mataeva ZT, Suleimenov MA, Ibrasheva RKh, Nakataev, ME, Nurgaliev ZhA. Effect of catalyst concentration on the oxidative cracking of the M-100 brand fuel-oil. *Khabarshysy Kazakstan Respublikasy Ul'tyik Gyl'm Akademiyasynyn* 2003; 47-53. Russian.
- [64] Jiang W, He M, Long J, Da Z, Tian H, Chen B, et al. Composite zeolites containing modified natural zeolites for cracking of heavy petroleum oils. Chinese Patent No. 1854253, 2006.
- [65] Chivadze GO, Naskidashvili TsI, Kvantaliani EK. Catalytic cracking of heavy petroleum fractions over modified natural zeolites. *Izvestiya Akademii Nauk Gruzinskoi SSR Seriya Khimicheskaya* 1990; 16: 186-9. Russian.
- [66] Sankey BM, Maa PS, Bearden R Jr, inventors; Exxon Research and Engineering Company, assignee. Conversion of the organic component from tar sands to lower boiling products. United States patent US 5795464. 1998 Aug 18.

- [67] Kuznicki SM, McCaffrey WC, Bian J, Wangen E, Koenig A, Lin CH. Natural zeolite bitumen cracking and upgrading. *Micropor Mesopor Mater* 2007; 105: 268–72.
- [68] Mier MV, Callejas RL, Gehr R, Cisneros BEJ, Alvarez PJJ. Heavy metal removal with Mexican clinoptilolite: multi-component ionic exchange. *Wat Res* 2001; 35: 373-8.
- [69] Inglezakis VJ, Grigoropoulou H. Effects of operating conditions on the removal of heavy metals by zeolite in fixed bed reactors. *J Haz Mat B* 2004; 112: 37-43.
- [70] Galli E, Gottardi G, Mayer H, Preisinger A, Passaglia E. The structure of potassium-exchanged heulandite at 293, 373 and 593 K. *Acta Crystallogr Sect B: Struct Sci* 1983; 39: 189-97.
- [71] Mondale KD, Carland RM, Aplan FE. The comparative ion exchange capacities of natural sedimentary and synthetic zeolites. *Miner Eng* 1995; 8: 535-48.
- [72] Dent LS, Smith JV. Crystal structure of chabazite, a molecular sieve, *Nature* 1958; 181: 1794-6.
- [73] Akgül M, Karabakan A, Acar O, Yürüm Y. Removal of silver (I) from aqueous solutions with clinoptilolite. *Micropor Mesopor Mater* 2006; 94: 99–104.
- [74] Hernández-Beltrán NA, Olguín MT. Elemental composition variability of clinoptilolite-rich tuff after the treatment with acid phosphate solutions. *Hydrometallurgy* 2007; 89: 374–8.
- [75] Semmens MJ, Martin WP. The influence of pretreatment on the capacity and selectivity of clinoptilolite for metal ions. *Wat Res* 1988; 22: 537-42.
- [76] Vlessidis AG, Triantafillidis CS, Evmiridis NP. Removal and recovery of p-phenyldiamenes developing compounds from photofinishing lab-washwater using clinoptilolite tuffs from Greece. *Wat Res* 2001; 35: 1603-8.
- [77] Blanchard G, Maunaye M, Martin G. Removal of heavy metals from waters by means of natural zeolites. *Wat Res* 1984; 18: 1501-7.
- [78] Kocaoba S, Orhan Y, Akyüz T. Kinetics and equilibrium studies of heavy metal ions removal by use of natural zeolite. *Desalination* 2007; 214: 1-10.
- [79] Junaid ASM, Street C, Wang W, Rahman MM, An W, McCaffrey WC, Kuznicki S.M. Integrated extraction and low severity upgrading of oilsands bitumen by activated natural zeolite catalysts. 2011. 30 p. Manuscript in submission as a journal article (JFUE-D-11-00663) with *Fuel* as of 17 May 2011, currently under review.

- [80] Junaid ASM, Rahman M, Yin H, McCaffrey WC, Kuznicki SM. Natural Zeolites for oilsands bitumen cracking: structure and acidity. *Micropor Mesopor Mater* 2011; 144: 148–57.
- [81] Junaid ASM, Yin H, Koenig A, Swenson P, Chowdhury J, Burland G et al. Natural zeolite catalyzed cracking-assisted light hydrocarbon extraction of bitumen from Athabasca oilsands. *Appl Catal A* 2009; 354: 44-9.
- [82] Junaid ASM, Rahman MM, Wang W, Street C, McCaffrey WC, Kuznicki SM. On the role of water in natural zeolite catalyzed cracking of oilsand bitumen: method and mechanism. 2011. 40 p. Unpublished manuscript currently in preparation for submission to *Energy Fuels* as a journal article; expected submission: October 2011.

Unique Features of Natural Zeolites for Oilsands Bitumen Cracking

2.1 INTRODUCTION

Zeolite catalyzed cracking reactions are carbocation-based [1] and therefore dependent on the surface acidity and the structure of the catalysts [2,3]. The selectivity and activity of these reactions depend on the amount of catalyst used, and on the strength and density of the acid sites dispersed over the catalyst surface. Acid strength is vital for breaking down the heavier molecules through cracking reactions. Strong acid sites are proton-donors which create carbocations, highly energetic species initiating cracking reactions, while a high site density increases the probability of catalytic reactions [4]. Surface acidity has been found to be somewhat dependent on the Si/Al ratio of the zeolite structures. Both theoretical calculations and experimental studies have demonstrated that increasing the Si/Al ratio increases acid strength at the expense of site density, which indicates that the maximum activity of a zeolite catalyst can be achieved by balancing these two [1,2]. In addition, high external surface area (attributed to both macropores and mesopores) allows increased accessibility of the acid sites to large hydrocarbon molecules. Therefore, accurate determination of the external surface area, micropore volume, Si/Al ratio, and, most importantly, strength and density of acid sites is critical for understanding

the cracking potential of zeolites [3], even though these factors may not always relate linearly to the effectiveness of cracking agents, particularly in the case of impure materials such as natural zeolites (NZ).

The surface area and porosity of the zeolites can be determined by standard BET measurement techniques [3,5], while their acid properties can be measured from desorption of basic probe molecules such as ammonia [1,3,5-9], alkylamines [10,11], pyridine [1,3,8,12,13], quinolone [12] and lutidine [12]. The acidity can be described in terms of concentration, strength, type and location of the acidic sites [2]. Although different types of acid sites vary in their strength and mechanism of cracking, their modes of acidity are not independent but rather interrelated [2]. Site distribution is also important because the strengths of different acid sites vary according to their location within the zeolite structure.

Multiple methods are available for the quantification of the acidic and basic properties of solids. Calorimetric or microcalorimetric measurements [14,15] provide heats of adsorption data but can be very cumbersome and have several inherent limitations for determining acid/base properties [1]. Frequently used surface science techniques like solid-state proton nuclear magnetic resonance ($^1\text{H-NMR}$) or infrared (IR) spectroscopy only provide semiquantitative results [2]. In addition, IR requires knowledge of extinction coefficient parameter values that are not readily available for the materials in question [1,2]. Other methods used less frequently, include carbon monoxide adsorption [16], NMR [17,18], potentiometric titration [19], and analysis of Argon adsorption [20]. With recent developments in computational approaches, the heats of adsorption of basic probe molecules on zeolite acid sites can be calculated by theoretical techniques such as density functional theory (DFT) [21,22]. However, application of these theoretical methods to the characterization of impure minerals such as NZs remains unrealistic.

Amine titration in presence of surface-adsorbed Hammett indicators is a proven technique that is currently widely employed to measure the acid properties of solids [23]. Originally developed by Johnson [24] and Benesi [25], the method is effectively employed to quantify both the site density and strength of solid acids [7,8]. The acid strength of a solid surface was defined by Hammett and Deyrup [26] as the ability of the surface to convert an adsorbed neutral base into its conjugate

acid. This is quantitatively expressed by Hammett and Deyrup's acidity function (H_0),

$$H_0 = pK_a + \log [B] / [BH^+] \quad (2-1)$$

where [B] and [BH⁺] are the concentrations of the neutral base and conjugate acid respectively and pK_a is pK_{BH⁺}. The strength of the solid acid sites can be determined from the pK_a values of the indicators, and the site density can be conveniently quantified from the amount of amine required to complete the titration.

Temperature-Programmed Desorption (TPD) is another simple and versatile method most frequently used to characterize the acidity of zeolites [1,2]. Quantification of species desorbed at specified temperatures provides information about the number, strength and heterogeneity of adsorption sites within the sample [27]. Ammonia TPD for example, can provide good estimates of the density [8,9] and strength [3] of the acid sites of NZs, although it does not distinguish between Brønsted and Lewis sites. The strength of adsorption of basic molecules on acid sites is correlated to the desorption temperature, which can be determined by single or multi-point calculations using desorption peak temperatures. However, a single point calculation is performed using the Redhead Equation (Equation 2-2), that uses an estimation of the pre-exponential factor of desorption (A) which may lead to inaccurate results [1,28].

$$E_d = RT_{max}[\ln(AT_{max}/\beta)-3.64] \quad (2-2)$$

Here, R is the gas constant, T_{max} is the peak temperature, and β is the heating rate. Multi-point methods use the linear form of the Polyani–Wigner equation, thereby eliminating the need for estimated parameters. With the carrier gas flow rate [29] or the heating rate [3,30] as the variable parameter, it may be possible to calculate heats of adsorption that are in agreement with reported experimental results. This method assumes a local equilibrium between the gas phase and the zeolite. In this study, the linear form of Polyani–Wigner equation is used to estimate heats of adsorption for first order desorption of ammonia by multi-point calculations:

$$\ln T_{\max}^2 / \beta = E_d / RT_{\max} + \ln E_d / AR \quad (2-3)$$

This chapter compares the acid properties of natural zeolites to those of commercial ZY and considers their potential to function as cracking agents for oilsands bitumen. Acid–base titration and ammonia TPD characterization results are used to complement acid strength measurements, providing insights into the structure and composition of the minerals.

2.2 MATERIALS AND METHODS

2.2.1 Catalyst preparation

Zeolite Y (ZY) was obtained as ammonium-exchanged Fluidized Catalytic Cracking (FCC) agent in the form of microspheres from Engelhard Corporation (currently a part of BASF). Two clinoptilolite samples (SC and A) were obtained from the Saint Clouds deposit in New Mexico (USA), and the Werris Creek deposit in New South Wales, Australia respectively. Raw sedimentary chabazite from the Bowie deposit was obtained from the GSA Resources of Tucson, Arizona. All these samples were finely ground to <74 μm particles and, with the exception of ZY, were ammonium-exchanged in slightly molar excess in a mildly acidic environment for 6–8 h. The raw calcium chabazite (CC) sample was also used to produce a highly exchanged variant using more than double molar quantity of ammonium ions. The sodium chabazite (NC) was exchanged two times with ammonium ions in more than double molar excess to stoichiometric quantity for each exchange. Samples were then calcined at 450 $^{\circ}\text{C}$ under nitrogen flow to convert the NH_4^+ -exchanged form of zeolites to the acid (H^+)-form for catalytic cracking reactions.

2.2.2 Catalyst characterization

X-ray diffraction (XRD) patterns of the raw catalyst samples were recorded at the Department of Earth and Atmospheric Sciences XRD facility at the University of Alberta using a Rigaku Geigerflex 2173 diffractometer with a CoK_α radiation source ($\lambda=1.79021 \text{ \AA}$). The patterns were acquired under air at room temperature for a 2θ range of 2–120 $^{\circ}$ with a scan speed of 0.033 $^{\circ} \text{ s}^{-1}$. The data were then corrected for background and converted to CuK_α radiation ($\lambda=1.54059 \text{ \AA}$) values using XRD

pattern processing software Materials Data Jade version 7.5, and matched with JCPDS data base Powder Diffraction Files (PDFs).

Scanning Electron Microscopy (SEM) images of the catalyst samples were captured under ultrahigh vacuum using Auger microprobe JAMP-9500F spectrometer from JEOL equipped with a Schottky field emission source that produces an electron probe with a diameter of about 3–8 nm at the sample. The accelerating voltage and emission current used for SEM imaging were 15 kV and 6 nA. The samples were kept at a working distance of 19.8–22.4 mm, and were tilted at an angle of 30° from the primary electron beam to face the electron energy analyzer. The analyses were conducted at the Alberta Centre for Surface Engineering and Sciences.

The catalyst surface areas were calculated from nitrogen adsorption isotherm data obtained at liquid nitrogen temperature with an Omnisorp 360 Analyzer, using 0.08–0.13 g of catalyst samples. The samples were outgassed at 350 °C for 4 h in vacuum before each adsorption measurement. Nitrogen was added to and withdrawn from the samples at a rate of 0.022 mmol min⁻¹ during adsorption and desorption processes. The linearized Brunauer, Emmett and Teller (BET) method was used to calculate the total specific surface area of the catalysts using adsorption data within P/P₀ range varying between 0.01 and 0.25, depending on linearity of the data. Macro and mesopore surface area and micropore volume were determined from *t*-plots. Pore Size Distributions (PSDs) and combined meso and macropore volume were obtained from the desorption branch of the N₂ physisorption isotherm with the Barrett–Joyner–Halenda (BJH) method. The analyses were conducted at a Department of Chemical and Materials Engineering BET facility at the University of Alberta.

2.2.3 Si to Al ratio measurement

The atomic compositions of Si and Al in the samples were determined by Energy Dispersive X-ray (EDX) analysis using a PGT (Princeton Gamma-Tech) PRISM IG (Intrinsic Germanium) detector attached to a Hitachi S-2700 Scanning Electron Microscope equipped with a PGT IMIX digital imaging system. The accelerating voltage and probe used for the analysis were 20 kV and 2.8 nA. The experiments were conducted at the EDX facility of the Department of Earth and Atmospheric Sciences at the University of Alberta.

Bulk phase Si and Al contents were determined by Inductively Coupled Argon Plasma-Atomic Emission Spectrometry (ICP-AES) at Exova Laboratory, Edmonton. Each sample, fused with lithium metaborate and lithium tetraborate at 1050 °C, was dissolved in a 1.5% HCl/8.5% HNO₃ solution prior to analysis.

2.2.4 Measurement of strength and density of acid sites

For strength and density measurement of acid sites using Hammett indicators, the catalysts were prepared by calcination in ceramic crucibles in a tube furnace at ~500 °C under helium flow for 2 h. The samples were then allowed to cool to 200 °C under the flow, and transferred immediately to dried screw capped vials and stored in vacuum desiccators. A set of Hammett indicators (pK_a = +6.8 to -8.2; Table 2-1) were selected and used to prepare a 0.1% solution of each in anhydrous benzene. Color tests were carried out using 0.1 g of dried catalysts, each in a screw capped vial, adding 3 mL of anhydrous benzene followed by three drops of 0.1% solution of a single Hammett indicator. The resulting suspension was then sonicated for 1h; during this time period the suspension was identified as acid or basic to a particular indicator. The process was repeated for all the selected indicators. The Hammett and Deyrup's acidity function (H₀) was determined to lie between the pK_a values of the indicator that demonstrate a shift from acidic to basic color.

Table 2-1: Basic indicators (Hammett indicators) used for measurement of strength of acid sites in catalyst samples.

Indicator	Base form color	Acid form color	pK _a value
Neutral Red (2-Methyl-3-amino-6-dimethylaminophenazine)	Yellow	Red	+6.8
Methyl Red (2-4-Dimethylamino-phenylazobenzoic acid)	Yellow	Red	+4.8
4-Phenylazo-1-naphthylamine	Yellow	Red	+4.0
p-Dimethylaminoazobenzene (Dimethyl yellow)	Yellow	Red	+3.3
o-Aminoazotoluene	Yellow	Red	+2.2
Crystal violet	Blue	Yellow	+0.8
Dicinnamalacetone	Yellow	Red	-3.0
1,3-diphenyl-2-propenone (Benzalacetophenone or Chalcone)	Colorless	Yellow	-5.6
Anthraquinone	Colorless	Yellow	-8.2

The acid site densities of the catalysts were determined by acid-base titration using a 0.05 M n-butylamine solution in anhydrous benzene and Crystal Violet

indicator. Three drops of the indicator were added to the catalyst samples (0.1 g each), followed by a 0.05 M n-butylamine solution in successive increments of 5-10 μL , until titration was complete. The resulting mixtures were shaken vigorously using a bench top shaker for at least 4 h until the end point (the point at which only a few particles display the acid color of the indicator) was detected [31].

Acidity measurements by ammonia TPD were done using Autochem II Micromeritics Chemisorption Analyzer. Samples (0.1-0.2 g) were placed in a U-shaped quartz tube reactor and preheated for 1 h at 700 $^{\circ}\text{C}$ for degasification to remove residual water and other species prior to each measurement. The samples were then cooled and saturated with ammonia using flow ($30\text{ cm}^3\text{ min}^{-1}$) of NH_3/He gas mixture (15% ammonia, 85% helium) for a few minutes at room temperature. The system was then purged with helium flow ($30\text{ cm}^3\text{ min}^{-1}$) to remove physically adsorbed ammonia. Desorption of ammonia was measured for a particular ramp rate up to 700 $^{\circ}\text{C}$ and the TPD spectra were recorded. After each desorption, samples were cooled, re-saturated with ammonia, purged with helium, and subsequently analyzed at another ramp rate. The process was completed for a total of five different ramp rates (5, 10, 15, 20 and 30 $^{\circ}\text{C min}^{-1}$).

The acid site density was measured by ammonia TPD, calibrating the thermal conductivity detector (TCD) for the analysis gas (15% ammonia, 85% helium). The TCD signals for individual analysis were converted to active gas (ammonia) volume data at STP. Assuming a one to one stoichiometry for ammonia adsorption, the volume data were converted to site density w.r.t. equivalent weight.

2.3 RESULTS

2.3.1 Catalyst characterization

The main phase present in ZY is faujasite, while all the NZ samples contain clinoptilolite phases, respectively. In addition, the clinoptilolite samples SC and A contain quartz and silica phases respectively. Figure 2-1 shows the powder diffraction patterns of the samples and Table 2-2 enlists the Bragg angles, corresponding d-spacings and identified phases. While clinoptilolite phases in SC are mostly in Na-form, A has a phase in K-form. Both chabazite samples (CC and NC) have chabazite phases in Ca- and Na-form.

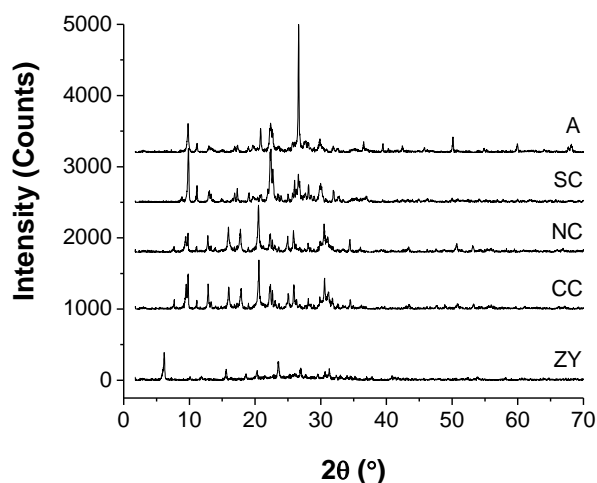


Figure 2-1: X-Ray powder diffraction pattern of the zeolite samples: commercial zeolite Y (ZY); raw sedimentary calcium chabazite (CC); sodium chabazite (NC); and raw clinoptilolites from Saint Cloud (SC) and Australia (A).

Table 2-2: Phase identification of zeolites: commercial zeolite Y (ZY); raw sedimentary calcium chabazite (CC); sodium chabazite (NC); and raw clinoptilolite from Saint Cloud (SC) and Australia (A).

Sample	2θ (°)	d (Å)	Reference data			
			2θ (°)	d (Å)	Material	PDF
ZY	6.16	14.33	6.18	14.30	Synthetic Na-Faujasite	00-038-0239
	20.32	4.368	20.36	4.36	Na-Al-Silicate Hydrate	00-043-0168
	23.52	3.78	23.58	3.77	Synthetic Na-Faujasite	00-038-0239
	30.67	2.91	30.81	2.90	Synthetic Na-Faujasite	00-038-0239
	31.29	2.86	31.36	2.85	Synthetic Na-Faujasite	00-038-0239
CC and NC	9.52	9.29	9.46	9.34	Chabazite Ca	00-034-0137
	9.81	9.01	9.87	8.95	Clinoptilolite Na	00-047-1870
	20.58	4.31	20.54	4.32	Chabazite Na	00-019-1178
	22.35	3.97	22.36	3.97	Clinoptilolite	01-070-1859
	25.04	3.55	25.05	3.55	Clinoptilolite K	01-089-7539
	25.91	3.44	25.83	3.45	Chabazite Ca	00-034-0137
	30.59	2.92	30.52	2.93	Chabazite Ca	00-034-0137
34.49	2.60	34.39	2.61	Chabazite Ca and Na	00-034-0137 and 00-019-1178	
SC	9.86	8.97	9.87	8.95	Clinoptilolite Na	00-047-1870
	22.41	3.96	22.42	3.96	Clinoptilolite Na	00-047-1870
	22.71	3.91	22.71	3.91	Clinoptilolite	01-070-1859
	26.59	3.35	26.62	3.35	Silica	01-077-1060
	30.03	2.97	30.04	2.97	Clinoptilolite Na	00-047-1870
A	9.80	9.02	9.86	8.96	Clinoptilolite K	01-089-7539
	20.84	4.26	20.86	4.25	Quartz	01-075-0443
	22.37	3.97	22.36	3.97	Clinoptilolite	01-070-1859
	22.71	3.91	22.71	3.91	Clinoptilolite	01-070-1859
	26.63	3.34	26.64	3.34	Quartz	01-075-0443
	50.14	1.82	50.14	1.82	Quartz	01-075-0443
59.94	1.54	59.97	1.54	Quartz	01-075-0443	

The SEM images show that in sharp contrast to ZY, the NZ samples have platy morphologies composed of layers of crystals (Figure 2-2).

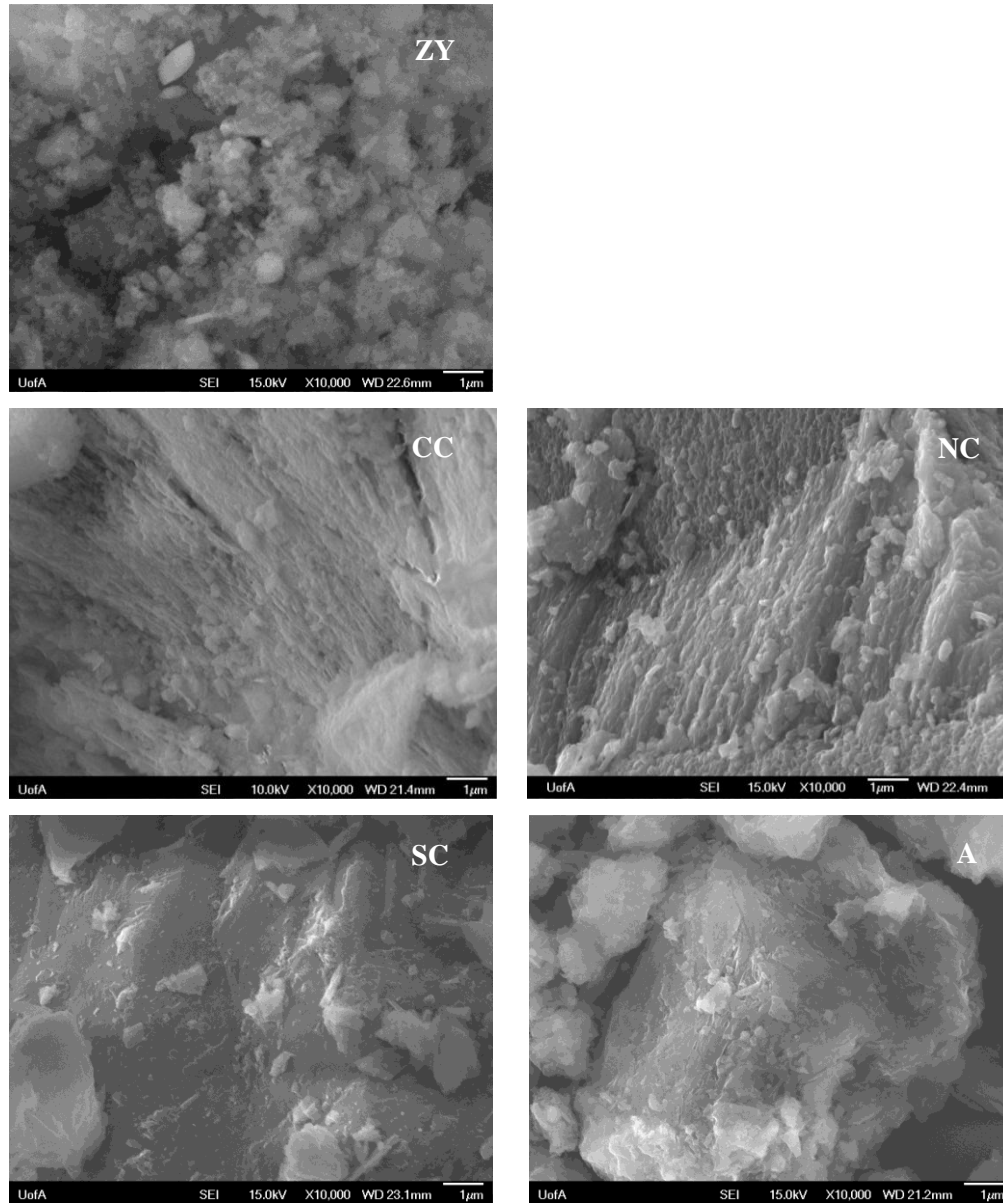


Figure 2-2: Scanning electron microscopy images of the zeolite samples: commercial zeolite Y (ZY); raw sedimentary calcium chabazite (CC); sodium chabazite (NC); and raw clinoptilolite from Saint Cloud (SC) and Australia (A).

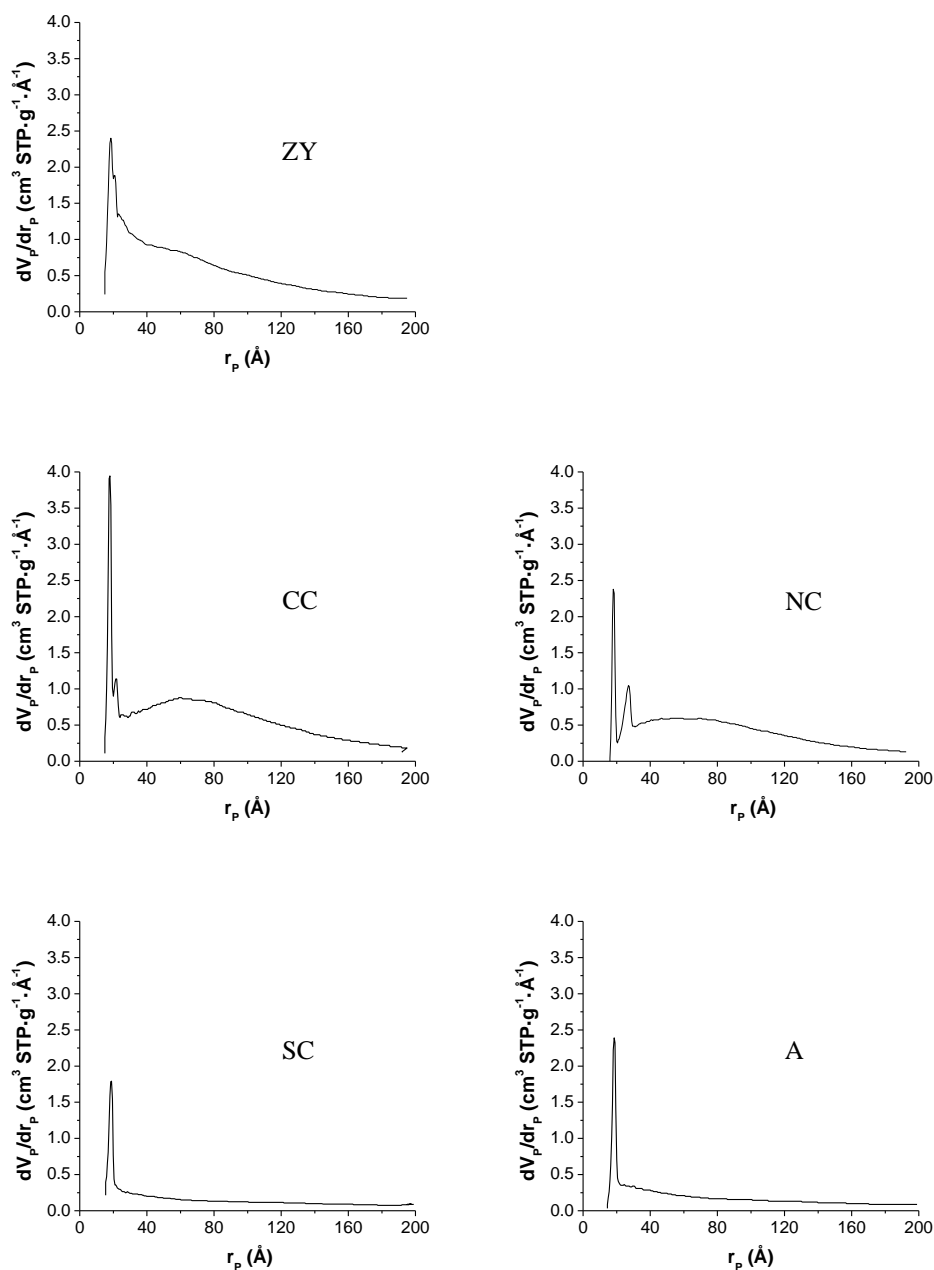
Surface area analysis reveal that macro and mesopores comprise 40-50% of the total surface area of the clinoptilolite, 29% of the total surface area of the ZY, and only 12-14% of the total surface area of the chabazite. (Table 2-3).

Table 2-3: Surface area and porous structure of the zeolite samples: commercial zeolite Y (ZY); raw sedimentary calcium chabazite (CC); sodium chabazite (NC); and raw clinoptilolite from Saint Cloud (SC) and Australia (A).

Sample	BET Surface Area (m ² g ⁻¹)	Meso & Macropore Surface Area (m ² g ⁻¹)	Micropore Surface Area (m ² g ⁻¹)	Micropore Volume (cm ³ g ⁻¹)	Approximate Average Micropore Diameter (Å)	Meso & Macropore Volume (cm ³ g ⁻¹)
ZY	268	78	190	0.0777	16.4	0.1667
CC	437	59	378	0.1472	15.6	0.1461
NC	417	48	369	0.1455	15.8	0.1154
SC	101	40	61	0.0305	20.0	0.0575
A	99	44	55	0.0268	19.6	0.0504

* The relative standard deviations for the BET surface area and pore volume analyses, based on 50 measurements performed on a standard alumina sample, are: 2.71% and 3.98%, respectively.

PSD analysis shows that the clinoptilolites have a uniform pore size distribution compared to ZY and the chabazites (Figure 2-3). Pore size refers to the diameter (d_p) as pores are assumed to be cylindrical. According to the PSD plots, the diameter of pores in clinoptilolites ranges between 36 and 39 Å, very close to the pore size of ZY (37 Å). However, PSD suggests that ZY also contains a large number of mesopores ($20 < d_p < 500$ Å) [32] ranging from 60-240 Å. (Figure 2-3). The chabazite samples also appear to have a wide distribution of mesopores, with the majority of the pores distributed around 36 Å (for CC and NC), 54 and 118 Å (NC) and 44 and 120 Å (CC). A sharp drop in distribution is observed for all the samples at approximately 36 Å. This suggests that the peaks at this pore size might be artifacts of the tensile strength effect caused by the presence of large fractions of micropores [33,34]. Micropore size distribution using the BJH method cannot be determined accurately as the Kelvin equation becomes invalid when pore sizes approach a few molecular diameters [33,34]. Therefore the average micropore size of the samples was approximated from the micropore volume of the samples (Table 2-3). These results show that the ZY and the chabazite samples have an average micropore size of ~16 Å compared to ~20 Å for clinoptilolite samples.



* The relative standard deviation for average pore size distribution analysis, based on 50 measurements performed on a standard alumina sample, is 3.98%.

Figure 2-3: Pore size distribution of the zeolite samples determined by BJH method: commercial zeolite Y (ZY); raw sedimentary calcium chabazite (CC); sodium chabazite (NC); and raw clinoptilolite from Saint Cloud (SC) and Australia (A).

2.3.2 Si to Al ratio measurement

EDX analysis shows that ZY has the lowest Si/Al ratio (2.41) of all samples ($\text{SiO}_2/\text{Al}_2\text{O}_3$ ratio: ~ 4.82). Among the NZs, the clinoptilolite samples have the highest Si/Al ratio of ~ 5.08 ($\text{SiO}_2/\text{Al}_2\text{O}_3$ ratio: ~ 10.16) (Table 2-4). ICP-AES analysis reconfirms the same order of the Si/Al ratio for the bulk phase of the samples, with values typically lower than those from the EDX analysis.

Table 2-4: Si/Al ratio of zeolite samples by EDX and ICP analysis: commercial zeolite Y (ZY); sedimentary calcium chabazite (CC); sodium chabazite (NC); and clinoptilolite from Saint Cloud (SC) and Australia (A).

Sample	Si/Al Ratio	
	EDX	ICP-AES
ZY	2.41	1.69
CC	3.55	2.65
NC	3.68	2.63
SC	4.98	3.44
A	5.08	3.85

2.3.3 Strength and density of acid sites

The pK_a values for the zeolites, determined from color tests using Hammett indicators, fall between the Hammett and Deyrup's acidity function values of -3.0 and -5.6 (Table 2-5). The catalyst-indicator mixtures in anhydrous benzene shift from acidic to basic color when the indicator is dicinnamalacetone ($\text{pK}_a = -3.0$), but remain unchanged with indicators of lower pK_a values.

Acid base titration using Hammett indicators shows that among the zeolite samples used in this study the raw untreated CC inherently possesses the highest density of acid sites (0.65 meq g^{-1}), while the raw SC has the lowest (0.05 meq g^{-1}) (Table 2-5). The order of site density is as follows:

Raw CC > Double exchanged NC > Ammonium-exchanged CCs \geq Commercial ZY > Ammonium-exchanged clinoptilolites (A and SC) \geq Raw SC.

Table 2-5: Strength and site density of the raw and acidified samples determined by acid-base titration: commercial zeolite Y (ZY); calcium chabazite (CC); sodium chabazite (NC); and clinoptilolite from Saint Cloud (SC) and Australia (A).

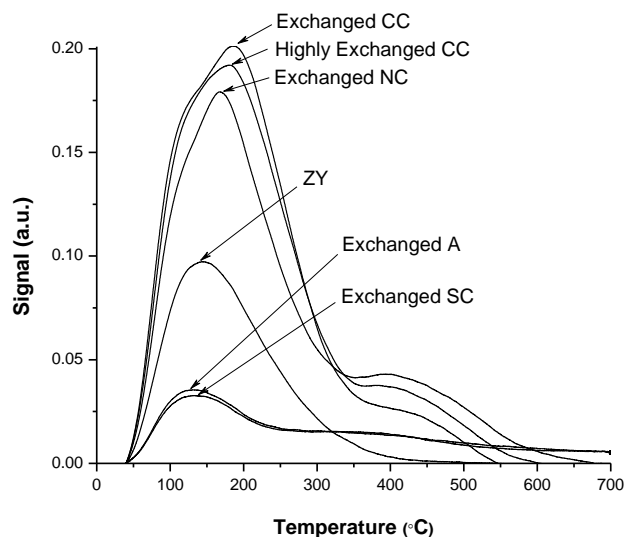
Sample	Hammett and Deyrup's acidity function (H_0)	Acid site density (meq g^{-1})
ZY	$-3.0 \leq H_0 \leq -5.6$	0.21
Exchanged CC	$-3.0 \leq H_0 \leq -5.6$	0.25
Highly exchanged CC	$-3.0 \leq H_0 \leq -5.6$	0.20
Double exchanged NC	$-3.0 \leq H_0 \leq -5.6$	0.35
Exchanged SC	$-3.0 \leq H_0 \leq -5.6$	0.06
Exchanged A	$-3.0 \leq H_0 \leq -5.6$	0.05
Raw CC	$-3.0 \leq H_0 \leq -5.6$	0.65
Raw SC	$-3.0 \leq H_0 \leq -5.6$	0.05

* The standard deviations of the site density of the samples based on multiple measurements performed on a single sample is 3.1%.

The TPD curves at different heating rates show that in every case the ammonia-exchanged NZs have at least one desorption peak appearing at a higher temperature than the corresponding peak for ZY. For example, at a heating rate of $15 \text{ }^\circ\text{C min}^{-1}$ the dominant desorption peaks for the exchanged and highly exchanged CCs appear at $186.2 \text{ }^\circ\text{C}$ and $179.4 \text{ }^\circ\text{C}$ respectively, while the only desorption peak for ZY appears at approximately at $143.8 \text{ }^\circ\text{C}$ (Figure 2-4). The analogous peak for ammonium-exchanged NC also appears at a higher temperature than ZY at $168.7 \text{ }^\circ\text{C}$. The ammonium-exchanged SC and A appear to be exceptions, as their dominant desorption peaks appear at temperatures lower than for ZY. However, just as the other ammonium-exchanged NZ they have multiple desorption peaks, with at least one peak appearing between $300\text{-}400 \text{ }^\circ\text{C}$, a considerably higher temperature range than the only peak temperature for ZY. The desorption peaks for raw NZ samples (CC and SC) also appear at higher temperatures than the peak temperature for ZY, at 178.8 and $144.2 \text{ }^\circ\text{C}$ respectively (Figure 2-5).

The heats of adsorption of ammonia on the dominant sites of the catalysts, calculated from the composite plots using Equation 2-3, are generally higher for NZs than for ZY (Table 2-6). Three representative composite plots are shown in Figure 2-6, while the heats of adsorption for the samples are calculated from Figure 2-7 constructed from individual TPD peaks for different ramp rates. The order of the heats of adsorption is as follows:

Ammonium-exchanged CCs > Raw CC > Double exchanged NC > Raw SC ≥ Commercial ZY > Ammonium-exchanged clinoptilolites (A and SC).



* The standard deviation of the peak temperature in ammonia TPD, based on multiple measurements performed on a single sample, is 4.1%.

Figure 2-4: Ammonia TPD curves of the ammonium-exchanged zeolites conducted at a ramp rate of 15 °C min⁻¹: commercial zeolite Y (ZY); calcium chabazite (CC); sodium chabazite (NC); and clinoptilolite from Saint Cloud (SC) and Australia (A).

Assuming a one to one stoichiometry for adsorption, the ammonia TPD measurements show that the NZ samples have much higher overall concentration of acid sites per unit weight compared to ZY (Table 2-6). The acid site density in the raw CC sample is 3.66 meq g⁻¹, more than fifteen times higher than that of ZY (0.23 meq g⁻¹) and the highest among all the samples tested. In fact, the acid site density of ZY is the lowest as shown below:

Raw CC > Ammonium-exchanged CCs ≥ Double exchanged NC > Ammonium-exchanged clinoptilolites (A and SC) > Raw SC ≥ Commercial ZY.

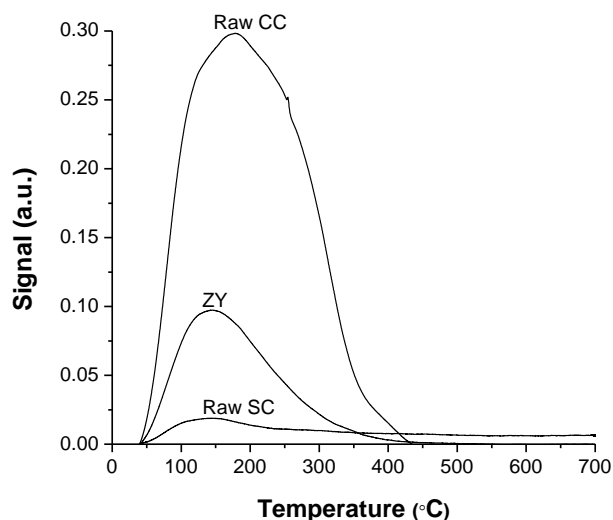


Figure 2-5: Ammonia TPD curves at a ramp rate of $15\text{ }^{\circ}\text{C min}^{-1}$ for raw sedimentary calcium chabazite (CC); and raw clinoptilolite from Saint Cloud (SC), compared to commercial zeolite Y (ZY).

Table 2-6: Heat of adsorption of the dominant acid sites, and overall site density measured by ammonia TPD for: commercial zeolite Y (ZY); calcium chabazite (CC); sodium chabazite (NC); and clinoptilolites from Saint Cloud (SC) and Australia (A).

Sample	Heat of adsorption of dominant sites (kJ mol^{-1})	Overall site density (meq g^{-1})
ZY	50.4	0.23
Exchanged CC	60.2	2.44
Highly exchanged CC	59.6	2.56
Double exchanged NC	55.3	2.45
Exchanged SC	46.6	0.53
Exchanged A	46.1	0.50
Raw CC	56.4	3.66
Raw SC	51.2	0.27

* The standard deviation of the site density of the samples based on multiple measurements performed on a single sample is 7.2%.

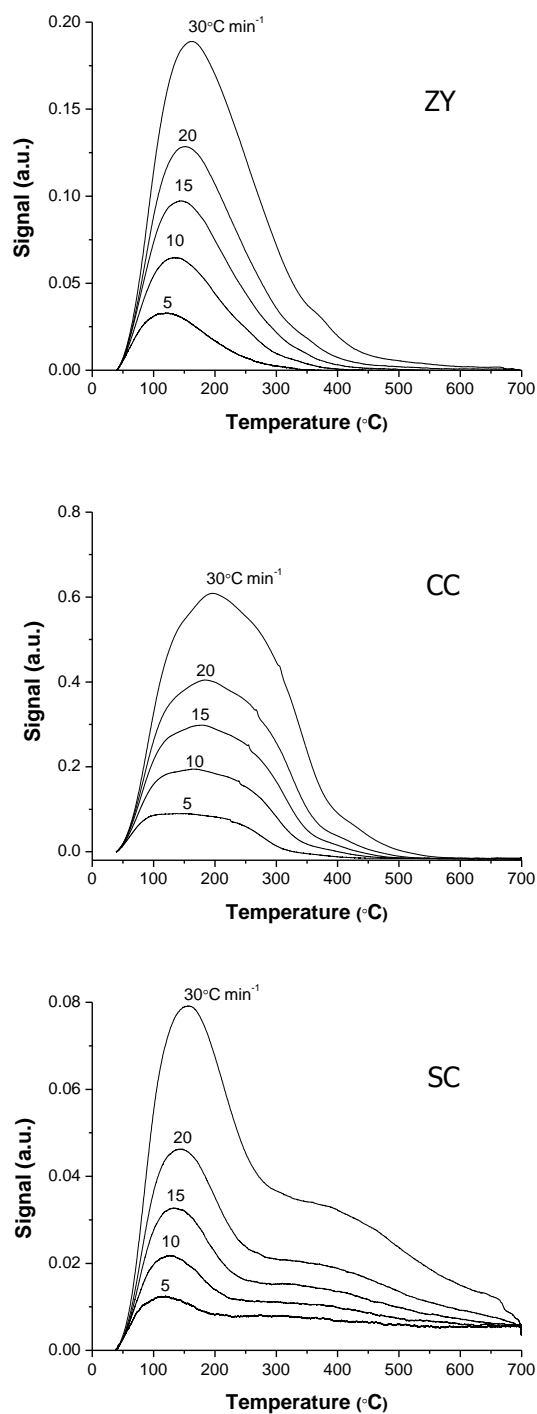


Figure 2-6: Representative composite ammonia TPD curves of the samples: commercial zeolite Y (ZY); raw sedimentary calcium chabazite (CC); and ammonium-exchanged clinoptilolite from Saint Cloud (SC).

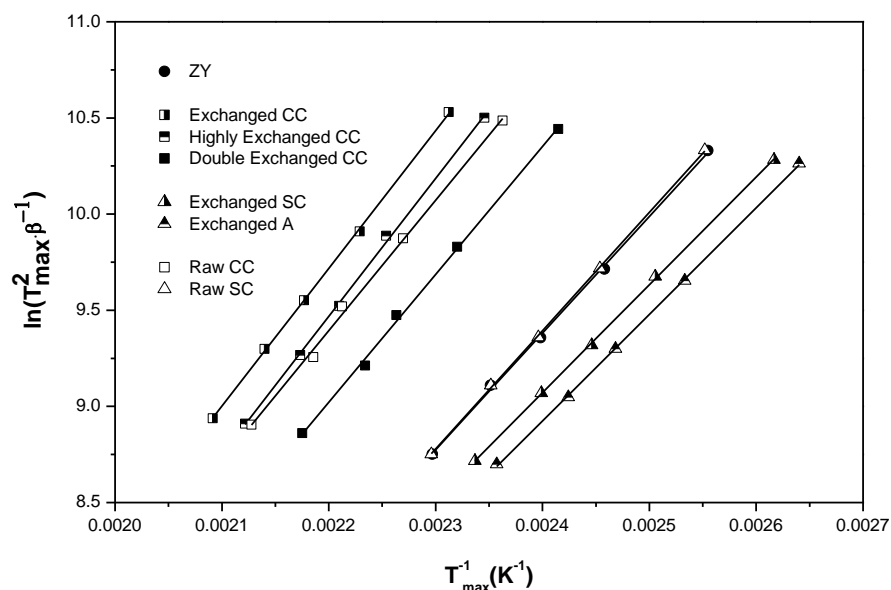


Figure 2-7: Heat of adsorption estimation for the dominant sites using Polyani-Wigner equation for commercial zeolite Y (ZY); raw sedimentary and ammonium-exchanged calcium chabazite (CC); ammonium-exchanged sodium chabazite (NC); and raw clinoptilolite from Saint Cloud (SC) and Australia (A).

2.4 DISCUSSION

2.4.1 Catalyst characterization

According to the XRD patterns, the NZ samples, composed mostly of clinoptilolite and/or chabazite phases, are more crystalline than the commercial ZY. The sedimentary chabazite samples (CC and NC) contain clinoptilolite impurities, whereas the quartz and silica phases present in the clinoptilolite samples (SC and A) are typical for any raw silica-alumina mineral. The fact that faujasite is the dominant phase in the ZY sample is in agreement with the literature [35].

SEM, BET surface area and pore size analysis demonstrate that the morphology and structure of the NZs are amenable to reactions involving large molecules present in bitumen. The SEM images (Figure 2-2) show that the NZs have platy morphology as opposed to ZY, and are able to accommodate large molecules on the surface easily. BET surface area analysis shows that the clinoptilolite samples

(SC and A), in particular, have a much larger fraction of the total surface area (40-50%) available as external surface (meso and macropore), compared to the other zeolite samples (Table 2-3). However, the meso and macropore surface area in ZY ($78 \text{ m}^2 \text{ g}^{-1}$), although only 29% of the total surface area, is still higher than for the clinoptilolites ($40\text{-}44 \text{ m}^2 \text{ g}^{-1}$) and is comparable to the chabazite samples ($48\text{-}59 \text{ m}^2 \text{ g}^{-1}$). Higher external surface area indicates accessibility of large organic molecules of oilsands bitumen such as asphaltenes to the acid sites within the samples. The cracking of these molecules is expected to take place on the external surface of the catalyst rather than the inaccessible surface of the micropores (diameter $>2 \text{ nm}$). However, once large molecules have been reduced in size by the initial cracking it is possible that a secondary cracking inside the micropores can occur. The average micropore size, approximated from the micropore volume of the samples, show that the ZY and the chabazite samples have an average micropore size of $\sim 16 \text{ \AA}$ compared to $\sim 20 \text{ \AA}$ for the clinoptilolite samples. The diameter of asphaltene molecules in bitumen has been reported to range between $12\text{-}24 \text{ \AA}$ by fluorescence correlation spectroscopy [36]; $7\text{-}9 \text{ nm}$ by freeze fracture-transmission electron microscopy [37]; and $1.26\text{-}3.6 \text{ nm}$ by small angle neutron scattering [38]. This reinforces the idea that following the preliminary cracking on the external surface the reduced fragments are able to undergo a secondary cracking within the micropores. PSD results, however, indicate the presence of some mesopores in chabazite and ZY samples that are accessible to large molecules (Figure 2-3).

To summarize, the NZ samples have favorable morphology and substantial fractions of external surface available for cracking of large molecules in bitumen. The large micropore surface in these samples can participate in secondary cracking of products.

2.4.2 Si to Al ratio measurement

EDX analysis results show that the NZs in general have stronger acid sites compared to the commercial ZY. Higher Si/Al ratio is an indicator of stronger acid sites. The reported Si/Al values (Table 2-4) are in good agreement with the ones reported in the literature ($4.25\text{-}5.25$ for clinoptilolite, $1.6\text{-}3.0$ for chabazite, and $>1.5\text{-}3.0$ for zeolite Y) [35] with the exception of chabazite (~ 3.6). The value is higher due to the presence of clinoptilolite phases in the chabazite samples. Si/Al ratios

determined by ICP-AES analysis demonstrate the same order of values in the bulk phase of the samples. The values, however, are lower compared to those determined by EDX analysis. This discrepancy is due to the semi-bulk, semi-surface sensitive nature of EDX analysis compared to direct bulk measurement by ICP-AES. In fact, the difference in Si/Al values by EDX and ICP-AES measurements indicate that Si/Al distribution in the samples is not uniform. Stronger acid sites, the presence of which is indicated by higher Si/Al values, are located on or in the proximity of the surface rather than in the bulk phase. It is also possible that a substantial amount of non-framework Al is present in the bulk phase of these samples. The difference in EDX and ICP-AES values are more noticeable in the NZ samples compared to ZY, which could indicate larger distribution of the stronger acid sites near the surface accessible to large molecules.

2.4.3 Strength and density of acid sites

Results of color tests and TPD measurements indicate that the NZs in general have stronger acid sites compared to ZY, while the strengths of the sites in every sample, including ZY, are of comparable magnitude. Color test using Hammett indicators show that the strength of the acid sites of every sample falls between the Hammett and Deyrup's acidity function values of -3.0 and -5.6 (Table 2-5). Ammonia TPD provided a more detailed analysis of their comparative acid strength. The desorption curves at different heating rates show that in every case the ammonia-exchanged NZs have at least one desorption peak appearing at a higher temperature than the corresponding peak for ZY. In general, the higher the temperature corresponding to a TPD peak the stronger the bond between the adsorbed species and the catalytic site, which in the case of a basic probe molecule such as ammonia, is a measure of the acidity of the site. Every ammonium-exchanged NZ sample have multiple desorption peaks, which indicate the presence of multiple types of chemisorption sites. However, due to an overlap of the peaks it is not always possible to determine the specific peak temperatures accurately and reliably. Methods such as deconvolution of peaks may lead to unique results that may not reflect the true desorption features of the samples. Interestingly, the two untreated raw NZ samples possess either equally (SC) or slightly stronger (CC) acidic sites than the commercial ZY. Unlike their ammonium-exchanged analogues, the raw samples have only one distinct type of chemisorption site.

The heats of adsorption of ammonia on the dominant sites of the zeolites reconfirm that NZs in general have stronger acid sites than ZY (Table 2-6). The values of the heat of adsorption also indicate that the acid strengths of the dominant sites in the zeolite samples used in the study are comparable, which supports the conclusion from the color tests. The order of acid strength, presented in terms of heats of adsorption, is consistent with the order of the TPD peak temperatures for the dominant sites.

The composite ammonia TPD plots for individual catalysts (Figure 2-6) show first order desorption kinetics for both ZY and the raw and exchanged NZ samples. The dominant TPD peaks for individual catalysts are asymmetric around the peak temperature, which is the characteristic trend for first order desorption [39,40]. This also implies that the TPD peak temperature is independent of the initial coverage [39,40] of ammonia. As expected, the TPD peaks for every sample shifted to lower values [39] as heating rates decreased, while maintained the same order of acid strength at each rate.

Acid-base titration and ammonia TPD measurements show that the NZ samples in general have higher numbers of acid sites per unit weight compared to commercial ZY. While the acid-base titration results show that the chabazites, both the exchanged and the raw forms, have equal or higher concentration of acid sites than ZY (Table 2-5), the TPD measurements show higher overall concentration for all NZ samples compared to ZY (Table 2-6). The order of acid site density determined by ammonia TPD measurements is generally consistent with the order determined by the acid-base titration with the notable exception of the positions of ZY and the clinoptilolite samples. It should also be noted that the site density of ZY measured by both these methods is essentially the same (Tables 2-5 and 2-6). This indicates that the acid sites in the ZY sample are mostly located on the external surface, equally available to small molecules such as ammonia and large molecules such as n-butylamine and the Hammett indicators. On the other hand, the acid site densities of the clinoptilolites are much higher when ammonia, a smaller molecule, is used (Tables 2-5 and 2-6) which indicates that a substantial fraction of these sites are located in the smaller pores. The chabazite samples, despite exhibiting similar trend, have equal or more acid sites available to larger molecules than the commercial ZY (Table 2-5), as indicated by the site densities determined from the acid-base titration.

Ammonium-exchange has some interesting impacts on the acid characteristics of the NZs. TPD plots show that ammonium-exchange generated a second type of chemisorption site with a higher desorption peak temperature, which was absent in the raw forms of the zeolites (Figure 2-8). The abundance of this site increases with higher exchange (Figure 2-8) as seen by comparing the TPD curves for the CC samples, which indicates that this is a typical Brønsted acid site generated by ammonium-exchange. For the double-exchanged NC, the site is even more abundant than for the CC because Na^+ , being smaller and lighter than Ca^{+2} is replaced more easily from the zeolite structure. The SC sample is also found to generate a similar second acid site upon ammonium-exchange, with a TPD peak appearing at a higher temperature.

While ammonium-exchange generates a second site in both NZ samples, it decreases the density of the dominant site in the CC samples as seen from the comparative normalized TPD peak intensities (Figure 2-8). The overall acid site density also decreases with a higher extent of exchange, while the strength of the dominant acid sites, measured by the heat of adsorption, increases (Table 2-6). This is possibly due to the loss of some initial acid sites by dealumination of the framework upon ammonium-exchange, which ultimately results in fewer overall numbers of sites but with stronger acid strength than the initial dominant sites. In SC, however, the opposite effect is observed; ammonium-exchange almost doubles the site density whereas there is a significant decrease in the heat of adsorption of the dominant sites. Clinoptilolites are more resistant to framework dealumination than chabazites.

To summarize, the raw untreated NZs possess acid sites with comparable or higher strength and higher density compared to the commercial ZY. Ammonium-exchange may either increase or decrease the strength or density of the sites in the raw NZs depending on the type of the zeolite, but it simultaneously generates a second and stronger acid site in every type. The commercial ammonium-exchanged ZY, on the other hand, has only one type of chemisorption sites of lesser strength than those of the raw NZs and most of the ammonium-exchanged NZs. In general, the acid site density in both the raw and exchanged forms of the NZ samples is much higher compared to ZY.

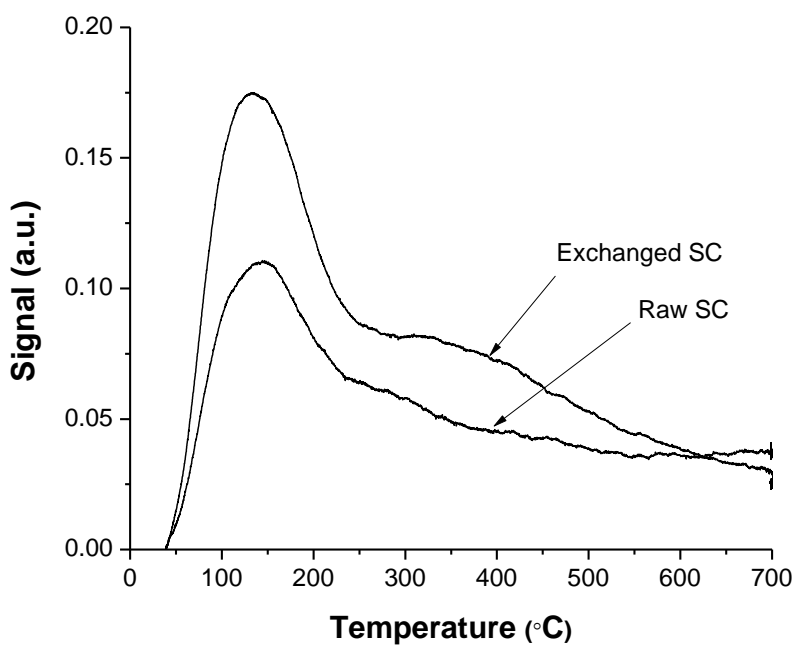
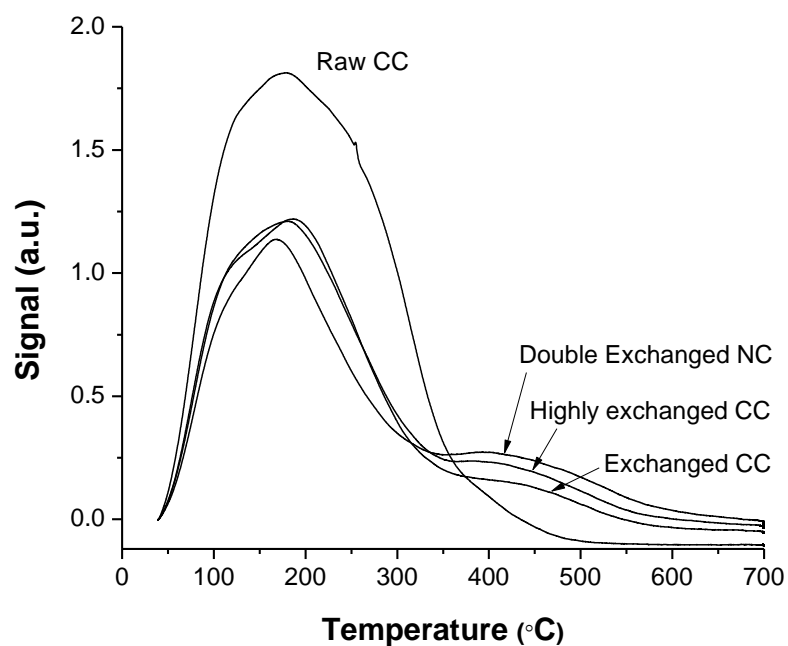


Figure 2-8: Effect of ammonium-exchange on the acid sites of chabazites (CC and NC) and clinoptillite (SC) demonstrated by ammonia TPD (normalized by sample weight).

2.5 CONCLUSION

This study shows that NZs possess morphology, structure and acid properties that are favorable for cracking of large molecules in bitumen. While the raw and ammonium-exchanged forms of NZs differ in their acidic features, in either form they are capable of performing as excellent cracking agents as compared to the commercial ZY. Especially the raw untreated NZs, available in multiple global deposits, can be utilized as better or equally effective petroleum cracking agents than ZY at a much lower cost. These abundant and economic natural mineral zeolites demonstrate a great potential for heavy oil and bitumen extraction and upgrading applications.

(A version of this chapter has been published. *Junaid ASM, Rahman M, Yin H, McCaffrey WC, Kuznicki SM. Natural zeolites for oilsands bitumen cracking: Structure and acidity. Micropor Mesopor Mater 2011; 144: 148-57.* Used with permission from Elsevier.)

BIBLIOGRAPHY

- [1] Farneth WE, Gorte RJ. Methods for characterizing zeolite acidity. *Chem Rev* 1995; 95: 615-35.
- [2] Weitkamp J. Zeolites and catalysis. *Solid State Ionics* 2000; 131: 175-88.
- [3] Tonetto G, Atias J., de Lasa H. FCC Catalysts with different crystalline sizes: acidity, structural properties and reactivity. *Appl Catal A* 2004; 270: 9-25.
- [4] Jentoft FC, Gates BC. Solid-acid-catalyzed alkane cracking mechanisms: evidence from reactions of small probe molecules. *Top Catal* 1997; 4: 1-13.
- [5] Katranas TK, Vlessidis AG, Tsiatouras VA, Triantafyllidis KS, Evmiridis NP. Dehydrogenation of propane over natural clinoptilolite zeolites. *Micropor Mesopor Mater* 2003; 61: 189-98.
- [6] Liu CY, Aika K. Ammonia adsorption on ion exchanged Y-zeolites as ammonia storage material. *J Jpn Petrol Inst* 2003; 46: 301-7.
- [7] Lertjiamratn K, Praserttham P, Arai M, Panpranot J. Modification of acid properties and catalytic properties of AlPO₄ by hydrothermal pretreatment for methanol dehydration to dimethyl ether. *Appl Catal A* 2010; 378: 119-123.
- [8] Sun L, Guo X, Liu M, Wang X. Role of acidity in the ethylation of coking benzene with ethanol over nanosized HZSM-5. *Ind Eng Chem* 2010; 49: 506-14.
- [9] Jong KP, Zečević J, Friedrich H, Jongh PE, Bulut M, Donk S, et al. Zeolite Y crystals with trimodal porosity as ideal hydrocracking catalysts. *Angew Chem Int Ed* 2010; 49: 10074-8.
- [10] Biaglow AI, Parrillo DJ, Gorte RJ. Characterization of H,Na-Y using amine desorption. *J Catal* 1993; 144: 193-201.
- [11] Biaglow AI, Parrillo DJ, Kokotailo GT, Gorte RJ. A study of dealuminated faujasites. *J Catal* 1994; 148: 213-23.
- [12] Dias SCL, de Macedo DL, Dias JA. Acidity measurements of zeolite Y by adsorption of several probes. *Phys Chem Chem Phys* 2003; 5: 5574-9.
- [13] Lima CL, Sousa HSA, Vasconcelos SJS, Filho JM, Oliveira AC, Sousa FF, et al. Effect of sulfation on the physicochemical and catalytic properties of molecular sieves. *Reac Kinect Mech Cat* 2011; 102: 487-500.
- [14] Quaschnig V, Auroux A, Deutsch J, Lieske H, Kemnitz E. Microcalorimetric and catalytic studies on sulfated zirconia catalysts. *J Catal* 2001; 203: 426-33.
- [15] Carre S, Tapin B, Gnep NS, Revel R, Magnoux P. Model reactions as probe of the acid-base properties of aluminas: Nature and strength of active sites.

Correlation with physicochemical characterization. *Appl Catal A* 2010; 372: 26-33.

- [16] Bolis V, Magnacca G, Cerrato G, Morterra C. Microcalorimetric Characterization of Structural and Chemical Heterogeneity of Superacid SO_4/ZrO_2 Systems. *Langmuir* 1997; 13: 888-94.
- [17] Haw JF, Zhang J, Shimizu K, Venkatramn TN, Luigi DP, Song W, et al. NMR and theoretical study of acidity probes on sulfated zirconia catalysts. *J Am Chem Soc* 2000; 122: 12561-12570.
- [18] Semmer V, Batamack P, Doremieux-Morin C, Vincent R, Fraissard J. The acid strength of sulfated zirconia measured by two ^1H NMR techniques in the presence of water: 4K broad-line and 300K high resolution MAS. *J Catal* 1996; 161: 186-93.
- [19] Younes MK, Ghorbel A, Rives A, Hubaut R. Acidity of sulphated zirconia aerogels: Correlation between XPS studies, surface potential measurements and catalytic activity in isopropanol dehydration reaction. *J Sol-Gel Sci Technol* 2004; 32: 349-52.
- [20] Matsuhashi H, Arata K. Measurement of the relative acid strength and acid amount of solid acids by argon adsorption. *Phys Chem Chem Phys* 2004; 6: 2529-33.
- [21] Yang G, Zhou L, Liu X, Han X, Bao X. Density functional calculations on the distribution, acidity, and catalysis of Ti^{IV} and Ti^{III} ions in MCM-22 zeolite. *Chem Eur J* 2011; 17: 1614-21.
- [22] Suzuki K, Nishio T, Katada N, Sastre G, Niwa M. Ammonia IRMS-TPD measurements on Brønsted acidity of proton-formed SAPO-34. *Phys Chem Chem Phys* 2011; 13: 3311-8.
- [23] Yazici DT, Bilgic C. Determining the surface acidic properties of solid catalysts by amine titration using Hammett indicators and FTIR-pyridine adsorption methods. *Surf Interface Anal* 2010; 42: 959-62.
- [24] Johnson O. Acidity and polymerization activity of solid acid catalysts. *J Phys Chem* 1955; 59: 827-31.
- [25] Benesi HA. Acidity of solid surfaces. II. Amine titration using Hammett indicators. *J Phys Chem* 1957; 61: 970-3.
- [26] Hammett LP, Deyrup AJ. A series of simple basic indicators. I. The acidity functions of mixtures of sulfuric and perchloric acids with water. *J Am Chem Soc* 1953; 54: 2721-39.
- [27] Webb PA. Introduction to chemical adsorption analytical techniques and their applications to catalysis. Norcross (GA): MIC Technical Publications; 2003.

- [28] Sakakini BH, Verbrugge AS. Temperature-programmed surface reaction as a means of characterizing supported-metal catalysts and probing their surface reactivity. *J Chem Soc Faraday Trans* 1997; 93: 1637-40.
- [29] Sharma SB, Meyers BL, Chen DT, Miller J, Dumesic JA. Characterization of catalyst acidity by microcalorimetry and temperature-programmed desorption. *Appl Catal A* 1993; 102: 253-65.
- [30] Mao J, Guo Z, Poh CK, Ranjibar A, Guo Y, Yu X, et al. Study on the dehydrogenation kinetics and thermodynamics of $\text{Ca}(\text{BH}_4)_2$. *J Alloys Compd* 2010; 500: 200-5.
- [31] Hirschler AE. The measurement of catalyst acidity using indicators forming stable surface carbonium ions. *J Catal* 1963; 2: 428-39.
- [32] Rouquerol J, Avnir D, Fairbridge CW, Everett DH, Haynes JH, Pernicone N, et al. Recommendations for the characterization of porous solids. *Pure & Appl Chem* 1994; 66: 1739-58.
- [33] Coulter™ Omnisorp™ Manual. Hialeah (FL): Coulter Corporation; 1991.
- [34] Gregg SJ, Sing KSW. Adsorption, surface area and porosity, 2nd ed. London: Academic Press; 1982.
- [35] Breck DW. Zeolite molecular sieves: Structure, chemistry and use. New York: John Wiley & Sons Inc.; 1974.
- [36] Schneider MH, Andrews AB, Mitra-Kirtley S, Mullins OC. Asphaltene molecular size by fluorescence correlation spectroscopy. *Energy Fuels* 2007; 21: 2875-82.
- [37] Acevedo S, Rodríguez P, Labrador H. An Electron Microscopy Study of Crude Oils and Maltenes. *Energy Fuels* 2004; 18: 1757-63.
- [38] Barre´ L, Spinat D, Rosenberg E, Scarcella M. Colloidal structure of heavy crudes and asphaltene solutions. *Rev Inst Fr Pet* 1997; 52: 161-75.
- [39] Masel RI. Principles of adsorption and reaction on solid surfaces. New Jersey: Wiley-Interscience; 1996.
- [40] Kolasinski K. Surface science: Foundations of catalysis and nanoscience. West Sussex: John Wiley & Sons Inc.; 2002.

Light Hydrocarbon Extraction of Natural Zeolite-Cracked Oilsands Bitumen

3.1 INTRODUCTION

As previously mentioned in Chapter 2, natural zeolite (NZ) catalysts have surface and acidic properties suitable for reducing large petroleum molecules into smaller compounds. One potential use of these minerals is to crack the asphaltenes and other heavy components in oilsands bitumen to such an extent that the liquid products can be extracted by light hydrocarbons (pentane or hexane) without using water [1]. This novel waterless approach to bitumen extraction and upgrading addresses some of the environmental issues of the water-based processes, and could improve the long-term economics of oilsands extraction.

Light hydrocarbons such as pentane and hexane can be used to separate bitumen fractions and asphaltenes based on molecular weight and solubility [2]. If the selective extraction of the products by lighter hydrocarbon solvents could be combined with the unique cracking and adsorptive properties of NZs, it may be possible to recover less contaminated, lighter distillates of bitumen from the oilsands using a waterless recovery process [1]. Following cracking with NZs, lighter solvents could fully extract the valuable hydrocarbon fractions from the sands into low-

viscosity, readily pipelined petroleum fractions, while excluding residuum. Extensive zeolite-catalyzed cracking of bitumen in the oilsands may even be sufficient to generate the light hydrocarbon solvents *in situ* for immediate use in extraction.

In this preliminary proof of concept study, oilsands bitumen is cracked into pentane- and hexane-extractable fractions using a series of ammonium-exchanged natural and commercial zeolite catalysts in simple micro-batch reactor systems. When the results are compared to thermal visbreaking, the NZs are found to have cracked the bitumen into much lighter components that have lower boiling points and are almost entirely extracted using light hydrocarbons (pentane and hexane). Effective cracking of oilsands bitumen using economical, abundant and readily disposable NZs represents a potentially significant advance towards a waterless extraction process.

3.2 MATERIALS AND METHODS

3.2.1 Oilsands

A representative sample of Athabasca oilsands was obtained from the Syncrude Facility at Mildred Lake near Fort McMurray, Alberta, Canada.

3.2.2 Catalyst preparation

Standard commercial zeolite Y (ZY) was obtained as ammonium-exchanged fluidized catalytic cracking (FCC) microspheres from Engelhard Corporation. A raw sedimentary Ca-chabazite sample (CC) from the Bowie deposit was obtained from the GSA Resources of Tucson, Arizona. Clinoptilolite samples SC and A are obtained from the Saint Clouds deposit in New Mexico, USA, and the Werris Creek deposit in New South Wales, Australia, respectively. All these samples were finely ground to <74 μm and then, with the exception of ZY, ammonium-exchanged in a slightly acidic environment for 6–8 h. A sodium-rich variant of the chabazite (NC) was double-exchanged with a molar excess of ammonium ions. Samples were then calcined to ~450 °C under nitrogen flow to convert to the hydrogen form for catalytic cracking reactions. For cracking reactions, all catalysts (ZY, NC, CC, SC and A) were used in their partially ammonium-exchanged, calcined forms.

3.2.3 Test reactions

Thermal and catalytic cracking reactions were performed in custom-designed stainless steel micro-batch reactors loaded with approximately 13 g of a 10:1 weight mixture of oilsands and the selected catalyst. The reactor was sealed and leak tested at >1380 kPa, then purged with nitrogen gas. Samples were heated in a tube furnace at a constant ramp rate of $10\text{ }^{\circ}\text{C min}^{-1}$, and soaked for 1 h at $\sim 385\text{ }^{\circ}\text{C}$. Reactions were quenched by immersing the reactor in cold water.

3.2.4 Extraction by organic solvents

Following the cracking reactions, samples were thoroughly mixed and 10 g of the reacted mixture was transferred into a double thickness, porous extraction thimble for solvent extraction and quantitative analysis. The hydrocarbon products were recovered by a 6-h reflux at moderate temperature in a Soxhlet apparatus, using 150 cm^3 of the specified organic solvent (hexane, pentane or toluene). Finally, the solvents were evaporated under vacuum, and the bituminous products were recovered and stored at room temperature. For visual analysis, a separate, smaller portion (approximately 1.1 g) of the reacted oilsands and catalyst mixture was transferred into a disposable pipette, and the hydrocarbon products were extracted using 3 cm^3 of pentane by a once-through process. A photographic representation of the reaction and extraction operations is presented in Figure 3-1.

3.2.5 Characterization of reaction products

Mass loss in the solvent-extracted samples was measured by vacuum distillation thermogravimetric analysis (TGA), a process analogous to ASTM D1160, using a Netzsch Thermogravimetric Analyzer. The organic solvent-extracted product (10–12 mg) was heated from 30 to $380\text{ }^{\circ}\text{C}$ at a constant ramp rate of $10\text{ }^{\circ}\text{C min}^{-1}$ under 1 mm Hg vacuum pressure, and then maintained at approximately $380\text{ }^{\circ}\text{C}$ for an additional 20 min period; sample temperature was kept at $\sim 380\text{ }^{\circ}\text{C}$ to prevent cracking of the extracted hydrocarbons. Temperature change inside the vacuum chamber was recorded during each thermogravimetric analysis and was essentially identical for all analyses; a typical temperature change curve is shown in Figure 3-2. Vacuum temperatures were converted to atmospheric pressure values using the ASTM D1160 temperature-pressure conversion table for petroleum hydrocarbons to

Light Hydrocarbon Extraction of Natural Zeolite-Cracked Oilsands Bitumen

approximate standard petroleum fractions [3] as illustrated in Figure 3-3. The difference between the effective and vacuum temperatures decreased with increasing vacuum chamber temperature, and was approximately 240 °C at the experimental soaking temperature (380 °C).

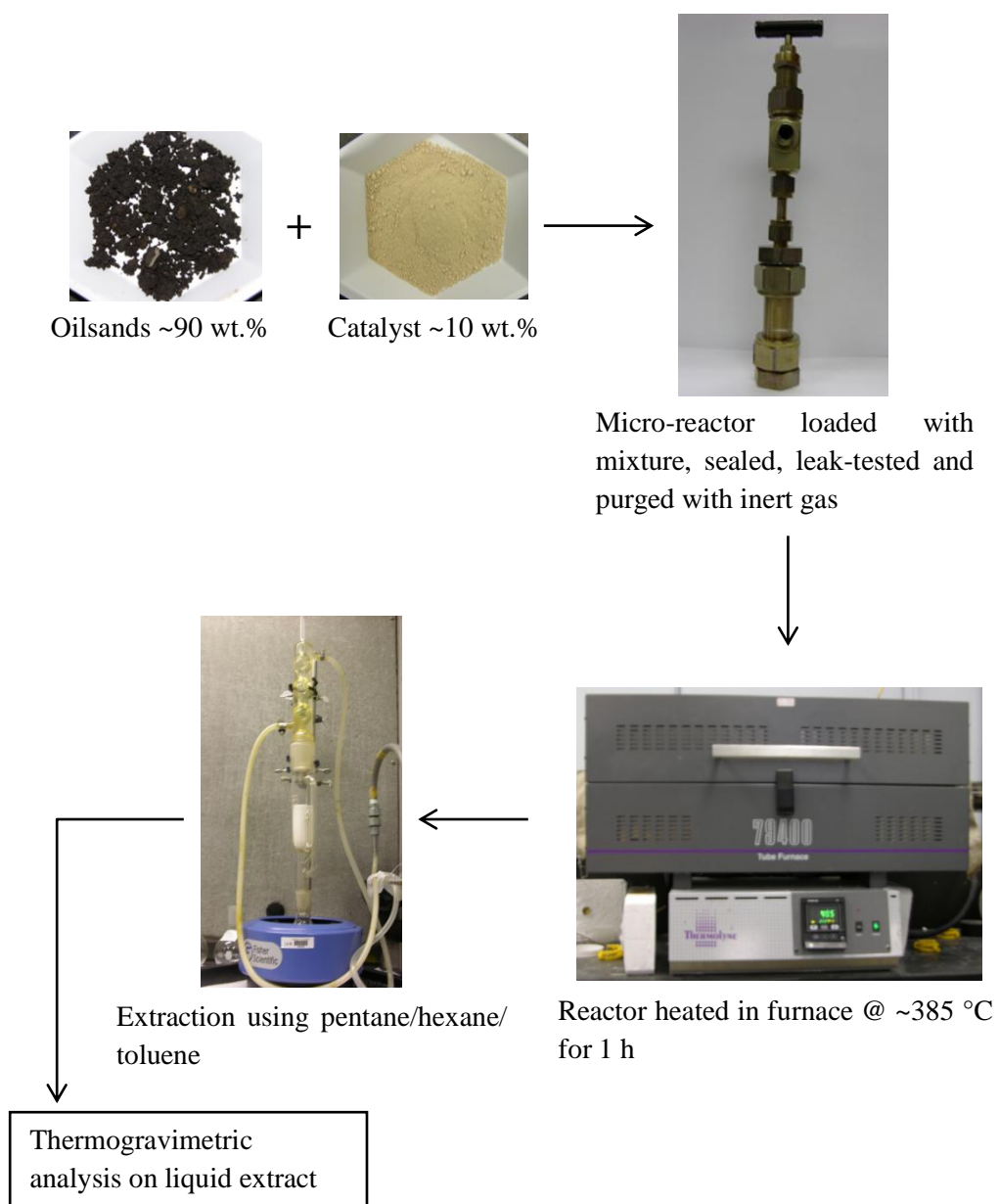


Figure 3-1: A photographic representation of the reaction and extraction experiments.

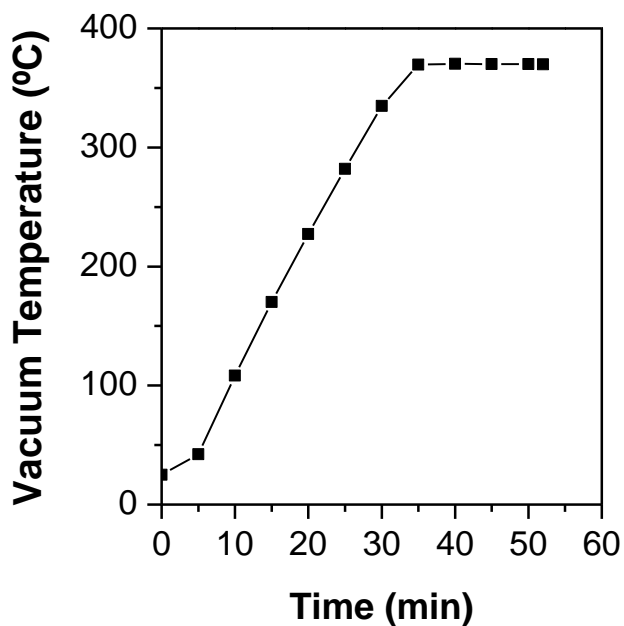


Figure 3-2: A representative time-temperature plot for the TGA experiments.

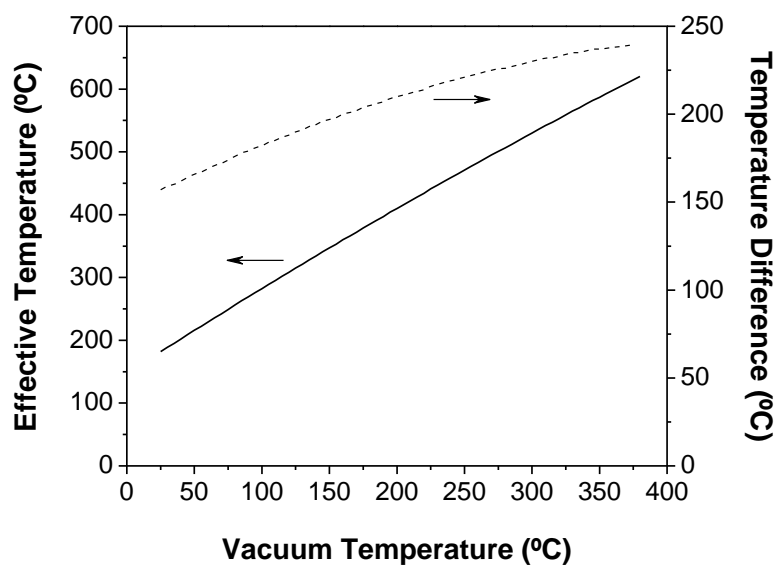


Figure 3-3: Conversion of boiling points under vacuum to effective atmospheric boiling temperatures for TGA of liquid hydrocarbon samples (—), and the difference between the effective and vacuum temperatures (---).

3.3 RESULTS AND DISCUSSION

3.3.1 Cracking and bitumen recovery

Generally, pentane and other light hydrocarbons cannot efficiently dissolve and extract bitumen and asphaltenic materials from oilsands because of the large difference in cohesive energy densities between the solvent and the solute [4]. Catalytic cracking by the NZs, however, yields products which are readily extracted with light aliphatic solvents. Pentane extraction of liquid hydrocarbons from oilsands increases when NZs are used as cracking catalysts, as compared to pentane extraction from analogous raw and thermally cracked samples (Figure 3-4). As expected, the sand from a pentane-extracted raw oilsands sample retains most of its initial structure and color, indicating that little bitumen has been extracted. The raw sample also produces an intermediate-colored pentane extract, indicating that, while no hydrocarbon content has been lost to gas production, most of the high molecular weight components of the bitumen remain insoluble in pentane. In contrast, pentane extraction of a zeolite-cracked sample leaves the sands lighter in color and collapsed. The pentane extract from this NZ-cracked sample is a deep brown color, demonstrating that cracking has resulted in products that are readily extracted by pentane, a light hydrocarbon solvent. The pentane extract from the thermally cracked sample is the lightest in color, while the sands from a thermally cracked sample assume an intermediate structure and a dark color. Thermal cracking leads to the production of low molecular weight products and to the formation of solid coke, which is deposited on the sand and results in visual blackening. In contrast, the light colored sand in the catalyst-cracked sample is indicative of reduced coking, suggesting that the catalyst suppresses the thermal reactions that would normally result in coke formation at these temperatures. This is consistent with previous studies which showed that thermal cracking of hexadecane is suppressed in the presence of NZ catalysts [5].

NZ cracking of oilsands samples results in enhanced extractability with light hydrocarbons, high recovery of liquid hydrocarbon and high gas make. Table 3-1 shows the weight percent of liquid hydrocarbons recovered by extensive Soxhlet extraction of pentane-, hexane- and toluene-extracted cracked and uncracked oilsands samples. Values assume complete (100 wt.%) extraction of the liquid hydrocarbons from the raw oilsands sample using toluene. When liquid hydrocarbons are extracted

from the sand matrix with pentane, the highest weight percent of liquid hydrocarbons is recovered from the SC-cracked oilsands sample (84.9 wt.%). In comparison, the raw, thermally cracked, NC-cracked, CC-cracked and ZY-cracked samples have recoveries of 72.0, 77.5, 82.9, 73.1 and 76.9 wt.% of total liquid hydrocarbon content, respectively.



Figure 3-4: Oilsand samples after extraction with pentane: raw (left); thermally cracked (middle) and cracked using clinoptilolite (right).

Average gas production associated with the NZ-catalyzed cracking is also higher than that from thermal or ZY cracking. Generally, there are more hexane-extractable liquid hydrocarbons in raw (85.5 wt.%) or thermally cracked (79.4 wt.%) sand samples, than in catalytically cracked samples. The data in Table 3-1 represents the results of individual experiments and, as such, does not include error values. When randomly selected experiments are repeated using independent oilsands samples, liquid hydrocarbon recovery varies by $\pm 5.5\%$. In general, the size of this error is smaller than the differences between the results for different catalysts and the controls. The variability in these results reflects both the heterogeneous nature of the

oilsands and the combined influence of the errors associated with each experimental step. Because the gas production values vary by up to 10.0%, with the value for clinoptilolite cracking showing the greatest observed variation, this parameter was not focused on when comparing the catalytic activity of the zeolites.

Table 3-1: The effect of cracking agents and extraction solvents on liquid hydrocarbon recovery from oilsands samples.

Sample *	Average gas production (g per g of reacted oilsands)	Liquid hydrocarbon recovery (wt.%)		
		Toluene extracted	Hexane extracted	Pentane extracted
Raw oilsands	-	100.0	85.5	72.0
Thermal cracking	0.0247	85.3	79.4	77.5
ZY	0.0301	89.4	79.4	76.9
CC	0.0338	97.0	64.6	73.1
NC	0.0465	88.3	78.7	82.9
SC	0.0493	78.3	69.3	84.9
A	0.0267	79.3	76.3	73.8

* All catalysts were used in their partially ammonium-exchanged, calcined forms.

It should be reiterated that all the catalysts used in this work were used in their partially ammonium-exchanged, calcined forms. While unexchanged forms of the catalysts have some limited cracking activity, comparative visual inspection of cracked oilsands and once-through pentane-extracts suggests that ammonium-exchange and calcination significantly improves catalyst performance. The activity of raw catalysts will be discussed in details in subsequent chapters of this thesis.

The pentane- and hexane-extracted products from ZY-catalyzed reactions had good recoveries (76.9 and 79.4 wt.%, respectively) of liquid hydrocarbons (Table 3-1). However, analysis of the boiling point distribution (Table 3-2 (a)–(c)) reveals that the liquid products from NZ-cracking have lighter components than those from the thermal or ZY-catalyzed reactions. This point will be discussed in greater details in the next sub-section of this chapter.

Toluene extracts more hydrocarbons from oilsands than either pentane or hexane. For example, pentane and hexane extraction of liquid hydrocarbons from raw oilsands results in 72.0 and 85.5 wt.% recoveries, respectively (Table 3-1), nearly 30 and 15% lower than toluene extraction from the same starting material. Extractability, which corresponds to relative solubility of petroleum fractions in hydrocarbon solvents, can be considered in terms of the Hildebrand solubility parameter (δ). This parameter is a numerical estimate of the degree of interaction between materials, which is widely used as an indicator of the solubility of non-polar materials, including the solubility of asphaltene fractions in hydrocarbon solvents [4]. Materials with similar δ values (such as asphaltenic materials and toluene) are more likely to be miscible than those with considerably different δ values (such as asphaltenic materials and pentane/hexane). The Hildebrand solubility parameter values for pentane, hexane, toluene are 14.4, 14.9 and 18.3 MPa^{0.5}, respectively [5]. Experimental and calculated solubility parameter values for Athabasca bitumen range from 18.9 to 19.6 MPa^{0.5} [6-8]. Calculated solubility parameters for asphaltenes range from 21.0 to 25.8 MPa^{0.5} [9,10], and the experimental values are in agreement with the lower end of this range [11]. Thus, toluene is predicted to extract unconverted bitumen from the oilsands that the lighter hydrocarbons cannot. However, having a closer solubility parameter to the asphaltenes, toluene will co-extract a larger fraction of the remaining asphaltenes with the light hydrocarbons, which is undesirable.

Table 3-2(a): Boiling point distribution of toluene ($\delta=18.3$ MPa^{0.5})-extracted liquid products from thermal and catalytic cracking reactions with zeolite Y (ZY), Na-chabazite (NC), Ca-chabazite (CC), and clinoptilolites from Saint Clouds (SC) and Australia (A).

Sample *	Petroleum Fractions (wt.%)		
	Distillate oil (277-343 °C)	Gas oil (343-566 °C)	Residuum (566 °C+)
Raw oilsands	0.6	33.3	65.9
Thermal cracking	8.0	49.5	42.0
ZY	6.5	50.5	42.6
CC	9.4	52.4	36.7
NC	8.1	52.1	39.7
SC	7.3	54.2	37.2
A	12.7	51.4	34.3

* All catalysts were used in their partially ammonium-exchanged, calcined forms.

Table 3-2(b): Boiling point distribution of hexane ($\delta=14.4 \text{ MPa}^{0.5}$)-extracted liquid products from thermal and catalytic cracking reactions with zeolite Y (ZY), Na-chabazite (NC), Ca-chabazite (CC), and clinoptilolites from Saint Clouds (SC) and Australia (A).

Sample *	Petroleum Fractions (wt.%)		
	Distillate oil (277-343 °C)	Gas oil (343-566 °C)	Residuum (566 °C+)
Raw oilsands	0.7	42.9	56.3
Thermal cracking	2.8	53.7	43.0
ZY	4.9	55.5	39.1
CC	7.2	57.3	34.5
NC	3.2	56.2	40.0
SC	7.3	54.2	37.2
A	11.3	56.6	30.0

* All catalysts were used in their partially ammonium-exchanged, calcined forms.

Table 3-2(c): Boiling point distribution of pentane ($\delta=14.3 \text{ MPa}^{0.5}$)-extracted liquid products from thermal and catalytic cracking reactions with zeolite Y (ZY), Na-chabazite (NC), Ca-chabazite (CC), and clinoptilolites from Saint Clouds (SC) and Australia (A).

Sample *	Petroleum Fractions (wt.%)		
	Distillate oil (277-343 °C)	Gas oil (343-566 °C)	Residuum (566 °C+)
Raw oilsands	1.3	55.4	43.3
Thermal cracking	1.7	53.2	44.9
ZY	8.0	56.2	35.8
CC	9.9	53.4	35.9
NC	6.5	56.9	36.2
SC	8.9	57.0	33.0
A	22.0	50.3	25.1

* All catalysts were used in their partially ammonium-exchanged, calcined forms.

3.3.2 Thermogravimetric analysis of liquid products

Following thermal or catalytic cracking, the bitumen from oilsands samples was extracted with pentane and evaporated, and the recovered products were analyzed by thermogravimetry. Thermogravimetric mass loss plots of the pentane-extracted liquid samples are shown in Figure 3-5. The NZ catalysts crack the bitumen into lighter components, with lower boiling points, than thermal cracking or catalytic cracking with commercial ZY. The pentane-extracted bitumen sample from oilsands cracked with A is reduced to 12% of its initial mass after heating under a vacuum to 380 °C. In comparison, extracts from raw and thermally cracked oilsands have residual masses of 22 and 25% of their initial masses (Figure 3-5). The residual mass from the clinoptilolite sample is approximately 10% lower than that generated by cracking with ZY; this indicates that the liquid generated using the inexpensive clinoptilolite catalysts contain the lightest hydrocarbon fractions. This trend is consistent whether the bitumen is extracted using pentane or hexane, however, when the cracked samples are extracted with hexane instead of pentane, increased residual masses are observed, indicating that hexane extracts heavier hydrocarbon fractions, as would be predicted based on the relative Hildebrand solubility parameters for pentane and hexane. The repeatability of this experiment is high; the standard deviation in the observed residual mass percentage for a single, representative, catalytically cracked and extracted sample was 1.3%, based on four repeated experiments conducted on the sample.

Thermogravimetric mass loss plots of the products of individual cracking reactions demonstrate that pentane and hexane extract lighter hydrocarbons and smaller amounts of residuum from oilsands samples than toluene (Figure 3-6). Light hydrocarbon extracts of clinoptilolite A-cracked samples reduce to 12, 16 and 22% of their initial masses from pentane, hexane and toluene extracts, respectively, which is significantly lower residuum than that observed in thermally cracked or uncracked samples (Figure 3-6). In contrast, raw oilsands extracted using toluene reduce to 43% of initial mass after distillation under vacuum; when pentane or hexane is used, the residual masses are much lower (22 or 33% of initial mass, respectively; Figure 3-6).

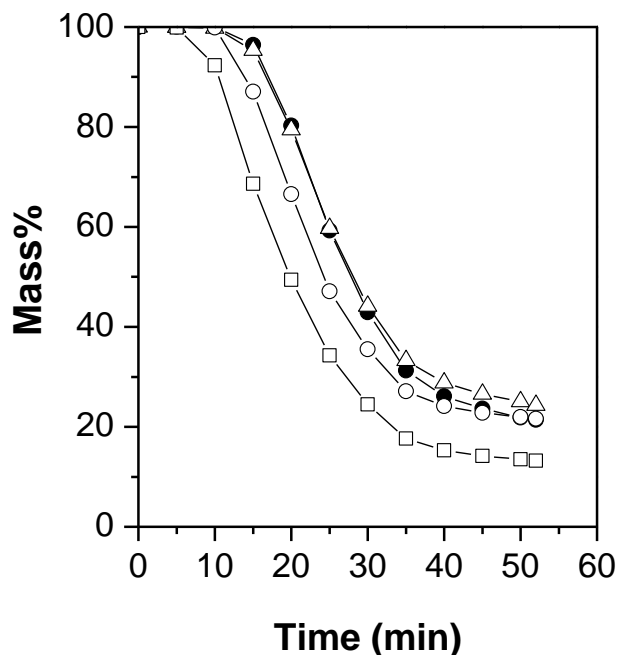


Figure 3-5: Effect of natural zeolite cracking on product quality: boiling point distribution of pentane-extracted liquid products from unreacted raw oilsands (●), and thermally cracked (Δ), zeolite Y (ZY) cracked (○) and Australian clinoptilolite (A) cracked (□) oilsands as determined by thermogravimetric analysis.

When the boiling points of the oilsands extracts measured under vacuum are converted to atmospheric pressure values to approximate standard petroleum fractions, the natural zeolite-cracked products are distributed into much lighter components than raw, thermally cracked, or ZY-cracked samples. The weight percent of these fractions from toluene, hexane and pentane extractions are presented in Table 3-2 (a)–(c). In toluene extracts, the raw oilsands sample has the highest residuum content (65.9 wt.%), while the clinoptilolite-catalyzed samples have the lowest (37.2 and 34.3 wt.%). The reduction in residuum content in the NZ-cracked liquid hydrocarbon samples corresponds to increases in the light and middle fractions (Table 3-2 (a)–(c)), as compared to raw, thermally cracked or ZY-cracked oilsands. This trend is consistent for toluene, hexane and pentane extraction. Weight percent values for the lighter petroleum fractions (including naphtha and kerosene) are not reported in the tables, as a significant fraction of these hydrocarbons can be lost by evaporation with the solvent after the extraction, and, as a result, the values measured for the light fractions are not reliable.

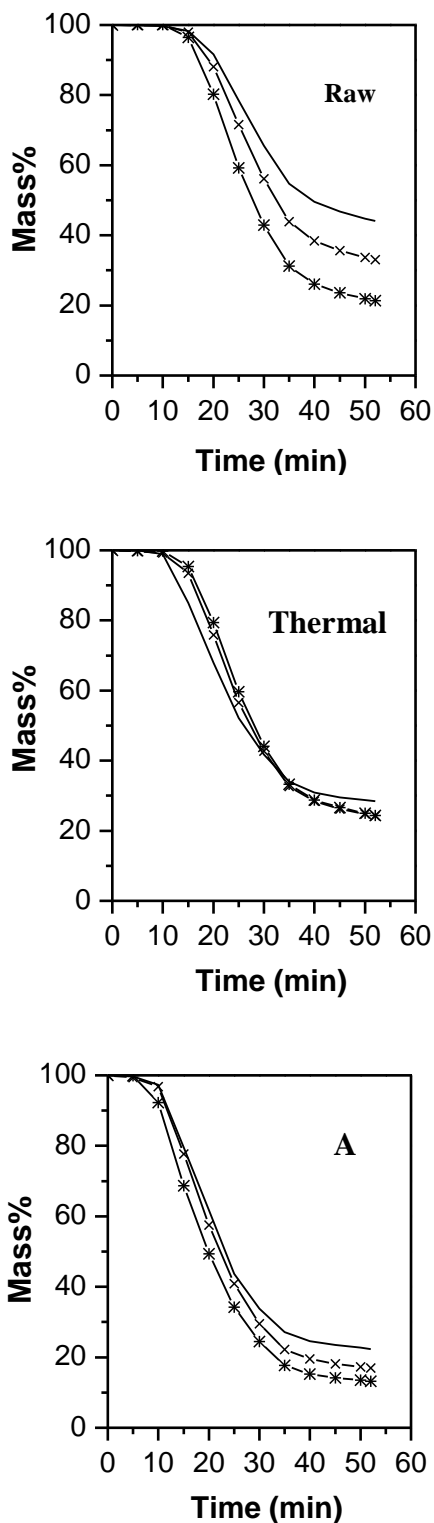


Figure 3-6: The effect of selected extraction solvents (toluene (no symbol), hexane (x), and pentane (*)) on the distribution of boiling points in extracted samples as determined by thermogravimetric analysis.

NZ cracking reduces the asphaltene content of bitumen significantly. Asphaltenes are soluble in toluene, but insoluble in lighter n-alkane hydrocarbons [11]. When the bitumen is cracked with clinoptilolite and extracted by lighter hydrocarbons (Table 2 (b) and (c)), the residuum content decreases by only 4–9 wt.%, compared to the analogous toluene-extracted samples (Table 2 (a)), indicating that few asphaltenes remain after the cracking reactions. In contrast, pentane and hexane extraction of raw oilsands reduces the residuum content by 13–23 wt.%, compared to toluene extraction, indicating that a significant portion of the asphaltene content of raw oilsands is not extracted using the lighter hydrocarbons.

Comparison of thermogravimetric mass loss plots and liquid hydrocarbon recovery from oilsands samples establishes that NZs break down the heavier hydrocarbons (like asphaltenes) in bitumen into much lighter components than thermal cracking or commercial ZY-catalyzed cracking. Light n-alkanes such as pentane or hexane can selectively extract those commercially valuable fractions from zeolite-cracked samples, leaving the few remaining asphaltenes and other undesirable heavier components in the exhausted sands. This waterless extraction method results in the production of lighter, less viscous and, therefore, more transportable, petroleum fractions that contain a higher proportion of fuel-grade hydrocarbons.

3.3.3 Cracking and acidity

It was shown in Chapter 2 that the NZs have stronger and/or higher density of acid sites compared to the commercial cracking catalyst ZY. Theoretically, stronger and larger number of acid sites lead to greater degree of cracking. The smaller residue fractions (Table 3-2 (a)–(c)) and larger gas makes (Table 3-1) in the NZ-cracked products, as compared to those of ZY, generally support this idea. However, the residue cracking did not follow the exact order of strength or density of acid sites. Considering the extremely complex and non-homogeneous nature of the feed, particularly in absence of mixing to provide effective and uniform contact with the acid sites, this is not unexpected. Moreover, secondary cracking of light products and generation of gas and coke leave a concentration effect on the residue fraction in the liquid products which makes it difficult to establish a direct relationship between the acidity and the residue content. Because of the small amounts of feed materials and the simple setup used for these experiments, it was not possible to account for

these factors. However, the objective of this study was to conduct a preliminary assessment of the efficacy of waterless (light hydrocarbon) extraction of NZ-cracked bitumen from oilsands. A more engineered approach, with provisions for mixing and measurement and analysis of all product fractions, is taken to conduct the advanced studies presented in the subsequent chapters.

3.4 CONCLUSION

NZs such as chabazite and clinoptilolite can break down the heavy molecules, especially asphaltenes, within oilsands bitumen into lighter fractions more effectively than thermal visbreaking or cracking with ZY, an expensive commercial catalyst. Light hydrocarbons such as pentane and hexane can then fully extract the lighter petroleum fractions from the sands, excluding residuum while extracting the valuable components of the bitumen. The combination of efficient, natural zeolite-catalyzed cracking and light hydrocarbon extraction is a step towards waterless liquid hydrocarbon extraction. The next objective will be to develop an effective engineered system that requires smaller amounts of catalysts and less processing steps to be practically feasible as well as economical.

(A version of this chapter has been published. *Junaid ASM, Yin H, Koenig A, Swenson A, Chowdhury J, Burland G, et al. Natural zeolite catalyzed cracking-assisted light hydrocarbon extraction of bitumen from Athabasca oilsands. Appl Catal A 2009; 354: 44-9.* Used with permission from Elsevier.)

BIBLIOGRAPHY

- [1] Kuznicki SM, McCaffrey WC, Junaid ASM, Yin H, Koenig A, Swenson P, et al. Advances in Natural Zeolite Bitumen Cracking. 57th Canadian Chemical Engineering Conference; 2007 Oct 28-31; Edmonton, Canada. Ottawa (ON): Canadian Society for Chemistry; 2007 Oct. 168 leaves.
- [2] Zhao S, Kotlyar LS, Woods JR, Sparks BD, Gao J, Chung KH. The chemical composition of solubility classes from Athabasca bitumen pitch fractions. *Pet Sci Technol* 2003; 21: 183-99.
- [3] Giles HN. Analysis of crude oils. In: Drews AW, editor. ASTM manual on hydrocarbon analysis, ASTM Manual Series, MNL 3. 4th ed. Philadelphia: American Society for Testing and Materials; 1989. p. 20-7.
- [4] Mitchell DL, Speight GJ. The solubility of asphaltenes in hydrocarbon solvents. *Fuel* 1973; 52: 149-52.
- [5] Kuznicki SM, McCaffrey WC, Bian J, Wangen E, Koenig A, Lin CH. Natural zeolite bitumen cracking and upgrading. *Micropor Mesopor Mater* 2007; 105: 268-72.
- [6] Zhao S, Xu Z, Xu C, Chung KH, Wang R. Systematic characterization of petroleum residua based on SFEF. *Fuel* 2005; 84: 635-45.
- [7] Corraera S, Merlini M, Lullo AD, Merino-Garcia D. Estimation of the solvent power of crude oil from density and viscosity measurements. *Ind Chem Res* 2005; 44: 9307-15.
- [8] Gray MR, Jokuty P, Yeniova H, Nazarewycz L, Wanke SE, Achia U, et al. The relationship between chemical structure and reactivity of Alberta bitumens and heavy oils. *Can J Chem Eng* 1991; 69: 833-43.
- [9] Akbarzadeh K, Dhillon A, Svrcek WY, Yarranton HW. Methodology for the characterization and modeling of asphaltene precipitation from heavy oils diluted with n-alkanes. *Energy Fuels* 2004; 18: 1434-41.
- [10] Rogel E. Theoretical estimation of the solubility parameter distributions of asphaltenes, resins, and oils from crude oils and related materials. *Energy Fuels* 1997; 11: 920-5.
- [11] Wiehe IA, Liang KS. Asphaltenes, resins, and other petroleum macromolecules. *Fluid Phase Equilib* 1996; 117: 201-10.

Activation of Natural Zeolite Catalysts by Water Addition

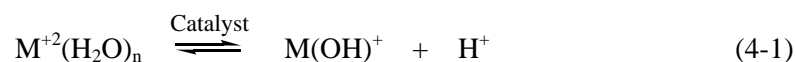
4.1 INTRODUCTION

The studies presented in the previous chapters demonstrated that natural zeolites (NZ), economic minerals found abundantly in multiple global deposits, when acidified by ammonium-exchange, are capable of breaking heavier fractions in oilsands bitumen into lighter components that are readily recoverable using light hydrocarbon, leading to a waterless recovery process [1]. Ammonium-exchange followed by calcination generates Brønsted acid sites on zeolite surfaces [2], which donate protons to generate carbocations that participate in cracking of large petroleum molecules [3]. A study conducted in our lab demonstrated that the extent of catalytic cracking of oilsands bitumen with raw unexchanged clinoptilolite is comparable to that achieved with clinoptilolite acidified by ammonium-exchange [4]. This study demonstrates that with a small amount of water addition (3 wt.% of feed oilsands), the extent of NZ-assisted cracking is enhanced significantly compared to that achieved by the waterless raw catalysts. Based on these results, water addition can essentially eliminate the need for the ammonium-exchange step required for acidification of the catalysts. This can offer great advantages from a process

perspective. The study presented in this chapter investigates the method and mechanism for water-activation of NZs.

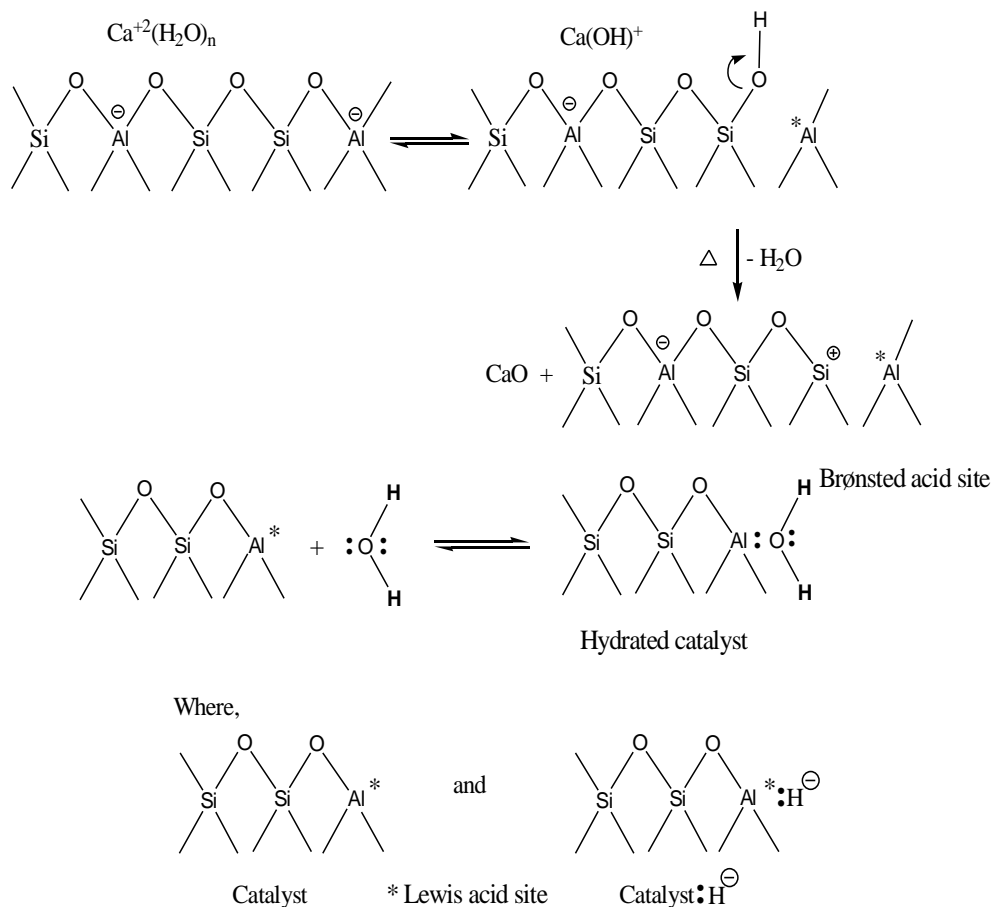
The role of water in heavy oil exploration and processing is of great interest to researchers for a couple of reasons. Water has a positive impact in extraction and upgrading of heavy feedstock in a world where conventional energy sources are diminishing. Research in this field encompasses studies on hydrous pyrolysis of kerogen [5], coal liquefaction [6] and upgrading of extra-heavy crude by methane and water [7]. Detailed proposed mechanisms on the role of water in these processes are available in the literature [5,8-12]. In oilsands processing, bitumen from oilsands is successfully extracted by Clark's hot water extraction process at low operating temperatures [13,14]. Quantity and quality of bitumen extraction can be increased by high temperature water-based extraction [15]. Another study conducted by Dutta et al. found that the presence of steam in fluidized coking of bitumen suppresses coke formation from thermal cracking [16]. The use of large amounts of water in these processes, however, has been subject of growing environmental concern about the consumption and pollution of fresh water [15].

In NZ-assisted reactions, water addition may generate acid hydroxyl groups on the catalyst surface which then participate in catalytic cracking. It is reported in literature that by a series of reactions including dehydroxylation and water regeneration, hydroxyl groups and acid sites are generated on silica-alumina surface by water [17,18]. Water molecules undergo dissociation by the electrostatic interaction of the divalent cations (M^{+2}) present on silica-alumina surface and generate $M(OH)^+$ and H^+ ions according to the following reaction [17,18]:



The generated proton may readily combine with the lattice oxygen of the catalyst framework and produce hydroxyl groups ($-SiOH$), the Brønsted acid. The Lewis acid site (tricoordinated aluminium) is simultaneously generated by cleavage of Al-O coordination bond. Ward et al. [19-21] observed that interaction of $-SiOH$ and $M(OH)^+$ groups may dehydrate the zeolites by producing tricoordinated silicon

and MO (Scheme 1). Furthermore, addition of water to the dehydrated zeolite catalyst transforms its Lewis acidity into Brønsted acidity and vice versa (Scheme 1):

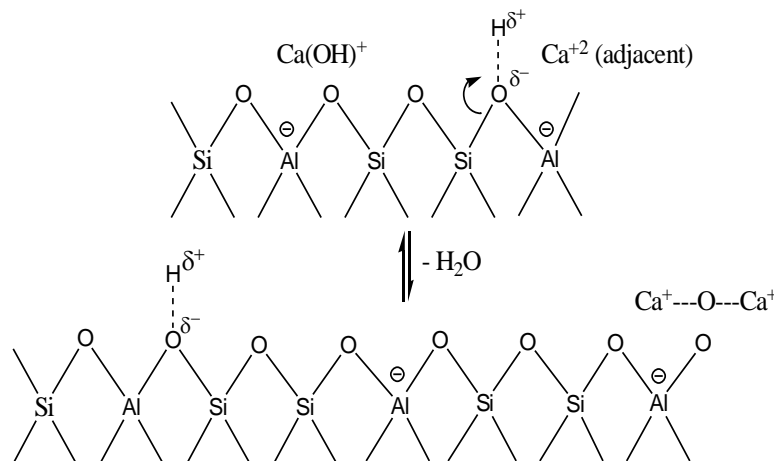


Scheme 1: Dehydroxylation and formation of Brønsted and Lewis acidity on divalent cation (Ca^{+2}) enriched zeolite surface [19-21].

$\text{M}(\text{OH})^+$ is very unstable and tends to undergo dehydration reactions even at 300-350 °C. It produces bridged cation species and regenerates a proton, essential for catalytic cracking, as follows:



According to another very similar mechanism [17,18], a silica-alumina structure may undergo acidification by self-ionization of externally added or lattice water by acid-base reaction. Water combines to generate hydroxyl and hydronium ions, which may undergo further dissociation to produce water and proton that reacts with lattice oxygen to regenerate -SiOH groups (Scheme 2).



Scheme 2: Dehydroxylation of the Ca(OH)^+ zeolite to form bridged cation species [17,18].

Either way, water addition may generate acid groups capable of participating in catalytic cracking on NZ surface. This study presents an investigation on the role of added water in activation of NZs for catalytic cracking. To understand the method and mechanism, a series of analytical and surface sensitive techniques are employed. Surface sensitive techniques such as infrared spectroscopy (IR) and solid state nuclear magnetic resonance (NMR) spectroscopy can detect presence of acid hydroxyl groups on the surface. On the other hand, tracer experiments, when combined with stable isotope mass spectrometry and NMR spectroscopy, can provide useful information on proton transfer from added water to the catalyst surface and liquid bitumen fractions [7,16,22-24]. Using D_2O -traced experiments, the extent and nature of the proton transfer from water-added reactions to bitumen is investigated. The results are helpful to gain insight and speculate on the possible mechanisms of catalytic cracking by self-acidified NZs.

4.2 MATERIALS AND METHODS

4.2.1 Materials

Saint Cloud Clinoptilolite (SC) and sedimentary Ca-chabazite (CC) were obtained from Saint Clouds, New Mexico and Bowie, Arizona, respectively. The samples were ground to $<44\ \mu\text{m}$ particles. Ammonium-exchanged forms (NH_4^+ -forms) of the catalysts were prepared following the procedure described in Section 3.2.2. Protonated forms (H^+ -forms) of the ammonium-exchanged catalysts, and calcined forms of the raw catalysts were prepared by drying the ammonium-exchanged forms and raw catalysts, respectively, at $\sim 450\ ^\circ\text{C}$ under helium flow.

Athabasca oilsands sample were obtained from the Syncrude Facility at Mildred Lake near Fort McMurray, Alberta, Canada. The oilsands samples were thoroughly mixed, homogenized and refrigerated prior to use.

4.2.2 Dean Stark analysis

Water content of the oilsands sample was determined by Dean Stark analysis at the Minerals Processing Laboratory in the Department of Chemical and Materials Engineering at the University of Alberta. 50 g of the sample was separated into oil, water and solids fraction using 200 mL of toluene in a Dean Stark apparatus. Details of the method can be found elsewhere [25].

4.2.3 Test reactions and gas separation

A 1000 mL capacity stainless steel custom-designed autoclave, equipped with a continuous stirred system was used to carry out catalytic cracking of oilsands bitumen. The experimental setup is illustrated and described in greater details in Chapter 5. A specified amount (0 and 5% of oilsands weight) of NZ catalyst was added and mixed with 500 g of oilsands with and without addition of 3 wt.% water. The mixture was loaded in to the autoclave, purged and leak tested with helium at a pressure $>1400\ \text{kPa}$. The stirred reactor was heated to $300\ ^\circ\text{C}$ and maintained for 1 h, then immediately quenched and allowed to reach thermal equilibrium. D_2O doped reactions were performed the same way with the exception of using 3 wt.% D_2O as a tracer instead of regular water.

4.2.4 Gas and light fractions separation

The gaseous products were analyzed in a calibrated Shimadzu 14B gas chromatograph equipped with a 3 m Haysep Q packed column and thermal conductivity detector. The degasified products were stripped off the light oil fractions by re-heating at 150 °C, and condensation using a cold trap. Water and oil contents in the condensate were separated based on density, and weighed. Gas and light fractions separations are described in greater details in Chapter 5.

4.2.5 Extraction of liquids by organic solvents

Liquid products were stripped from 80 g of the reacted mixture by Soxhlet extraction by pentane or toluene in a double thickness, porous extraction thimble for 8-12 h, until a clear solvent appears. Extracted products were collected by evaporating the solvents under vacuum using a rotary evaporator. The solvent-extracted liquid products and spent sands were dried in an oven by maintaining the temperature slightly higher than the boiling point temperature of the solvents (40 °C for pentane and 115 °C for toluene extractions) until a constant weight was achieved. Proportional amounts of liquid condensate were added back to liquid products prior to analyses.

4.2.6 Maltenes, asphaltenes and coke measurement

Maltenes content, the liquid fraction extractable by pentane, was determined as the combined mass of the light oil fraction from the cold trap plus the pentane-extracted liquid from the Soxhlet extraction. C₅-asphaltene contents, fractions unextractable by pentane but extractable by toluene, were measured by re-extracting the pentane-extracted and dried spent sands with toluene using a Soxhlet extractor, maintaining a toluene to bitumen ratio of at least 40:1. The extract was then dried at 115 °C until a stable mass was achieved and weighed. Evaporation of residual solvents from the spent sands was conducted in a tube furnace maintained at ~250 °C for 2 h under helium flow. The dried and depleted sands were weighed, and placed in a high temperature muffle furnace maintained at 850 °C for 5 h in the presence of air to combust the remaining organic solids. The amount of coke was determined from the weight loss of the depleted sands.

4.2.7 Simulated distillation

A high temperature simulated distillation (HTSD) method [26] was used to determine the boiling point distribution of the liquid products. The boiling range (up to 720 °C) corresponds to the n-alkane range of C₅-C₁₂₀. This is a modified version of the ASTM standard test method for determination of boiling range distribution of crude petroleum by gas chromatography (ASTM D5307) [27]. Each sample was used to prepare a 2 wt.% solution of toluene-extracted liquid dissolved in CS₂. 0.2 µL of each solution was injected into a WCOT Ultimet non-polar column (Varian Micron, 5 m×0.53 mm, 0.09 µm film thickness) on a Varian Micron 450 GC equipped with an on-column injector and flame ionization detector (FID). The oven was heated from 308 to 673 K, and the injector was programmed from 373 to 673 K at a constant temperature ramp of 20 K min⁻¹ and 150 K min⁻¹ respectively. The final temperature of 673 K was maintained throughout the acquisition. The chromatographic elution times for low carbon number hydrocarbons (C₇-C₁₂) were calibrated with the Supelco ASTM D2887 pure paraffin standard mixture (Belletonte, USA). A mixture of linear, even polyethylene (Polywax 655, Supelco) was used as the calibration standard for higher range carbons (C₅-C₁₂₀). The detector signal was integrated every 0.2 min. To confirm system performance, each injection was preceded by an injection of the same sample plus 0.2 wt.% (based on the weight of CS₂) internal standard reference sample of known boiling point composition (Supelco ASTM D5307 crude oil internal standard). Several blank CS₂ injections were made to clean the column residues between injections. SIMDIST analysis was performed on the portion of the chromatograms falling between 5% of the n-C₁₄ retention time, and 95% of the n-C₁₇ retention time. To ensure a baseline signal free from extraneous peaks and drifts, a blank run was performed under the same conditions, and the corresponding signals were subtracted from each analysis using SIMDIST software to provide bleed-corrected chromatograms.

4.2.8 Mass balance and yield-calculations

The masses of the liquid products were distributed into naphtha (>191 °C), kerosene (191-277 °C), distillate oil (277-343 °C), gas oil (343-566 °C) and residuum (566 °C+) fractions according to their boiling points [28]. The %-yields of gas, coke,

maltenes, asphaltenes, residue-free liquid and total liquid are calculated based on 500 g of oilsands feed using the following equation:

$$\% \text{ - Yield} = \frac{M_i}{M_G + M_{TL} + M_C} \times 100\% \quad (4-3)$$

Where M_i , M_G , M_{TL} and M_C represent the mass of the particular component 'i', gas, total liquid (combined mass of all liquid fractions) and coke respectively.

4.2.9 Average molecular weight (AMW) measurement

AMW of liquid product samples were measured with a KNAUER Vapor Pressure Osmometer (model K-7000) following ASTM standard D2503 [29]. The instrument was calibrated with sucrose octacetate (AMW=679 g mole⁻¹) as an internal standard and 1,2-dichlorobenzene as a solvent at 130 °C in order to minimize the molecular associations. A commercially available polybutene (AMW=920 g mole⁻¹) (Sigma Aldrich 388696) was used as a standard material for testing the accuracy of the calibration curve. Calibration constant (K_C) was calculated by extrapolating a standard (MV C⁻¹ versus C) plot to zero concentration, where MV=measurement value (kg g⁻¹) and C=known concentration (mole kg⁻¹) (Appendix A). The measurement constant (K_M) values for the unknown samples were determined from the MV C⁻¹ versus C plots (Appendix A). The AMW (g mole⁻¹) was calculated using the following equation:

$$\text{AMW} = K_C / K_M \quad (4-4)$$

4.2.10 Viscosity measurement

A Brookfield DV-E chamber and spindle viscometer was used to measure viscosity of samples at three different temperature set points (40, 50 and 60 °C). The viscometer was pre-calibrated and tested with several standard silicone oil samples. For each measurement, 2-3 mL of each of the liquid product samples was allowed to

reach thermal equilibrium at the specified temperature. In this chapter, for the sake of brevity only viscosity values measured at 50 °C are used.

4.2.11 Fourier transform infrared spectroscopy (FTIR) analysis of catalysts

FTIR analysis of the catalysts was conducted at the Alberta Center for Surface Engineering and Science using a Thermo Nicolet 8700 FTIR spectrophotometer with a Smart Collector device. The spectra were recorded from 400-5000 cm^{-1} range in the transmission mode with a resolution of 4 cm^{-1} . Determination of peak intensities was performed using Nicolet OMNIC software.

4.2.12 Nuclear magnetic resonance (NMR) spectroscopic analysis

^{29}Si NMR spectra for solid catalysts were recorded with a Chemagnetics CMX Infinity 200 NMR Spectrometer, operating with a proton frequency of 200.1469 MHz and a ^{29}Si frequency of 39.7604 MHz. The cross-polarization magic angle spinning (CP/MAS) ^{29}Si NMR acquisition method was used with a 4.0 μs proton 90° pulse flip angle, a CP contact time of 10 ms, an acquisition time of 14.6 ms and a recycle delay of 3 s. The MAS frequency was 8 kHz. The spectra were referenced such that the chemical shift of tetramethylsilane (TMS)=0 was set so the silyl ^{29}Si of tetrakis (trimethylsilyl) silane peak appeared at -9.843 ppm.

Quantitative ^1H NMR and ^{13}C NMR spectroscopic analyses of liquid products were performed using a Varian Inova-400 NMR spectrometer operating at 399.794 MHz for proton and 100.54 MHz for carbon. Deuterated chloroform (CDCl_3) was used to dissolve the petroleum compounds for ^1H NMR analysis. The sample concentration was maintained approximately at 5.71 mg mL^{-1} CDCl_3 . All the ^1H NMR data were acquired using a 2.5 s acquisition time, 4799.0 Hz sweep width, a 45° pulse flip angle and a recycle delay of 0.10 s. The proton spectra were recorded by performing 128 scans and were referenced to the residual chloroform (CDCl_3) peak resonance at 7.26 ppm. The ^{13}C NMR spectra were recorded at a sweep width setting of 26990.6 Hz. Each liquid sample was maintained at a concentration of 0.05 g mL^{-1} of CDCl_3 containing 10% chromium (III) acetylacetonate [$\text{Cr}(\text{acac})_3$] as a paramagnetic relaxation agent in the presence of TMS in chloroform (0.15 $\mu\text{L g}^{-1}$) as an internal reference. All data were acquired using a pulse flip angle of 30°, a pulse

width of 3.2 Hz and a pulse repetition time of 3 s. The acquisition time and relaxation delay were 1 and 2 s respectively. The ^{13}C NMR spectra were recorded with 1000 scans and were referenced to the CDCl_3 resonance peak at 77.06 ppm. For each spectrum a 10 Hz line broadening was used for signal to noise ratio improvement. All ^1H and ^{13}C NMR peaks and percentage of each region were assigned and recorded in accordance with the data presented in Table 4-1 [30,31]. A procedure similar to the one for ^1H NMR was used for the ^2D NMR analysis, with CHCl_3 used as a solvent without any internal standard instead of CDCl_3 . All NMR analyses were conducted at the Department of Chemistry NMR facilities at the University of Alberta.

Table 4-1: Assignment of ^1H and ^{13}C NMR bands [30,31].

NMR peak range (ppm)	Assignment	Symbol
9.30-6.30	Hydrogen attached to aromatic carbons	H_{ar}
6.30-4.50	Hydrogen attached to olefinic carbons	H_{al}
4.50-1.85	Hydrogen attached to aliphatic carbons at α -position to an aromatic ring	H_{α}
1.87-1.00	Hydrogen attached to aliphatic carbons at β -position to an aromatic ring	H_{β}
1.00-0.50	Hydrogen attached to aliphatic carbons at γ - δ or positions further to an aromatic ring	H_{γ}
11.00-60.00	Aliphatic carbons	C_{al}
100.00-160.00	Aromatic carbons	C_{ar}

4.2.13 Energy dispersive X-ray (EDX) analysis

EDX analysis of the catalyst samples was conducted using a liquid nitrogen cooled lithium drifted silicon detector with a Norvar window (Princeton Gamma-Tech) attached to a JEOL 6301F field emission scanning electron microscope. The accelerating voltage used for the analysis was 20 kV.

4.2.14 Stable isotopic mass spectrophotometric analysis

A Finnigan MAT 252 stable isotope mass spectrometer was used to quantify deuterium incorporation in liquid products. The analyses were conducted at the Department of Earth and Atmospheric Sciences at the University of Alberta. 2-5 mg of liquid sample was placed in a copper foil and then carefully inserted into a quartz tube. Approximately 2.0 g of CuO and pure silver and copper wires were added to

convert sulfur and nitrogen oxides generated from the reactions. The tubes were evacuated at ~4 Pa vacuum to remove air and moisture, and sealed with a torch. The sealed tubes were placed in a furnace, preheated to 800 °C for 20-24 h, and then cooled gradually for another period of 12-24 h. The tubes were placed in a bath of dry ice and ethanol mixture to condense and separate combustion water vapor from the CO₂. The CO₂ was then collected in the vacuum line after breaking the tube, and then frozen in a separate liquid nitrogen trap. The collected water was removed from the tubes by heating at 80 °C under vacuum, then frozen in a sample tube containing 0.5 g of zinc metal, and finally converted to hydrogen gas for the mass spectrometric analysis. The concentrations of deuterium in the hydrogen gas, determined from mass spectrometric measurements, were used to calculate deuterium incorporation according to the following equation:

$$\%D \text{ incorporation} = \frac{\text{D in bitumen}}{\text{D added to reaction}} \times 100\% \quad (4-5)$$

4.3 RESULTS AND DISCUSSION

4.3.1 Characterization of feed

Dean Stark analysis indicates that the feed oilsands is a medium-high grade ore (~12 wt.% bitumen) with ~1 wt.% water and ~87 wt% solids. The maltenes and asphaltenes content are typical for Athabasca oilsands bitumen [32,33]. All characterization data including residue (566 °C+) [28] content, aromaticity, and aliphatic and aromatic hydrogen and carbon distribution are presented in Table 4-2.

Table 4-2: Characterization of feed oilsands and bitumen.

Fraction	Wt. %
Dean Stark analysis of oilsands	
Solids	86.9
Bitumen (Oil)	12.1
Water	1.0
Pentane-toluene extraction of bitumen	
Maltenes	76.7
C ₅ -asphaltenes	19.5
Insoluble organic solids	3.8

Table 4-2 (cont.): Characterization of feed oilsands and bitumen.

Fraction	Wt.%
Boiling point distribution of toluene-extracted bitumen by SIMDIST	
Naphtha (>191 °C)	0.0
Kerosine (191-277 °C)	2.0
Distillate Oil (277-343 °C)	9.2
Gas Oil (343-566 °C)	46.8
Residuum (566 °C+)	42.0
Aliphatic and aromatic H and C fractions of toluene-extracted bitumen by ¹ H and ¹³ C NMR	
¹ H _{al}	94.58
¹ H _{ar}	5.42
¹³ C _{al}	68.05
¹³ C _{ar}	31.95
Proton distributions of toluene-extracted bitumen by ¹ H NMR	
H _α	9.03
H _β	58.79
H _γ	26.04

4.3.2 Upgrading and product recovery

Addition of 3 wt.% water resulted in higher yields of residue free liquid, maltenes and gas fractions for both SC and CC catalyzed reactions compared to the analogous reactions conducted without water addition (Table 4-3). The increase in maltenes yield is due to a higher conversion of the heavier asphaltenes fraction. However, as the crackable components in the feed are exhausted, overcracking resulted in increased gas make. Such overcracking of feeds is typical in other catalytic cracking processes [34]. Water addition also increased the yield of the residue free liquid product from thermal reaction, although the amount was lower (~62 wt.%) compared to those of the NZ-catalyzed reactions (~68 wt.%).

Dry composition of gaseous products shows the increased catalytic effects of NZ-assisted reactions from water addition (Figure 4-1). SC and CC added reactions generate significantly higher amounts of C₂₊ fractions from catalytic carbocationic reactions [3] compared to the analogous reactions conducted without water addition. Moreover, water added catalytic reactions produce substantially larger amounts of paraffins, possibly by hydride ion transfer [3] compared to the waterless catalytic or

thermal reactions. This is also indicative of a higher extent of catalytic cracking in water-added NZ-assisted reactions. The water added thermal reaction, however, have a high paraffin fraction. Both water-added thermal and catalytic reactions produced large amounts of sour gases (H₂S and CO₂) from decarboxylation and desulfurization reactions.

Table 4-3: Products from thermal and 5 wt.% (of feed oilsands) NZ catalyzed reactions with 0 and 3 wt.% water addition, presented as percent of feed bitumen present in reactant oilsands.

Reaction products	Thermal reaction		SC catalyzed reaction		CC catalyzed reaction	
	<i>Water addition</i>					
	0%	3%	0%	3%	0%	3%
Residue Free Liquid	48.8%	62.2%	59.1%	67.5%	49.2%	68.3%
Total Liquid	95.4%	94.4%	95.7%	94.0%	97.3%	90.4%
<i>Maltenes</i>	75.1%	71.8%	79.5%	82.8%	68.1%	76.0%
<i>C₅-Asphaltenes</i>	20.3%	22.6%	16.2%	11.2%	29.2%	14.4%
Gas	4.6%	5.1%	3.4%	5.6%	2.7%	5.3%
Coke	0.0%	0.5%	0.9%	0.5%	0.0%	4.3%

* The standard deviations of the amounts of gas, maltenes, asphaltenes and coke make are 1.7, 3.4, 6.4 and 1.9 wt.% of feed bitumen respectively, based on three repeated experiments conducted on a single sample.

Water addition promoted cracking of the heavier fractions into lighter low boiling point products. Simulated distillation results (Table 4-4) show that the toluene-extracted liquid products from SC and CC catalyzed reactions conducted with water have smaller residue fractions compared to the analogous products from reactions conducted without water addition. It is worth noting that while the addition of water to all the reactions resulted in lower residue content compared to the raw bitumen, this effect was minimal on the thermal cracking reaction (34.1% compared to 42.0% in raw bitumen).

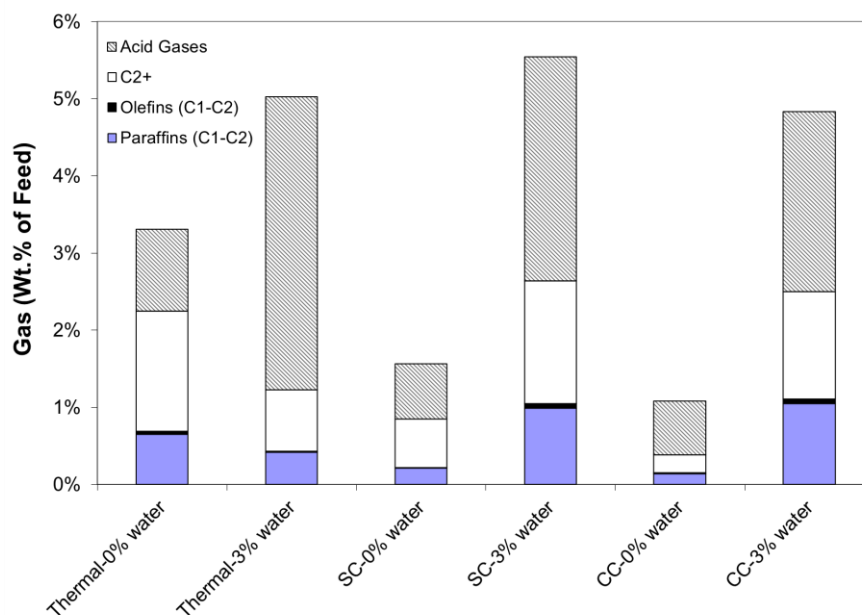


Figure 4-1: Composition of gaseous products from 0 and 3 wt.% (based on feed oilsands) water added thermal and NZ-catalyzed reactions.

Table 4-4: Petroleum fractions based on boiling point distribution of toluene-extracted liquid products from thermal and 5 wt.% (of feed oilsands) NZ catalyzed reactions with 0 and 3 wt.% water addition, as determined by SIMDIST analysis.

Boiling point fractions	Thermal reaction		SC catalyzed reaction		CC catalyzed reaction	
	<i>Water addition</i>					
	0%	3%	0%	3%	0%	3%
Naphtha (>191 °C)	1.9%	1.6%	1.7%	4.5%	2.8%	5.0%
Kerosine (191-277 °C)	3.4%	3.4%	1.2%	2.0%	2.9%	2.4%
Distillate Oil (277-343 °C)	7.9%	9.9%	8.0%	9.4%	6.2%	12.4%
Gas Oil (343-566 °C)	37.9%	51.0%	50.8%	56.0%	38.7%	55.9%
Residuum (566 °C+)	48.9%	34.1%	38.3%	28.1%	49.3%	24.3%

* The standard deviation of the boiling point fractions varied 1.5-3.8% from the mean value, depending on the fraction, as determined by three repeated experiments conducted on a single representative sample.

Interestingly both the thermal reaction and CC catalyzed reactions without water addition resulted in slightly higher residue content than the raw bitumen. This could be due to a number of factors. First, the concentration of the residue fractions in the remaining liquid may increase following conversion into gas, condensate and coke. The sand matrix and/or the catalysts may also cause polymerization of the compounds to increase the residue fraction within bitumen. Another possible explanation is the dismutation of the resins fraction, typically observed in visbreaking operations at mild temperatures, which can destabilize and therefore increase the heavy fractions in bitumen [35].

Further evidence of the impact of water addition on catalytic cracking reactions is demonstrated by the lower average molecular weight and viscosity values of the liquid products (Figures 4-2 and 4-3) compared to those of the products from analogous reactions conducted without water. Water addition also reduced the average molecular weight of the liquid product during the thermal reaction but the same was not true for its viscosity. Viscosities of the liquid products are highly sensitive to generation of lighter components which may act as diluents, reducing the overall viscosity of bitumen despite the remaining significant amounts of heavy constituents.

In summary, the results of the upgrading reactions demonstrate that water addition significantly enhances the cracking ability of the NZ catalysts.

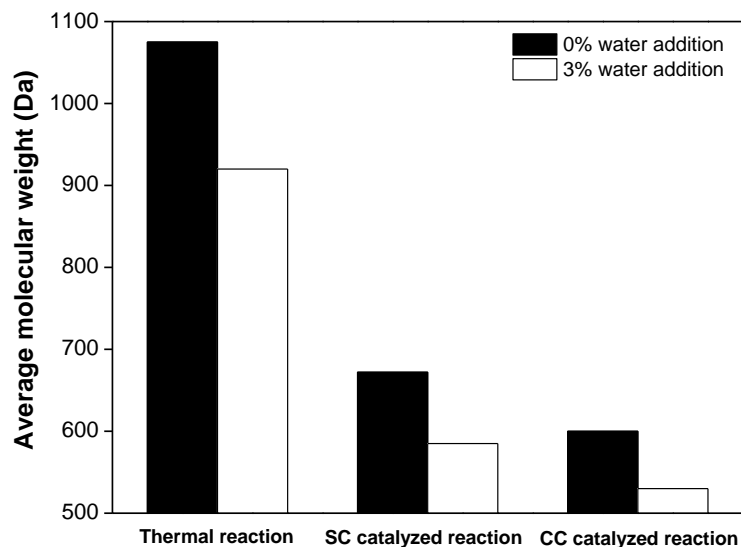


Figure 4-2: Average molecular weight (AMW) of liquid products from 0 and 3 wt.% (of feed oilsands) water-added thermal and 5 wt.% NZ-catalyzed cracking of oilsands, determined by vapor pressure osmometry. The standard deviation of AMW of a product is 1.6%, based on three repeated experiments performed on a single representative sample.

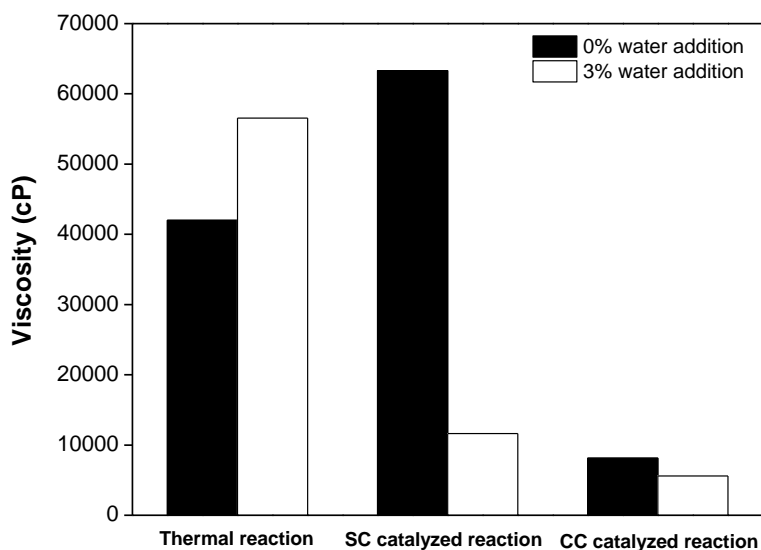


Figure 4-3: Viscosity of the liquid products from 0 and 3 wt.% (of feed oilsands) water-added thermal and 5 wt.% NZ-catalyzed cracking of oilsands, measured at 50 °C. The standard deviation of viscosity of liquid products is 3.0%, based on five repeated experiments performed on a single representative sample.

4.3.3 Characterization of product bitumen by ^1H and ^{13}C NMR

The ^1H and ^{13}C NMR results show a slight decrease in aliphatic hydrogen (H_{al}) in liquids from catalytic reactions with the addition of water (runs 3 to 4, and 5 to 6 in Table 4-5). Generally, a greater increase in aromaticity (C_{ar}) with water addition is observed for thermal cracking (runs 1 to 2) compared to NZ-assisted cracking reactions (runs 3 to 4, and 5 to 6). Increase in C_{ar} suggests the possibility of some aromatization occurring via cyclization reactions, and/or dehydrogenation of cyclic compounds, and/or loss of aliphatic carbons from gas make. Correspondingly, aromatic hydrogen (H_{ar}) of liquid products from catalyzed reactions increases, while the opposite is observed for the thermal reaction (Table 4-5).

Table 4-5: Characterization of toluene-extracted liquid products from 0 and 3 wt.% (of feed oilsands) water-added thermal and 5 wt.% NZ-catalyzed reactions by ^1H and ^{13}C NMR.

Sample	Run	Water addition (wt.% of oilsands)	$\text{H}_{\text{ar}}(\%)$	$\text{H}_{\text{al}}(\%)$	$\text{C}_{\text{ar}}(\%)$	$\text{C}_{\text{al}}(\%)$
Thermal	1	0	7.4	92.6	34.2	65.8
	2	3	7.2	92.8	37.6	62.5
SC	3	0	8.3	91.7	31.7	68.3
	4	3	9.2	90.8	33.8	66.2
CC	5	0	8.1	91.9	36.1	64.0
	6	3	9.4	90.6	34.9	65.1

* Typical error associated with NMR analysis of bitumen samples is $\pm 5.0\%$.

The ^1H NMR results (Table 4-6) show that water addition generally increased the H_{α} fraction of the aliphatic components in both thermally cracked and catalyzed reactions. In thermal cracking, the aliphatic chains bonded to the aromatic rings are broken and hydrogen radical is added from water to the benzyl radicals [7], increasing the H_{α} fraction. Similarly in the catalytic reactions the aliphatic chain is cracked at the β -position to the aromatic ring by benzyl carbocation generation, which then abstracts a hydride ion (from a catalyst hydride) to form an alkyl aromatic compound, increasing the H_{α} fraction. Benzyl carbocations are more stable than 1, 2 and 3 $^{\circ}$ carbocations [16], and hence is the favored product). Methylation of the

aromatic rings may also yield the same result, although will be rare because of the low rate of formation for methyl carbocation [3]. The H_α fraction generated from thermal cracking is larger than that from the catalytic reactions while the opposite is true for H_β and H_γ fractions.

Table 4-6: Proton distributions of aliphatic chains in toluene-extracted liquid products from 0 and 3 wt.% (of feed oilsands) water-added thermal and 5 wt.% NZ-catalyzed reactions by ^1H NMR.

Sample	Run	Water addition (wt.% of oilsands)	H_α (%)	H_β (%)	H_γ (%)
Thermal	1	0	16.7	54.2	21.7
	2	3	20.8	56.0	17.2
SC	3	0	9.3	58.2	24.2
	4	3	18.8	54.9	18.2
CC	5	0	11.6	60.1	20.2
	6	3	12.5	60.0	19.9

4.3.4 Proton incorporation from water addition

The upgrading reaction results showed that water addition significantly increases cracking and enhances product quality. Product characterization by ^{13}C and ^1H NMR demonstrated that water addition impacts the liquid product composition and distribution. In order to understand the important role of water in NZ-catalyzed upgrading, it is essential to trace its incorporation from the beginning. 3 wt.% D_2O -doped (as a substitute of water) reactions and isotopic analysis of the toluene-extracts were conducted to investigate incorporation of the added water to the liquid products. The results show that 52.7% of the total deuterium used in the CC-catalyzed reaction was incorporated in the liquid products, followed by 26.0% for the SC-catalyzed reaction (Table 4-7). Thermal reaction on the other hand, incorporated only 19.6% of the added deuterium. The results clearly indicate incorporation of large numbers of protons to the liquid products by analogous water-added catalyzed reactions.

Deuterium distribution by ^2D NMR shows that for both thermal and catalytic reactions the majority of the proton incorporation (~73-82%) from water to bitumen

takes place in the aliphatic fractions (D_{al}) (Table 4-7). 1H and ^{13}C NMR results show a slight decrease in aliphatic hydrogen (H_{al}) with the addition of water (Table 4-5). Combined, these results suggest that protons from the added water participate mainly in the rearrangement and substitution reactions in the aliphatic chains. The distribution also shows incorporation of deuterium at all positions of the crude oil molecules that can be differentiated by 2D NMR, which is in agreement with previous reports on tracer-based experiments conducted on extra-heavy crude oil [7]. The catalytic cracking reactions, however, had more incorporation at β - (D_{β}) and γ -positions (D_{γ}) and less incorporation at α -positions (D_{α}) of the aliphatic chains compared to the analogous thermal reactions. This is in general agreement with the proton distribution of products by 1H NMR (runs 2, 4 and 6, Table 4-6), and also with the literature reports on preferential enrichment of D_{α} in the rings or chains for thermal reactions in the presence of water [7]. This enrichment, observed in thermal reactions, progresses via deuterium abstraction by benzyl radicals. Deuterium distribution also shows substantial incorporation in the aromatic rings (D_{ar}) indicating substitution and/or dehydrogenation of cyclic compounds and/or aromatization by cyclization reactions from water addition, which is consistent with the 1H and ^{13}C NMR findings.

Table 4-7: Deuterium incorporation and distribution of toluene-extracted bitumen from 3 wt.% (of feed oilsands) D_2O added reacted oilsands, determined by stable isotopic and 2D NMR analyses.

Run	Sample	Deuterium incorporation (%)	Deuterium distribution				
			D_{ar} (%)	D_{al} (%)			
				Total	D_{α}	D_{β}	D_{γ}
1	Thermal	19.6	20.7	81.3	59.9	18.8	0.6
2	SC	26.0	27.4	72.6	45.1	23.4	4.1
3	CC	52.6	17.9	82.1	40.0	34.8	7.4

The catalyzed reactions are found to incorporate much larger amounts of D_2O than the analogous thermal reactions. It is therefore evident that with water added NZs, protons are transferred to liquid products mainly via catalytic reactions. Water addition generates acid sites on the NZ surface by hydrolysis reactions in

presence of multivalent cations, as demonstrated in Schemes 1 [19-21] and 2 [17,18]. These acid hydroxyl groups then supply protons to participate in carbocation-based cracking. Ultimately, these protons are incorporated into liquid products following a series of reactions. The limited proton incorporation from the water-added thermal reaction is possibly due to the activity of the silica-alumina sand matrix.

4.3.5 Acid hydroxyl groups on raw NZ surface

Having found evidence for proton incorporation from water-added catalytic reactions, the next logical step was to investigate the presence of hydroxyl groups on the catalyst surface. ^{29}Si and ^1H NMR analyses showed that acid hydroxyl groups are present on raw hydrated NZ catalysts but are absent or suppressed in their calcined forms. NMR spectra show a peak at ~ 94 ppm (Figures 4-4(a) and (c)), that corresponds to the SiOH group in the zeolite lattice. The peak value is consistent with reported literature data [36]. NMR analysis also shows that this peak is either absent (CC), or present only as a small shoulder (SC) (Figure 4-4(d) and (b)) in the spectra for the calcined forms of the catalysts, confirming that the hydroxyl groups are generated from hydration. This is further supported by the EDX analysis results: Ca^{+2} and Mg^{+2} , multivalent cations essential for formation of acid hydroxyl groups (Schemes 1 and 2), are present in substantial quantities on the raw uncalcined catalyst surface (Table 4-8).

FTIR analysis further confirms the presence of acid hydroxyl groups and physically adsorbed water on raw hydrated NZ catalysts (Figure 4-5). Reported values for OH- stretching frequencies on zeolite surfaces range between 3520-50 and 3640-50 cm^{-1} [37,38]. Particularly, structural hydroxyl groups generated from cation hydrolysis or NH_4^+ -exchange are observed between 3540-50 and 3640-50 cm^{-1} [37,39]. The peaks at 3541 and 3547 cm^{-1} on raw SC and CC respectively correspond to this group. The IR spectra also show presence of peaks at ~ 3650 cm^{-1} , although these are difficult to distinguish due to overlapping (Figure 4-5). A small peak at 3624 cm^{-1} for raw, NH_4^+ -exchanged and H^+ -form of SC is observed. According to Bolton this peak is attributed to both OH- formation by H^+ liberated from hydrolysis and the lattice oxygen, and H^+ -exchange [38]. Physically adsorbed water (3280-90 and 1631-41 cm^{-1}) especially on the raw form of the catalysts and a large peak (1041-62 cm^{-1}) due to Si-O-Si bonds [40] are also observed.

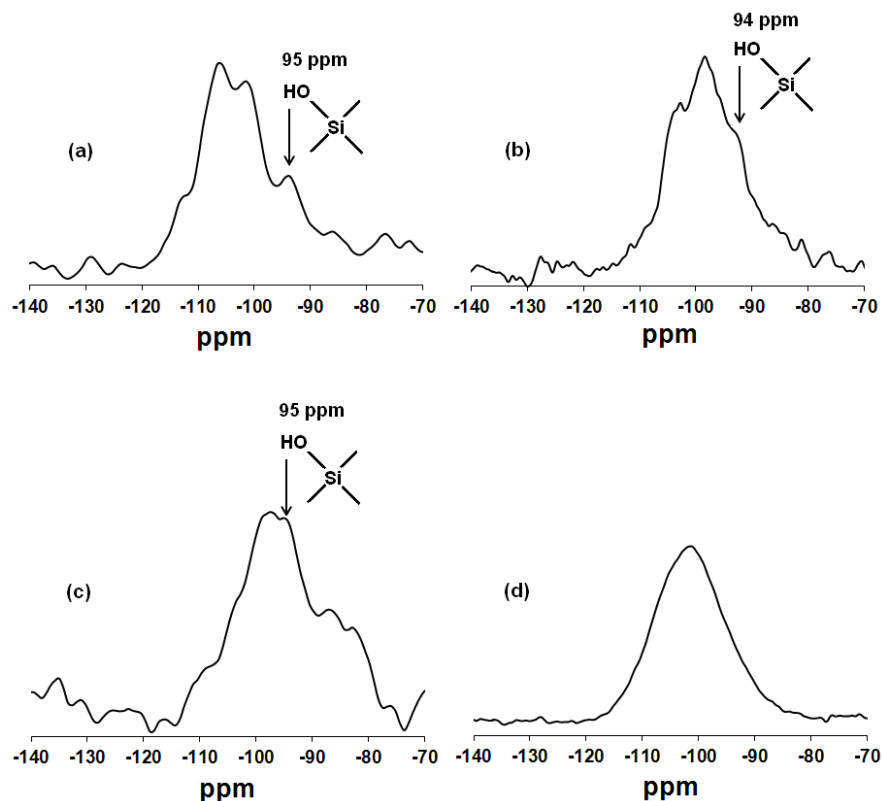


Figure 4-4: High-resolution ^{29}Si NMR of (a) uncalcined SC (b) calcined SC (c) uncalcined CC and (d) calcined CC catalyst.

Table 4-8: Atomic composition of the raw and protonated forms of the SC and CC catalysts determined by EDX analysis.

Elements	Atomic Wt. (%)			
	SC		CC	
	Raw form	Protonated-form	Raw form	Protonated-form
Na	0.00	0.00	5.99	1.35
K	1.15	0.76	0.47	0.38
Ca	1.45	0.34	0.73	0.20
Mg	0.93	0.50	0.42	0.44
Al	6.40	6.67	7.08	7.88
Fe	0.73	0.69	1.52	1.38
Ti	0.00	0.00	0.00	0.05
Si	25.36	26.38	22.42	24.49
O	64.00	64.67	61.36	63.81

* Typical error associated with EDX analysis of samples is <0.1%.

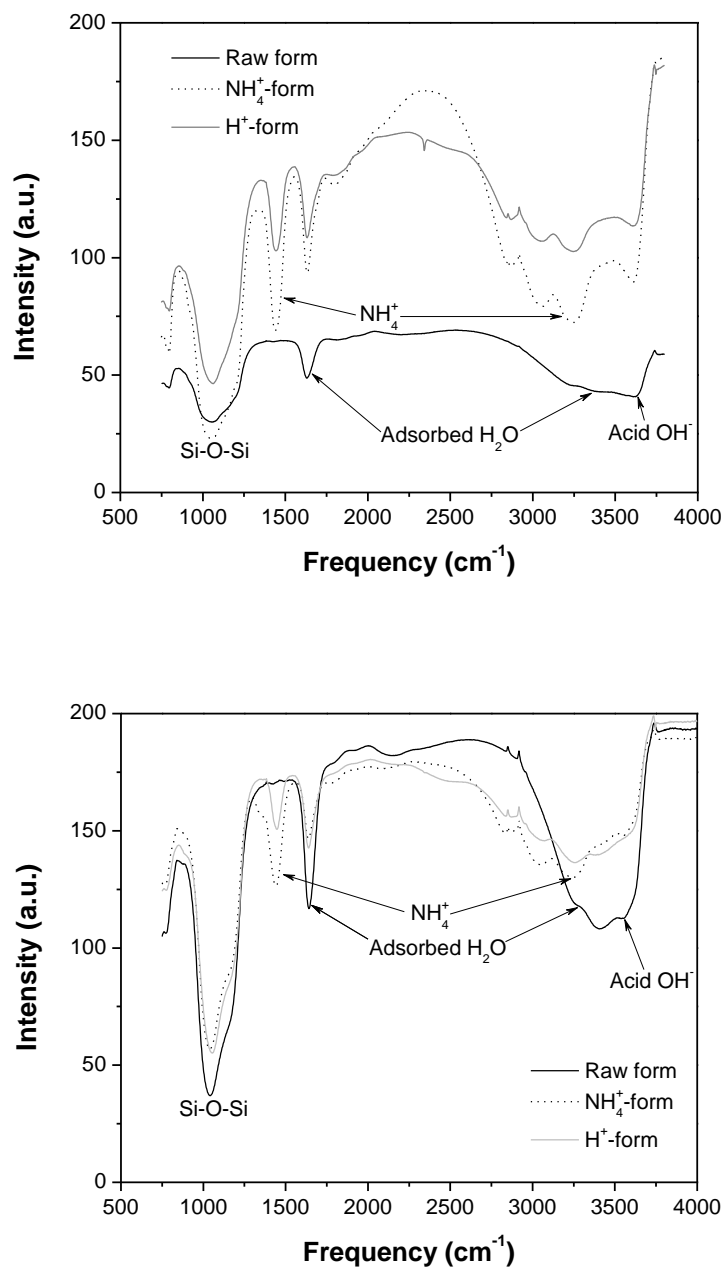


Figure 4-5: FTIR analysis of raw, ammonium-exchanged (NH₄⁺-form), and ammonium-exchanged and calcined (H⁺-form) SC (top) and CC (bottom) catalysts.

The FTIR peaks for OH- stretching and adsorbed water are absent or suppressed in the NH_4^+ -exchanged and H^+ -forms of the catalyst. The peak intensities related to OH- stretching ($\sim 3550\text{-}3560\text{ cm}^{-1}$) are generally lower in the NH_4^+ -exchanged and H^+ -forms of the catalysts compared to the raw hydrated forms. In the NH_4^+ -exchanged forms of the catalysts the additional bands for NH_4^+ (~ 3244 and 1442 cm^{-1}) are formed at the expense of those for OH- stretching. Proton formation by NH_4^+ -exchange exhausts the divalent metal ions from the zeolite surfaces (Table 4-8), eliminating or reducing the hydroxyl groups formed by hydrolysis. This indicates that while the catalytic cracking activity of the H^+ -forms of the NZs (Chapter 3) [1] is due to the Brønsted acid sites generated by NH_4^+ -exchange, the greater activity of the raw catalysts is due to the larger amounts of Brønsted sites generated by hydrolysis reactions from water addition.

4.3.6 Carbocationic reactions using water-added NZs

As discussed in the preceding sections, NMR and FTIR analyses detected presence of acid sites on the raw hydrated catalysts generated from water. Stable isotopic mass spectrophotometric analysis and proton and deuterium distribution by NMR analysis suggest the possibility of different catalytic reactions such as: aromatization, rearrangement and substitution in the aliphatic chains, β -scission, dehydrogenation, and increased hydrogen enrichment at β - and γ -positions. This section incorporates these findings to illustrate some possible reactions occurring during catalytic cracking of bitumen by self-acidified NZs.

Catalytic cracking of bitumen is an ionic process during which carbocations generated by the catalysts participate in the chemical transformation of the organic compounds. Water addition generates Brønsted and Lewis acid sites on raw NZ catalysts by cation hydrolysis (Schemes 1 and 2), which then generate carbocations via three possible mechanisms: (1) by protons supplied directly from the Brønsted acid sites; (2) by protons generated from the hydrolysis reactions (Equations 4-1 and 4-2); and (3) by hydride ion abstraction by the Lewis acid sites of the catalysts.

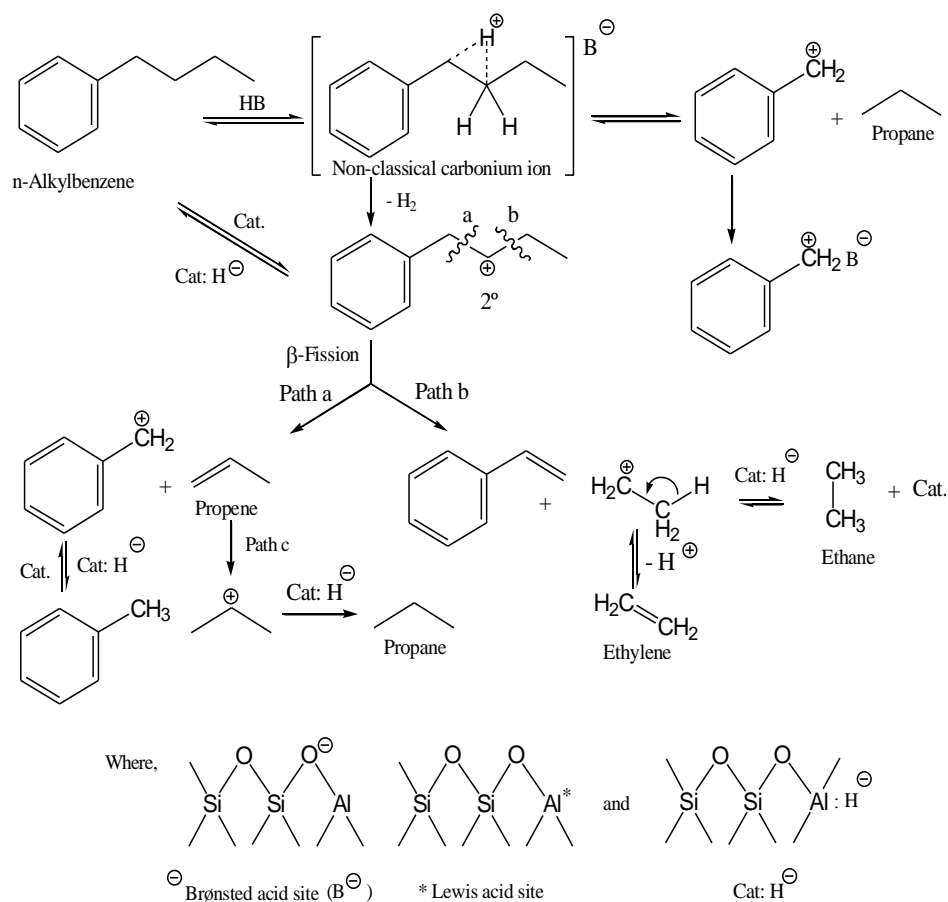
A simplified conversion mechanism for the alkyl aromatic constituents of bitumen is presented in Scheme 3 by a representative molecule. This, of course, is one of the many possible reaction schemes, speculated to provide a general understanding only of the complex nature of catalytic conversion of bitumen by

hydrolyzed acid catalysts. The side chain, upon reaction with a proton supplied by a Brønsted acid site on the hydrolyzed catalyst, forms a non-classical pentacoordinated carbonium ion [41,42] which readily undergoes decomposition to form a 2° carbocation. Alternatively, the carbocation may be generated via hydride ion abstraction by the Lewis acid site of the catalyst. In either case the carbocation may undergo β -scission and follow two different pathways: (a) initially producing a primary carbocation and an olefin, which, abstracting a proton from the Brønsted site and generating another 2° carbonium ion (Path (c)) interacts with the catalyst hydride (cat:H-) to produce a paraffin; or (b) initially generating an unstable 1° carbocation which readily undergoes deprotonation, or in presence of a Lewis acid site, hydride addition to produce an olefin or paraffin respectively. Possibly, in the absence of water, Brønsted and Lewis sites are not available for conversion of the formed olefins to paraffins. A hydrated catalyst, on the other hand, is able to produce paraffin via carbocation generation by Brønsted sites followed by hydride ion abstraction and supply by Lewis acid sites, or by hydride ion abstraction and supply by Lewis acid sites alone. Following either of these pathways, the hydrated catalyst generates more paraffinic gases than olefins (Scheme 3) compared to the waterless catalysts, which is consistent with the experimental data on gas production and composition presented in Table 4-3 and Figure 4-1.

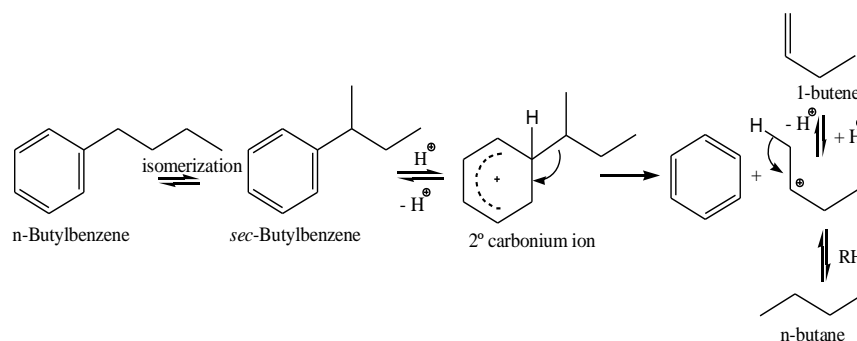
The pentacoordinated carbonium ion may also decompose to a paraffin molecule and a primary carbocation, which, just like the benzyl carbocation formed by pathway (a), may undergo a hydride addition at α -position from a catalyst hydride to form an alkyl aromatic compound (Scheme 3). This is consistent with the NMR results that demonstrate preferential enrichment of protons at α -positions (Tables 4-6 and 4-7).

Addition of a proton from a Brønsted site, or a proton generation reaction (Equations 4-1 and 4-2) to the aromatic ring of a sec-alkyl aromatics produces a 2° carbocation by dealkylation as well as an aromatic molecule (Scheme 4). Subsequent deprotonation (by the catalyst) or hydride transfer to the alkyl carbonium ion produces an olefin or a paraffin compound respectively. In both Schemes 3 and 4, the gaseous compounds generated from conversion of carbocations make the liquid products concentrated and enriched in aromatics, which is consistent with the general increase in aromaticity and decrease in aliphaticity in liquid products from catalyzed

reactions, as shown by the ^1H and ^{13}C NMR data (Table 4-6). Aromaticity may also increase due to cyclization reactions of the hydrocarbon chains, which progress via hydride abstraction by the Lewis sites and deprotonation by the catalyst, leading to the formation of aromatic rings [43]. This can explain the increase in H_{ar} and C_{ar} and simultaneous decrease in H_{al} and C_{al} in the liquid products from water added catalyzed reactions.



Scheme 3: Possible conversion mechanism for a representative alkyl aromatic molecule by cracking with water-added NZ catalysts. The double headed arrow indicates double electron transfer.



Scheme 4: Dealkylation of alkyl aromatics to produce aromatics and light hydrocarbons. The double headed arrows indicate double electron transfer.

4.4. CONCLUSIONS

Two established oilsands cracking agents, Clinoptilolite and Ca-chabazites, demonstrate remarkable catalytic activity in their raw state with the addition of 3 wt.% water. This moderate water addition causes self-acidification of the zeolite surface and generates Brønsted and Lewis acid sites by hydrolysis reactions. The protons generated from the added water undergo a series of surface reactions involving the acidic sites to actively participate in catalytic cracking of heavy molecules in bitumen, before incorporating into the liquid products. Water addition essentially eliminates the requirement for the ammonium-exchange step needed for acidification of the catalysts, offering great advantages for practical application.

(A version of this chapter is in preparation for submission as a journal article. *Junaid ASM, Rahman MM, Wang W, Street C, McCaffrey WC, Kuznicki SM. On the role of water in natural zeolite catalyzed cracking of oilsand bitumen: method and mechanism. Energy & Fuels. Expected submission: October 2011.*)

BIBLIOGRAPHY

- [1] Junaid ASM, Yin H, Koenig A, Swenson P, Chowdhury J, Burland G, McCaffrey WC, Kuznicki SM. Natural zeolite catalyzed cracking-assisted light hydrocarbon extraction of bitumen from Athabasca oilsands. *Appl Catal A: Gen* 2009; 354: 44-9.
- [2] Schwochow F, Puppe L. Zeolites-Their synthesis, structure, and applications. *Angew Chem Inter* 1975; 14: 620-8.
- [3] Raseev S. Thermal and catalytic processes in petroleum refining. New York: Marcel Dekkar, Inc.; 2003.
- [4] Wang W. Catalytic cracking of Athabasca Oilsands Using Clinoptilolite [dissertation]. Edmonton (AB): University of Alberta; 2010.
- [5] Lewan MD. Role of water in petroleum formation. *Energy Fuels* 1997; 61: 3691-23.
- [6] Song C, Saini AK, Schobert HH. Effects of drying and oxidation of Wyodak subbituminous coal on its thermal and catalytic liquefaction: Spectroscopic characterization and products distribution. *Energy Fuels* 1994; 8: 301-12.
- [7] Ovalles C, Hamana A, Rojas I, Bolivar RA. Upgrading of extra-heavy crude oil by direct use of methane in the presence of water. *Fuel* 1995; 74: 1162-8.
- [8] Alexander R, Kagi RI, Larcher AV. *Geochim Cosmochim Acta* 1982; 46: 219-22.
- [9] Werstiuk NH, Ju C. Protium-deuterium exchange of benzo-substituted heterocycles in neutral D₂O at elevated temperatures. *Can J Chem* 1989; 67: 812-5.
- [10] Hoering TC. Thermal reactions of kerogen with added water, heavy water and pure organic substances. *Org Geochem* 1984; 5: 267-78.
- [11] Stalker L, Larter SR, Farrimond P. Biomarker binding into kerogens: evidence from hydrous pyrolysis using heavy water (D₂O). *Org Geochem* 1998; 28: 238-53.
- [12] Lewan MD. Thermodynamics of reactions involving H₂O and hydrocarbon radicals between 27 and 374 °C. *Prepr Pap-Am Chem Soc, Div Fuel Chem* 1999; 44: 420-2.
- [13] Clark KA. Bituminous sands of Alberta. *Oil Weekly* 1945; 118: 46-51.
- [14] Clark KA. New technique taps Athabaska tar sands. *World Oil* 1951; 132: 205-8.

- [15] Masliyah J. Fundamentals of oilsands extraction (ChE 534 Course Materials). Edmonton (AB): University of Alberta; 2011.
- [16] Dutta RP, McCaffrey WC, Gray M. Thermal cracking of Athabasca bitumen: Influence of steam on reaction chemistry. *Energy Fuels* 2000; 14: 671-6.
- [17] Uytterhoeven JB. Hydrogen held by solids. XVI. Infrared spectroscopy of X- and Y-type zeolites containing univalent and divalent cations. *J Catal* 1969, 13: 425-34.
- [18] Breck, DW. Zeolite Molecular Sieves: Structure, Chemistry and Use, New York: John Wiley & Sons Inc.; 1974, p. 460-5.
- [19] Ward JW. Nature of active sites on zeolites. III. The alkali and alkaline earth ion-exchanged forms. *J Catal* 1968; 10: 34-46.
- [20] Ward JW. Spectroscopic study of the surface of zeolite Y. II. Infrared spectra of structural hydroxyl groups and adsorbed water on alkali, alkaline earth, and rare earth ion-exchanged zeolites. *J Phys Chem* 1968; 72: 4211-23.
- [21] Ward JW, Nature of active sites on zeolites. IV. Influence of water on the acidity of X and Y type zeolites. *J Catal* 1968; 11: 238-50.
- [22] Dutta RP, McCaffrey WC, Gray M. Use of ¹³C tracers to determine mass-transfer limitations on thermal cracking of thin films of bitumen. *Energy Fuels* 2001; 15: 1087-93.
- [23] Steer JG, Muehlenbachs K. Stable isotope analysis of hydrogen transfer during catalytic hydrocracking of residues. *Energy Fuels* 1992; 6: 540-4.
- [24] Sanford CS. Residuum hydrocracking with supported and dispersed catalysts: Stable hydrogen and carbon isotope studies on hydrogenation and catalyst deactivation. *Energy Fuels* 1995; 9: 928-35.
- [25] Dean EW, Stark DD. A Convenient method for the determination of water in petroleum and other organic emulsions. *J Ind Eng Chem* 1920; 12: 486-90.
- [26] Villalanti DC, Raia JC, Maynard JB. High-temperature simulated distillation applications in petroleum characterization. In: Meyers RA, editors. *Encyclopedia of analytical chemistry*, Chichester: John Wiley & Sons Ltd; 2000, p. 1-15.
- [27] Standard test method for determination of boiling range distribution of crude petroleum by gas chromatography, ASTM D 5307-97 (Reapproved 2007). Philadelphia: American Society for Testing and Materials; 2007. p. 1-7.
- [28] Giles HN. Analysis of crude oils. In: Drews AW, editor. *ASTM manual on hydrocarbon analysis*, ASTM Manual Series, MNL 3. 4th ed. Philadelphia: American Society for Testing and Materials; 1989. p. 20-7.

- [29] Standard test method for relative molecular mass (molecular weight) of hydrocarbons by thermoelectric measurement of vapor pressure, ASTM D 2503-92 (Reapproved 2007). Philadelphia: American Society for Testing and Materials; 2007. p. 1-3.
- [30] Gillet S, Rubini P, Delpuech J-J, Escalier J-C, Valentin P. Quantitative carbon-13 and proton nuclear magnetic resonance spectroscopy of crude oil and petroleum products. I. Some rules for obtaining a set of reliable structural parameters. *Fuel* 1981; 60: 221-5.
- [31] Díaz C, Blanco CG. NMR: A powerful tool in the characterization of coal tar pitch. *Energy Fuels* 2003; 17: 907-13.
- [32] Agarwala M, Yarranton W. An asphaltene association model analogous to linear polymerization. *Ind Eng Chem Res* 2001; 40: 4664-72.
- [33] Peramanu S, Pruden B, Rahimi P. Molecular Weight and Specific Gravity Distributions for Athabasca and Cold Lake Bitumens and Their Saturate, Aromatic, Resin, and Asphaltene Fractions. *Ind Eng Chem Res* 1999; 38: 3121-30.
- [34] Ding F, Ng SH, Xu C, Yui S. Reduction of light oil catalytic cracking of bitumen-derived crude HGOs through catalytic selection. *Fuel Process Technol* 2007; 88: 833-45.
- [35] Casalini A, Mascherpa A, Vecchi C. Modifications induced by visbreaking on composition and structure of atmospheric residues. *Fuel Sci Technol Inter* 1990; 8: 427-45.
- [36] Lippmaa E, Magi M, Samoson A, Tarmak M., Engelhardt G. Investigation of the structure of zeolites by solid-state high-resolution ^{29}Si NMR spectroscopy. *J Am Chem Soc* 1981; 103: 4992-6.
- [37] Corma A, Agudo AL, Fornés V. Infrared spectroscopic evidence for the presence of H^+ (H_2O)_n ions in a decationated Y-type zeolite. *J Chem Soc Commun* 1983; 557: 942-4.
- [38] Bolton AP. The nature of rare-earth exchanged Y zeolites. *J Catal* 1971; 22: 9-15.
- [39] Farneth WE, Gorte RJ. Methods for characterizing zeolite acidity. *Chem Rev* 1995; 95: 615-35.
- [40] Engelhardt VG, Kriegsmann H. Spektroskopische Untersuchungen an Siliciumverbindungen. XXVIII) Spektroskopische Untersuchungen zur Struktur der Silicium--Sauerstoff-Bindung in einigen substituierten Disiloxanen. *Zeitschrift für anorganische und allgemeine Chemie* 1965; 336: 286-294. German.

- [41] Boronat M, Corma A. Are carbenium and carbonium ions reaction intermediates in zeolite-catalyzed reactions? *Appl Catal A: Gen* 2008; 336: 2-10.
- [42] Haag WO, Dessau RM. Duality of mechanism for acid catalyzed paraffin cracking. In: *Proceedings of the Eighth International Congress on Catalysis*, Vol.2, 2nd ed., Berlin: Verlag Chemie, 1984; p. 305-16.
- [43] Hatch LF. A chemical view of refining. *Hydrocarb Process* 1969; 48: 77-88.

Activated Natural Zeolite-Based Integrated Extraction and Low Severity Upgrading

5.1 INTRODUCTION

As described in Chapter 1, bitumen extraction and upgrading from oilsands is associated with unique operational and quality issues. A substantial fraction of bitumen is heavy residue, which makes it too viscous for pipeline transportation to refining facilities [1-4], and requires the addition of naphtha, gas condensates, or other diluents to meet pipeline specifications [3,4]. Oilsands bitumen has a high asphaltene and polar resin content and a corresponding high boiling point distribution. It also has high heteroatom (N, S) and heavy metal (Ni, V and others) contents, and a low H/C ratio [1,2,5], all of which necessitate extensive treatment prior to conversion to useable fuels. In addition, conventional methods of bitumen extraction consume multiple barrels of fresh water that is discarded as waste in the tailings ponds, creating environmental issues [6,7].

Conventional primary upgrading techniques to reduce the heavy bitumen fractions to lighter hydrocarbons involve coking, thermal or catalytic cracking, visbreaking and hydrogen-added operations [2,5,8]. Severe thermal techniques such as delayed or fluid coking, with operating temperatures in the range of 487 to 537 °C

[9], produce somewhat lighter oil after hydrotreating, but result in large amounts of oil loss by carbon rejection from coke and gas make and considerable operational problems [4,5]. Typical synthetic crude oil (SCO) yield, coke make and gas make in these processes vary between 70.3-74.9%, 15.6-22.1% and 8.7-8.9 wt.%, respectively, after hydrotreating [4]. Loss of yield (typical yield) by carbon rejection has important economic implications, and a great deal of effort is directed to designing more efficient methods [4]. Visbreaking, a relatively mild and less expensive thermal cracking process, reduces the viscosity of bitumen but cannot significantly impact the boiling point distribution [8]. Visbreaking also produces less stable products at higher conversion [10] and some coke by polymerization and condensation reactions [2].

Upgrading techniques as hydroconversion, hydrocracking, hydrovisbreaking and hydrotreating involving hydrogen addition and/or simultaneous carbon rejection often either follow conventional coking processes [8], or are integrated into unique processes such as LC-Fining or H-Oil [4,9]. Despite their higher liquid product yields (58.0-89.2 wt.%), the value of these techniques is reduced by the high cost of catalysts and commodity hydrogen, capital costs, and substantial gas (2.1-14.7 wt.%) and coke make (5.2-15.4 wt.%) [4,9]. These methods also encounter reduced catalyst function due to inactivation by both trace metals in the visbreaking products and polymer formation from nitrogen and oxygen functional groups on the catalyst surface [5].

Compared to hydrogen-based processes, fluidized catalytic cracking (FCC) is a relatively low capital cost [11], high yield (85.1 wt.%) method employed in refineries to convert the SCO into middle distillates [11]. FCC, however, is applicable to pre-upgraded oil only [11,12] and requires even higher operating temperatures (524-529 °C) [9] and frequent catalyst regeneration as the heteroatoms in the oil quickly deactivate the expensive catalysts [12]. FCC processes also result in significant losses in yield by carbon rejection (10.8 wt.% coke) and gas make (4.1 wt.%).

To summarize, the large number of distinct steps involved in separate extraction and upgrading processes make bitumen processing highly capital-intensive and complicated. There is currently no single extraction and upgrading method for

oilsands bitumen that is effective, economical, and able to address all of the associated production and environmental issues.

The potential of natural zeolites (NZ) for oilsands bitumen cracking was reported in Chapter 3. It was found that, under low-to-moderate cracking conditions, the addition of ~10 wt.% ion-exchanged chabazites and clinoptilolites can convert the heavy fractions of oilsands bitumen into smaller components that can be easily extracted using light hydrocarbon solvents, eliminating the need for water extraction. The study demonstrated the potential of NZs as effective, economical and environmentally friendly catalysts for the rapidly growing oilsands industry. A follow up study found that with the addition of 3 wt.% water (less than one-tenth of the amount used in current conventional methods), untreated natural clinoptilolite and chabazite undergo self-acidification and act as very effective cracking agents even under low severity reaction conditions (Chapter 4). This eliminates the ion-exchange and preparation steps required to acidify these catalysts, simplifying their potential industrial application. If the high activity of these self-acidified NZs can be utilized in an engineered system with proper mixing, the catalyst loading and reaction temperature can be further reduced to develop a practical and economic process for integrated extraction and low temperature upgrading of oilsands bitumen. This chapter presents a systematic study on a scaled-up engineered system with mixing designed for solid oilsands cracking with reduced loadings of self-acidified NZ-catalysts. This study is intended to quantify the performance of the NZ-based process for potential larger (pilot/industrial) scale application. The performance of the process had been evaluated with respect to the total and residue-free oil recovery, and product quality (boiling point distribution, viscosity, average molecular weight, aromaticity, heteroatoms and heavy metals contents etc.).

5.2 MATERIALS AND METHODS

5.2.1 Materials

Finely ground (<44 μm particles) clinoptilolite (SC) and sedimentary Ca-chabazite (CC) samples were obtained from the deposits in St. Cloud, New Mexico and Bowie, Arizona, respectively.

Athabasca oilsands sample were obtained from the Syncrude Facility at Mildred Lake near Fort McMurray, Alberta, Canada. The oilsands samples were thoroughly mixed, homogenized and refrigerated prior to use. The analysis showed that the oilsands used in the study is a medium-high grade ore with oil and water contents as shown in Table 5-1. The measured maltenes, asphaltenes, heteroatoms and metals contents are in good agreement with the reported literature values for typical Athabasca bitumen [13-15].

Table 5-1: Composition of untreated feed oilsands and extracted bitumen.

Fraction	Amount
<i>Dean Stark analysis on feed oilsands</i>	
	<i>Wt.%</i>
Solids	86.9
Bitumen (oil)	12.1
Water	1.0
<i>Pentane-toluene extraction of bitumen</i>	
	<i>Wt.%</i>
Maltenes	76.7
C ₅ -asphaltenes	19.5
Insoluble organic compounds	3.8
<i>Boiling point distribution of toluene-extracted bitumen by SIMDIST and mass balance</i>	
	<i>Wt.%</i>
Naphtha (>191 °C)	0.0
Kerosene (191-277 °C)	2.0
Distillate Oil (277-343 °C)	9.2
Gas Oil (343-566 °C)	46.8
Residuum (566 °C+)	42.2
<i>Heteroatoms and metals contents of toluene-extracted bitumen by elemental analysis and INAA</i>	
Nitrogen	0.65 wt.%
Sulfur	5.18 wt.%
Vanadium	228 ppm

5.2.2 Test reactions

Catalytic cracking reactions were performed in a large custom-designed, stainless steel Parr autoclave (~1000 cm³ capacity) equipped with a spiral scraper-type impeller specially designed for handling oilsands, and heated with a 15 A, 115 V heating jacket. A detailed schematic diagram for the experimental setup including the

reactions were stripped off the light oil fractions and water by re-heating the reactor vessel at 150 °C. The condensate was collected using a cold trap with spiral tubing and a conical bottom placed in an ice-water bath. The light oil fraction and water were then separated as different layers by controlled drainage through the conical bottom using a stop-cock. The layers were weighed.

5.2.4 Extraction with organic solvents

The remaining liquid products were recovered by pentane- and toluene-extraction (80 g of the reacted mixture/extraction) in a Soxhlet extractor for 8-12 h until a clear solvent appeared. The pentane-extracted bitumen and depleted sands were dried at 40 °C, until a stable mass was achieved. The toluene-extracted bitumen and depleted sands were dried at 115 °C in a similar manner to evaporate the remaining solvent. The maltene fractions were determined from the combined weights of the pentane-extracts and the liquid hydrocarbon condensates collected in the cold trap. The condensate fractions were added back to the toluene-extracted bitumen in proportionate amounts prior to performing any analyses.

5.2.5 Asphaltenes and coke measurement

The C₅-asphaltene contents were determined by re-extracting the pentane-extracted depleted sands with toluene in a Soxhlet extractor, drying (at 115 °C) and weighing the extract. The depleted sands were dried at ~250 °C for 2 h under helium flow in a closed tube furnace to strip off any remaining toluene. The dried and depleted sands were weighed and placed in a muffle furnace at 850 °C for 5 h in the presence of air to combust the remaining organic solids. Coke was measured from the weight difference of the depleted sands before and after the combustion.

5.2.6 Simulated distillation

Boiling point distributions of toluene-extracted bitumen samples were determined by a high temperature simulated distillation (HTSD) method, covering the n-alkane boiling range of C₅-C₁₂₀ up to 720 °C [16]. This is a modified version of the ASTM D5307 method [17]. Each sample was used to prepare a 2 wt.% solution of toluene-extracted liquid dissolved in carbon disulfide. 0.2 µL of each of these solutions was injected into a WCOT Ultimetal non-polar column equipped on a pre-

calibrated and standardized Varian Micron 450 GC. Details of the method, instrument and standardization were presented in Section 4.2.7.

5.2.7 Mass balance, liquid yields and residue conversion calculation

From the mass balance performed on the products (including gas, condensate and coke) and the boiling point distribution of toluene-extracted liquid determined by simulated distillation, the individual masses of naphtha (>191 °C), kerosene (191-277 °C), distillate (277-343 °C), gas oil (343-566 °C) and residuum (566 °C+) [18] were measured. The following parameters are calculated based on 500 g of feed oilsands:

$$\% \text{ - Residue free liquid yield} = \frac{M_{\text{RFL}}}{M_{\text{G}} + M_{\text{TL}} + M_{\text{C}}} \times 100\% \quad (5-1)$$

$$\% \text{ - Total liquid yield} = \frac{M_{\text{TL}}}{M_{\text{G}} + M_{\text{TL}} + M_{\text{C}}} \times 100\% \quad (5-2)$$

$$\% \text{ - Residue Conversion} = \frac{M_{\text{RP}} - M_{\text{RB}}}{M_{\text{RB}}} \times 100\% \quad (5-3)$$

Where M_{RFL} , M_{TL} , M_{G} and M_{C} represent masses of residue free liquid (combined mass of naphtha, kerosene, distillate and gas oil), total liquid (combined mass of all liquid fractions), gas and coke respectively. M_{RP} and M_{RB} are masses of residue in product liquid and unreacted bitumen, respectively.

5.2.8 Viscosity measurement

Viscosities of toluene-extracted liquid samples were measured by a Brookfield DV-E chamber and spindle viscometer. The instrument was calibrated using multiple samples of standard silicone oil of different viscosities. Measurements for a single sample was conducted at least at three different temperature set points out of five chosen levels (40, 45, 50, 60 and 70 °C), depending on the extent of the

measured viscosity values and the measurement limits for the instrument. 2-3 mL of each sample was allowed to reach thermal equilibrium at the specified temperature prior to each measurement. The dependence of viscosity of bitumen and heavy oil on temperature is very accurately represented by a double logarithmic two parameter model [3, 19-21]. The two parameters (a_1 and a_2) in the following ASTM equation were determined from data fitting (Appendix B):

$$\ln [\ln (\mu)] = a_1 + a_2 \ln (T) \quad (5-4)$$

Here, μ is the viscosity measured at temperature T . All viscosity data were converted to equivalent 50 °C values, if not measured at this temperature.

The samples were also checked for time dependent effects by extending wait time for measurements and observing the variation in values. Possibilities of viscous heating were minimized by maintaining minimum shear rates. To test the shear thinning/thickening properties of the bitumen, viscosities of three representative samples produced from different reaction conditions (temperature, catalyst type and loading) were measured after subjection to varying shear rates (0.5-10.0 rpm).

5.2.9 Average molecular weight (AMW) measurement

Average molecular weight (AMW) of toluene-extracted liquid products was measured with a calibrated and standardized KNAUER Vapor Pressure Osmometer (model K-7000) following ASTM D2503 method [22] and using Equation (4-4). Details of the measurement and calibration method were presented in Section 4.2.9.

5.2.10 Aromaticity measurement

Aromaticity of toluene-extracted liquid products was determined by quantitative measurement of aromatic carbon by ^{13}C NMR spectroscopic analyses using a Varian Inova-400 NMR spectrometer operating at 100.54 MHz. The spectra were recorded at a sweep width setting of 26990.6 Hz and with 1000 scans. Each bitumen sample was maintained at a concentration of 0.16g 3.5 mL⁻¹ of deuterated chloroform containing 10% chromium (III) acetylacetonate [$\text{Cr}(\text{acac})_3$] as a

paramagnetic relaxation agent in the presence of tetramethylsilane (TMS) in chloroform (15 μL 100 g^{-1}) as an internal reference. All data were acquired using a pulse flip angle of 30° , a pulse width of 3.2 Hz and a pulse repetition time of 3 s. The acquisition time and relaxation delay were 1 and 2 s respectively. The spectra were referenced to the CDCl_3 resonance peak at 77.06 ppm. For each spectrum a 10 Hz line broadening was used to improve the signal-to-noise ratio, and the peaks and percentage of each region were assigned based on literature data [23].

5.2.11 Elemental analysis and heteroatoms measurement

The total carbon, hydrogen, nitrogen and sulfur contents of toluene-extracted liquid products were measured simultaneously by a Carlo Erba EA1108 CHNS-O Elemental Analyzer. Tin containers of samples were weighed and placed into a high temperature (1000 $^\circ\text{C}$) reactor where the sample underwent 'dynamic flash combustion' with the aid of injected pure oxygen. The combustion gases were carried by pure helium through an oxidative catalytic stage (tungstic oxide on alumina) to achieve quantitative combustion. This was followed by a reductive stage using copper wires to remove excess oxygen and reduce nitrogen oxides to elemental nitrogen. The gases (N_2 , CO_2 , H_2O , SO_2) are then separated in a chromatographic column (Porapak QS, 4 mm ID, 2 m long) and detected by a thermal conductivity detector. The output signals are converted into a chromatogram displaying the gases by Eager 2000 software. The generated area count data are used to calculate the total percentage of C, H, N and S based on the calibration curves previously constructed for each element by analysis of standard samples. Two replicated measurements are conducted on each sample, and the result is reported as an average.

5.2.12 Heavy metal contents measurement

Instrumental neutron activation analysis (INAA) was applied to measure the vanadium content in toluene-extracted liquid samples using the SLOWPOKE-II nuclear reactor at the Nuclear Reactor Facility of the University of Alberta. Approximately 0.12-0.15 g of each bitumen sample was placed in a cleaned and dried capped polyethylene irradiation vial. The vials were placed in the SLOWPOKE-II nuclear reactor, irradiated for 5 minutes and counted for 300 s (live time) using an inhouse modified sample changer mechanism following a decay period of 20 ± 5

minutes. Spectral peak search was accomplished using SPAN software, and decay correction and quantification of elements were done by in-house coded programs.

Simultaneous measurement of vanadium and nickel contents in liquid products was conducted with inductively coupled plasma mass spectrophotometry (ICP-MS) at the Department of Earth and Atmospheric Sciences at the University of Alberta. Approximately 10 mg of each liquid sample was digested in a glass vial at ~150-200 °C on a hot plate with periodic addition of concentrated nitric acid over extended period of time until a colorless and solids-free homogeneous solution was obtained. The digested solution was diluted to a ~ 100 mL in a graduated volumetric flask with deionized water and then analyzed for vanadium and nickel. A Perkin Elmer 's Elan 6000 machine (35 sweeps reading⁻¹, 20 min dwell time) was used to conduct the ICP-MS analysis on the prepared sample. Three replicate measurements were conducted on each sample and the results were reported as an average. Blank runs were deducted from each measurement after internal standard correction.

5.3 RESULTS AND DISCUSSION

5.3.1 Stirred reactions on oilsands

Oilsands is a complex, non-uniform mixture of numerous organic compounds present in the form of bitumen, in a water and siliceous sand matrix. Even with constant stirring and monitoring, it is impossible to maintain uniform temperature and composition within the 1 L laboratory-scale reactor due to the presence of heterogeneous gas, liquid and solid phases, and due to the heating method: heat is added from the reactor wall. The outside wall of the reactor must be kept at higher temperature levels to maintain specified centerline temperatures (Figure 5-2), which results in significant radial temperature profiles. Because of this temperature gradient, it is not possible to assign a meaningful average temperature for the reaction. Also, because of the size and geometry of the reactor-impeller setup, it was not possible to generate adequate data points along the radial direction to calculate a logarithmic temperature profile. Instead, equivalent thermal severity is chosen for comparison.

Savage et al. used the concept of reaction severity, a composite function of operating temperature and residence time, to assess the extent of thermal reactions of

asphaltenes [24]. For a first order chemical reaction, such as the thermal cracking of heavy oil, the severity value is the same as the Damköhler number ($Da=kt$). A separate study on Athabasca bitumen vacuum residue cracking reports kinetics data and relates severity values to residue conversion [25]. The severity values for the reactions are calculated based on data fitting of the reported values (Appendix C), allowing for a very general comparison of the extent of the thermal reactions conducted in this study. This approach is solely intended to provide a general idea of the comparative thermal conditions of both of these low severity reactions. Thermal reactions with centerline temperatures maintained at 300 and 350 °C correspond to Da values of roughly 0.044 and 0.236. Such low values indicate very low severity of reactions within the reactor at either of the specified reaction temperatures, even compared to the visbreaking conditions of bitumen (≥ 400 °C) [10] or the pyrolysis of large hydrocarbon molecules [26-28]. However, the relative severity of the higher temperature thermal reaction is approximately ~5-6 times higher than that of the lower temperature reaction. Based on these values, for comparative purposes, the reactions conducted at 300 and 350 °C centerline temperatures are referred to as lower severity and higher severity reactions respectively from this point onwards.

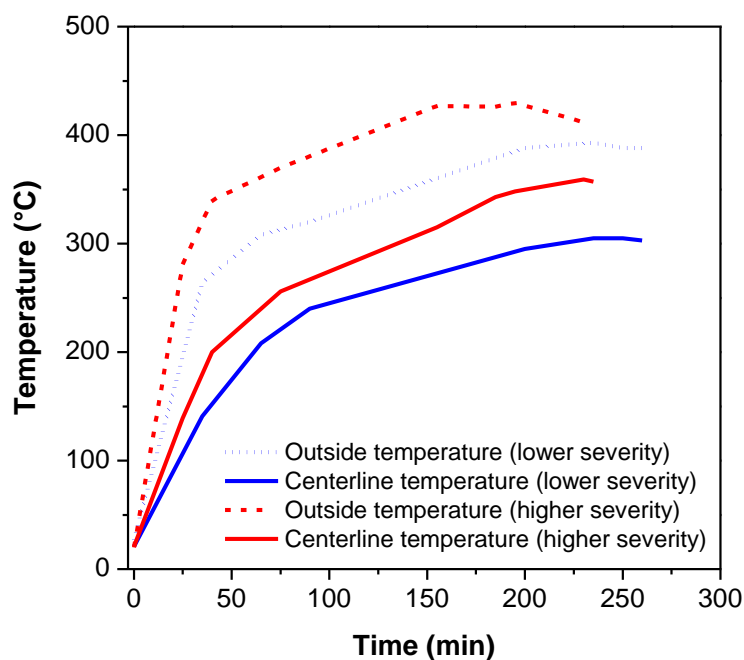


Figure 5-2: Typical wall and centerline temperature profiles for the thermal reactions conducted at different severities.

5.3.2 NZ catalyzed cracking and recovery

With the addition of 1-5 wt.% NZ, the residue conversion and residue-free liquid yield from oilsands bitumen increased significantly (Figure 5-3). The conversion was found to increase with higher NZ loading and increased reaction severity. However, at high conversions, the yield increased nonlinearly with residue conversion (Figure 5-3) due to overcracking which resulted in increased gas (Figure 5-4) and coke make (Figure 5-5). The total liquid yield, particularly at higher reaction severity, decreased with residue conversion (Figure 5-6) due to overcracking. Importantly, a high total liquid yield (~90-95%) and most of the increase in residue-free liquid yield (up to 10%) can be maintained while achieving substantial residue conversion (~29-47%) through lower severity NZ-added reactions.

Generally higher residue conversion is achieved with 5% loading than 1% loading of the catalyst. This suggests that higher numbers of acid sites available at higher loadings contribute to the increased cracking and conversion. Comparing the performance of the two types of NZs used in this study, higher residue conversion is achieved by CC, a catalyst with much higher acid site density (0.65 meq g⁻¹ by solid acid titration and 3.66 meq g⁻¹ by ammonia-TPD) and high strength (56.4 kJ mol⁻¹), than that achieved by SC with lower acid site density (0.05 meq g⁻¹ by solid acid titration and 0.27 by meq g⁻¹ ammonia-TPD) but comparable site strength (51.2 kJ mol⁻¹) [30]. External surface area may also have some contribution to the residue conversion; CC has a higher external area of 59 m² g⁻¹ over the 40 m² g⁻¹ of SC [30]. The surface and acid characteristics of these minerals were discussed in details in Chapter 2. The conversions observed in the thermal reactions, on the other hand, can be largely attributed to the higher temperatures near the reactor wall (Figure 5-2), and to the catalytic effects of the clay matrix present in oilsands.

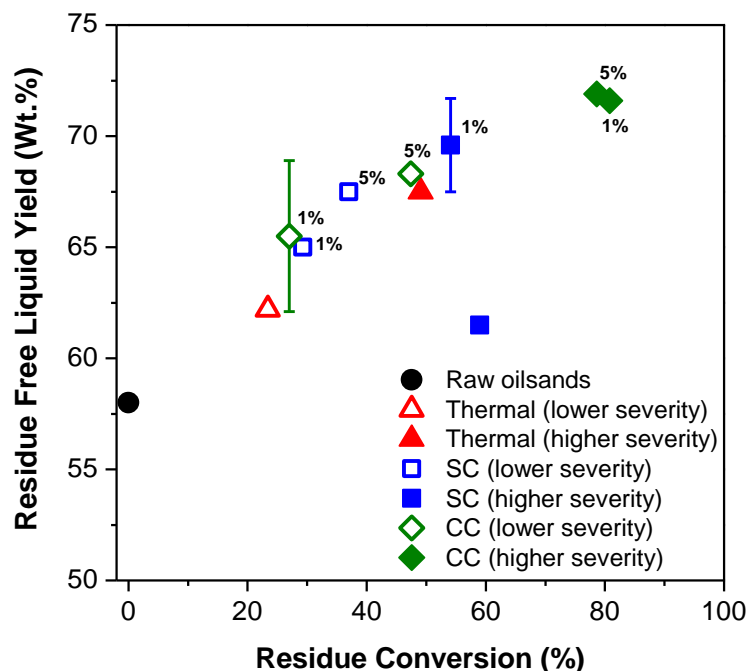


Figure 5-3: Residue free liquid yield from thermal and NZ catalyzed reactions. Error bars are for one standard deviation based on three repeated experiments conducted on each sample.

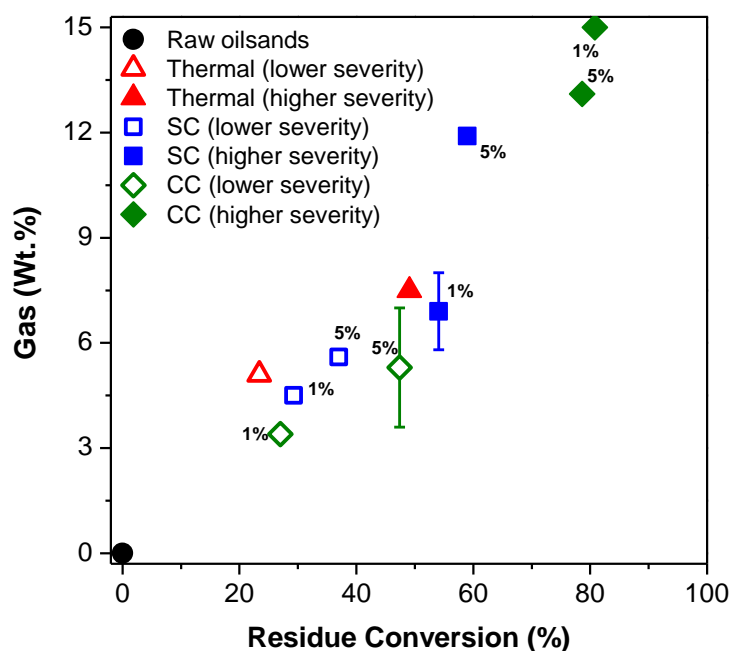


Figure 5-4: Gas make from thermal and NZ catalyzed reactions. Error bars are for one standard deviation based on three repeated experiments conducted on each sample.

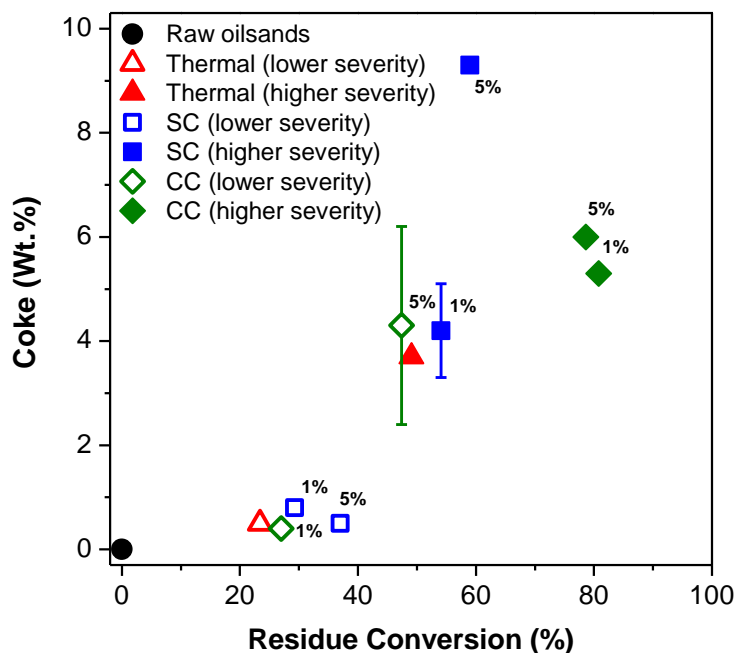


Figure 5-5: Coke make from thermal and NZ catalyzed reactions. Error bars are for one standard deviation based on three repeated experiments conducted on each sample.

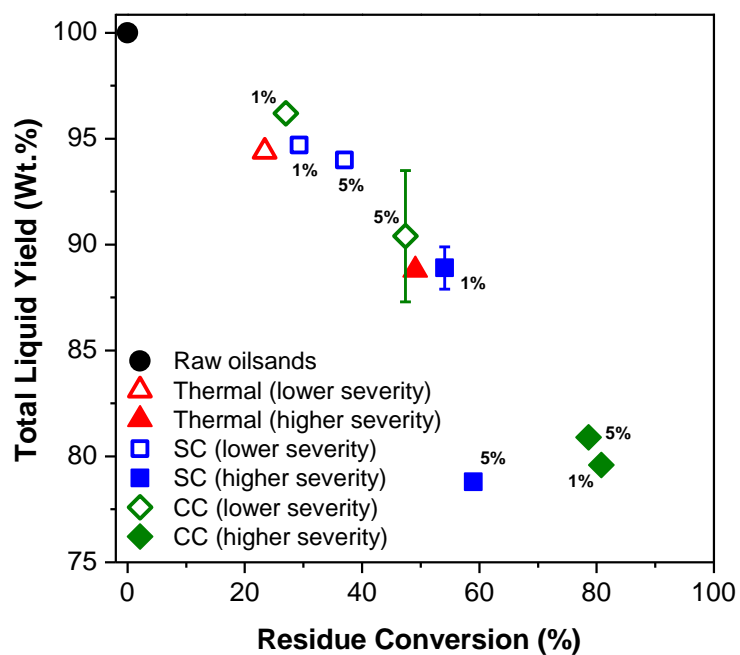


Figure 5-6: Total liquid yield from thermal and NZ catalyzed reactions. Error bars are for one standard deviation based on three repeated experiments conducted on each sample.

The gas compositions (Figure 5-7) show substantial olefin, paraffin and acid gas production. Formation of these gases are mainly attributed to β -scission of hydrocarbons by thermal and catalytic cracking, hydride ion transfer during catalytic reactions, and decarboxylation and desulfurization reactions by thermal and catalytic reactions respectively [29]. Formation of larger C_2+ fractions in the catalytic reactions indicates high extent of carbocationic reactions. However, it is very likely that thermal reactions simultaneously take place due to temperature effects.

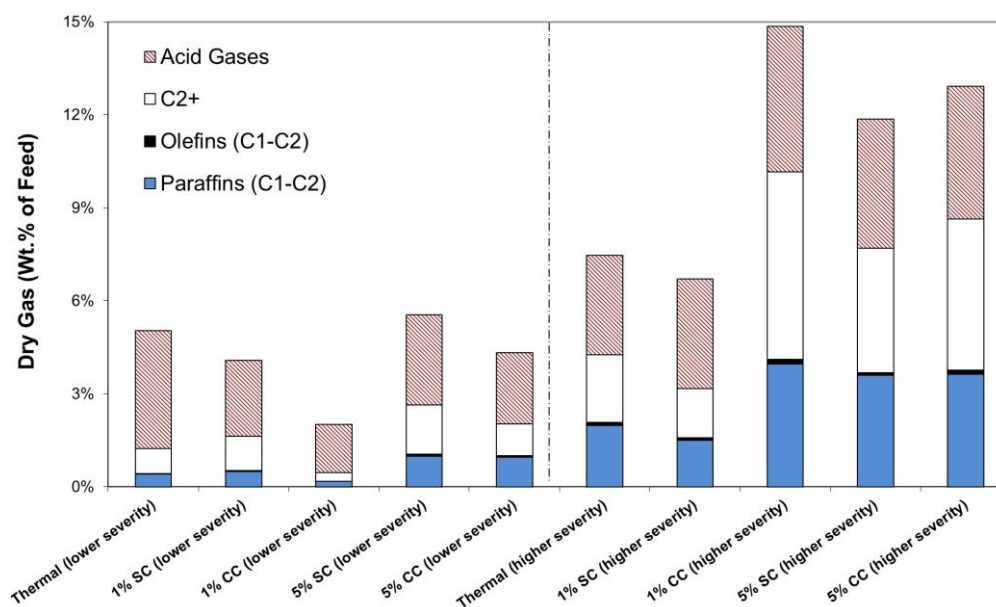


Figure 5-7: Composition of gases produced from thermal and NZ catalyzed reactions.

The mass balance on the products from these experiments is closed within $\pm 7\%$ of that observed for the oilsands bitumen feed, with the majority of reactions closing within $\pm 5\%$. Most of the error was introduced through difficulties in collection, separation and measurement of gaseous and liquid products from the sand phase. The general trends from the NZ-catalyzed oilsands cracking reactions remain clear, despite any difference in the mass balance closure resulting from the unique nature of these experiments.

5.3.3 Product quality

The objective of this study was to enhance cracking with NZs to increase the extractable liquid yield and simultaneously improve the liquid product quality under mild thermal conditions. A significant increase in the quality of the liquid products was observed as a result of NZ cracking. SIMDIST analysis of the liquid products shows that NZ cracking reduces the heavy fractions of bitumen into lighter, lower boiling point products, compared to raw, unreacted bitumen or analogous, thermally cracked bitumen. To illustrate this point, sample boiling point distribution curves of liquid bitumen from 5% NZ catalyzed reactions, uncatalyzed thermal reactions and raw oilsands are qualitatively compared in Figure 5-8. At lower severity, NZ cracking converted substantial amounts of residue, resulting in higher yields of gas oil and equal or higher yields of distillate fractions compared to raw or thermally cracked samples. Neither the raw nor the thermally-cracked sample contained any significant kerosene or naphtha fractions. This shift in the boiling point distribution of products was more pronounced for the higher severity reactions; for example, the bitumen from the calcium chabazite (CC)-catalyzed reaction had exceptionally low residue and gas oil and much higher distillate, kerosene and naphtha fractions than the raw or thermally cracked samples. Although the thermal and SC-catalyzed reactions produced similar residue contents, the SC-cracked product had lower gas oil and higher naphtha, kerosene and distillates. These observations indicate that, even at lower thermal severities, NZ addition effectively increases the proportion of lower boiling point petroleum fractions in liquid products. The boiling point fractions varied between 1.5-3.8% from the mean value (one standard deviation), as determined by three repeated experiments conducted on a single representative sample.

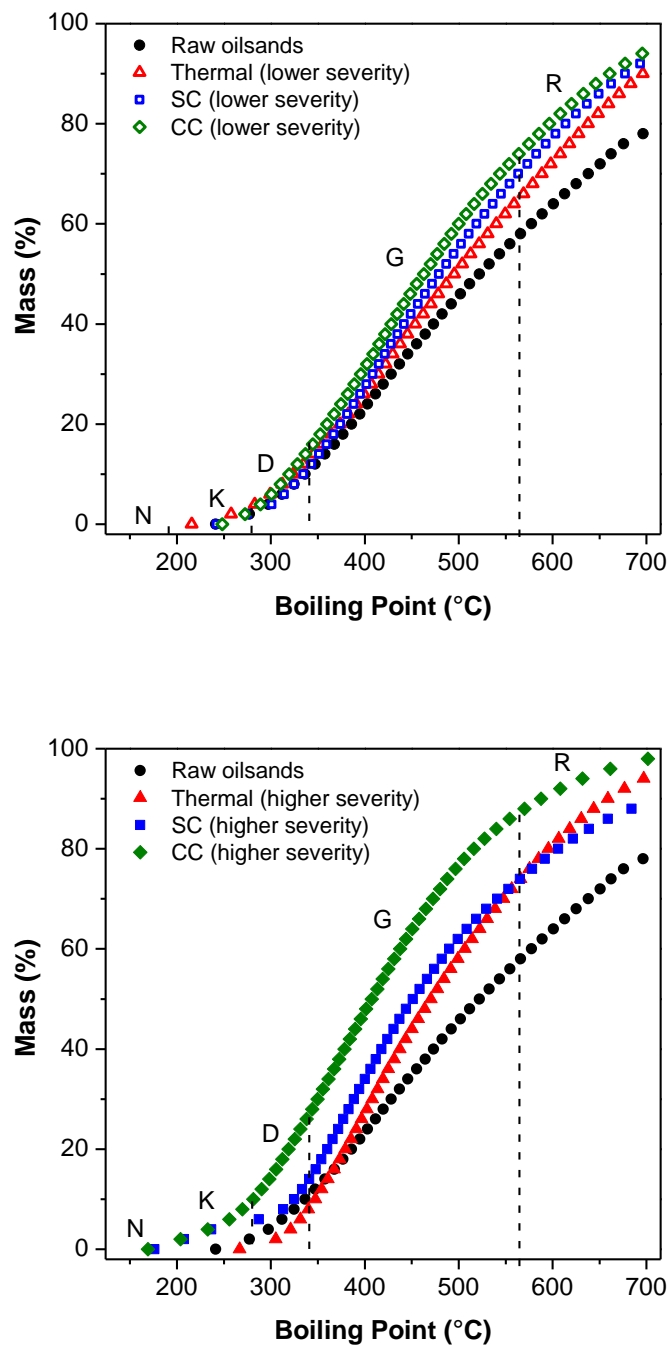


Figure 5-8: Sample boiling point distribution curves of toluene-extracted liquid products from lower severity (top) and higher severity (bottom) reactions compared to raw oilsands bitumen. N, K, D, G and R represent naphtha (>191 °C), kerosene (191-277 °C), distillate oil (277-343 °C), gas oil (343-566 °C) and residuum (566 °C+) fractions respectively.

C₅-asphaltenes comprise a significant portion of the residue fraction of bitumen, a fraction that was reduced to as low as ~5 wt.% of the feed by NZ cracking (Figure 5-9). This reduction was most significant in the higher severity reactions and in high NZ loadings, particularly at lower severity. As stated earlier, an increase in loading corresponds to a higher number of active sites in the catalyst, a substantial fraction of which are on the external surface and accessible to large hydrocarbon molecules such as asphaltenes for cracking. At higher severity, NZ surfaces are highly activated, desorption of products is spontaneous and asphaltene conversion is less dependent on the loading. This was particularly noticeable in CC-catalyzed cracking reactions. It is also possible that, at higher severity, the partially reduced asphaltenes can access the active sites within the pores of SC (average diameter 20.1 Å) more easily than the sites in CC, a material with smaller micropores (15.6 Å) (Chapter 2) [30]. Secondary cracking by a wider pore matrix is typical for zeolite-catalyzed acidic reactions [11]. The high variability of the asphaltenes yield associated with the low severity CC sample (Figure 5-9) was due to the variation of a single run compared to the other replicated experiments conducted on the sample.

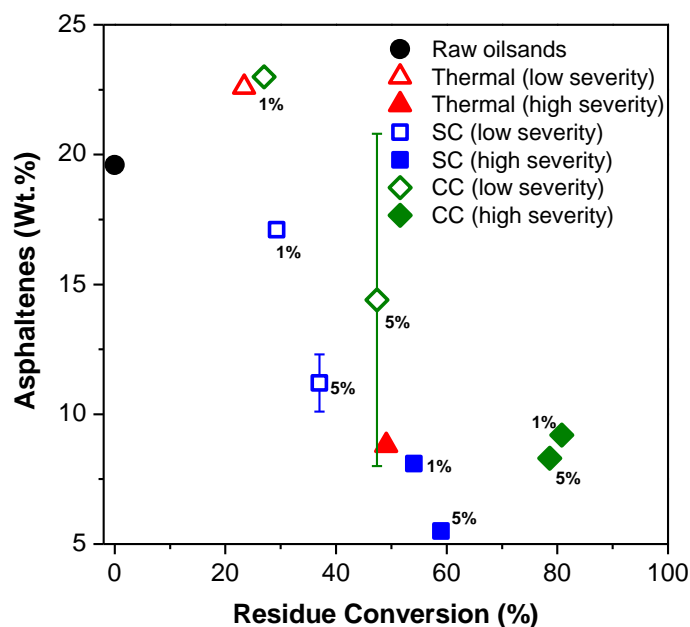


Figure 5-9: C₅-asphaltenes yield from thermal and NZ catalyzed reactions. Error bars are for one standard deviation based on three repeated experiments conducted on each sample.

NZ-added reactions reduced the average molecular weights (AMW) of liquid products significantly, with substantial reduction achieved at lower severity, and maximum reduction at higher severity (Figure 5-10). The AMW of bitumen from a catalytic reaction can be as low as 340-359 Da (molecular formulas determined by elemental analysis correspond to carbon skeletons of C₂₃-C₂₅) compared to the 1409 Da of raw oilsands bitumen (corresponds to C₉₈-skeleton). The thermally cracked samples, regardless of the reaction severity, have substantially higher AMW (629-920 Da, C₄₀-C₅₇). The standard deviation of the AMW of bitumen samples was 1.5% from the average value based on three repeated experiments conducted on a single sample.

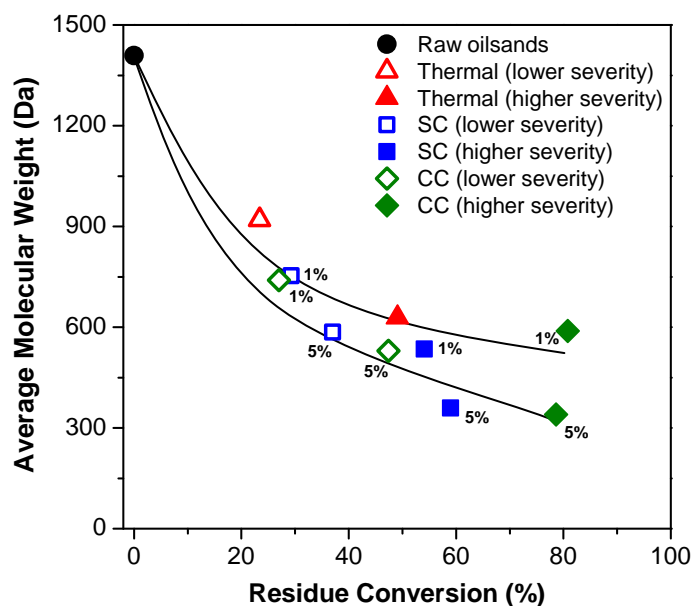


Figure 5-10: Average molecular weight of toluene-extracted liquid products from thermal and catalytic reactions as a function of residue conversion.

Cracking and residue conversion increased the transportability of liquid products dramatically. It was found that, with the addition of 1-5% NZ, even at lower severity, the viscosity of the liquid products was significantly reduced compared to analogous thermally cracked samples (Figure 5-11). As expected, the liquid products from higher severity catalytic reactions had the lowest viscosity values, orders of magnitude lower than the raw bitumen or thermally cracked bitumen. It was also found that for reactions with similar residue conversions, the viscosity of the liquid product from a high loading reaction was always lower than the viscosity from a low loading reaction, demonstrating a clear trend for viscosity as a function of residue conversion. A similar trend was observed for the AMW of the liquid products (Figure 5-10). At higher severity or NZ loading, viscosity is lower because more light petroleum fractions are formed (as seen in Figure 5-8), resulting in a greater impact on the transportability of the liquid. The standard deviation of the viscosity of bitumen samples was 3.0% from the average value based on five repeated experiments conducted on a single sample. The viscosity results were not impacted by shear thinning/thickening properties of bitumen (Figure 5-12) [31] and time effects which are detected by significant change in values with shear rate and time [32].

The liquid products from NZ-catalyzed reactions were low in aromaticity and had higher H/C ratios, parallel to the trend observed for analogous products from the thermal reactions (Figure 5-13). Some degree of aromatization and dehydrogenation of liquid products would be expected for both thermal and NZ-catalyzed cracking. Low aromaticity and high hydrogen content are desirable product qualities which further enhance the potential value of the high recovery, low viscosity and low boiling point distribution observed for liquid products from NZ-cracked reactions.

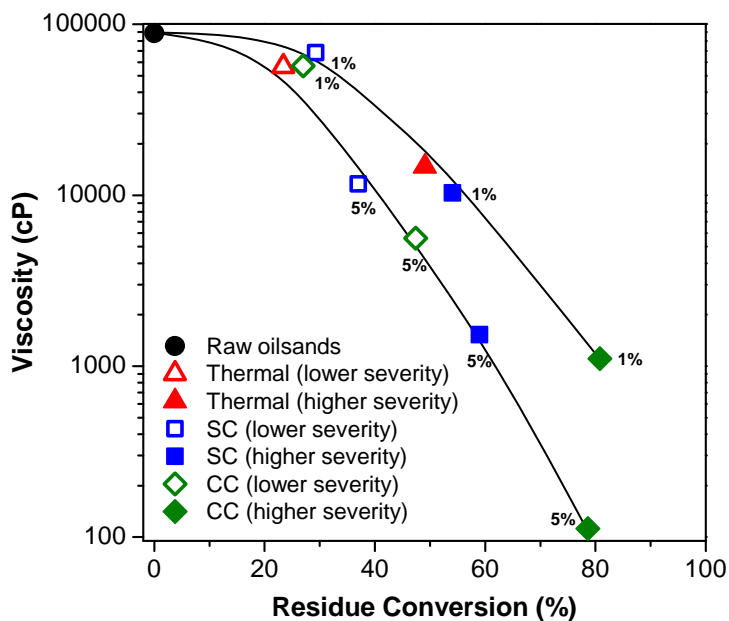


Figure 5-11: Viscosity of toluene-extracted liquid products from thermal and catalytic reactions as a function of residue conversion, measured at 50 °C.

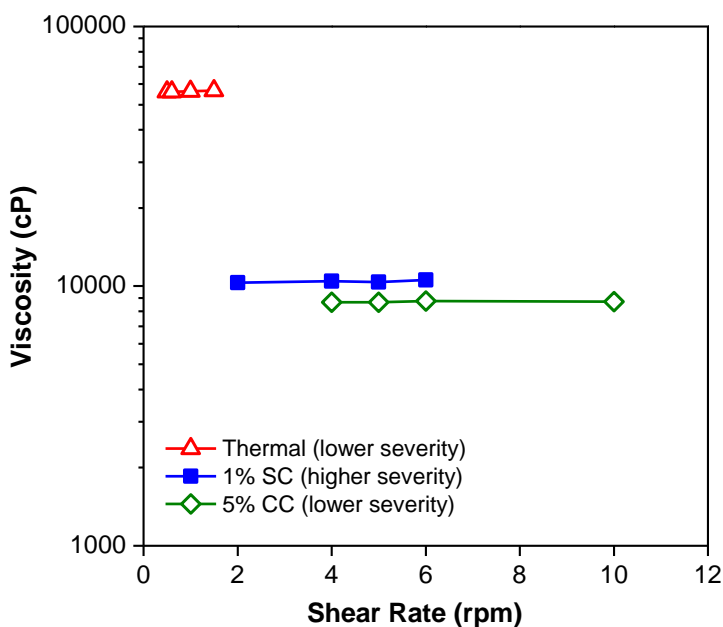


Figure 5-12: Effect of shear rate on the viscosities of liquid products. Three representative liquid samples from reactions conducted at different conditions were subjected to varying shear rates. The viscosity values remained unchanged [31]. Reused with permission from the World Academy of Science, Engineering and Technology.

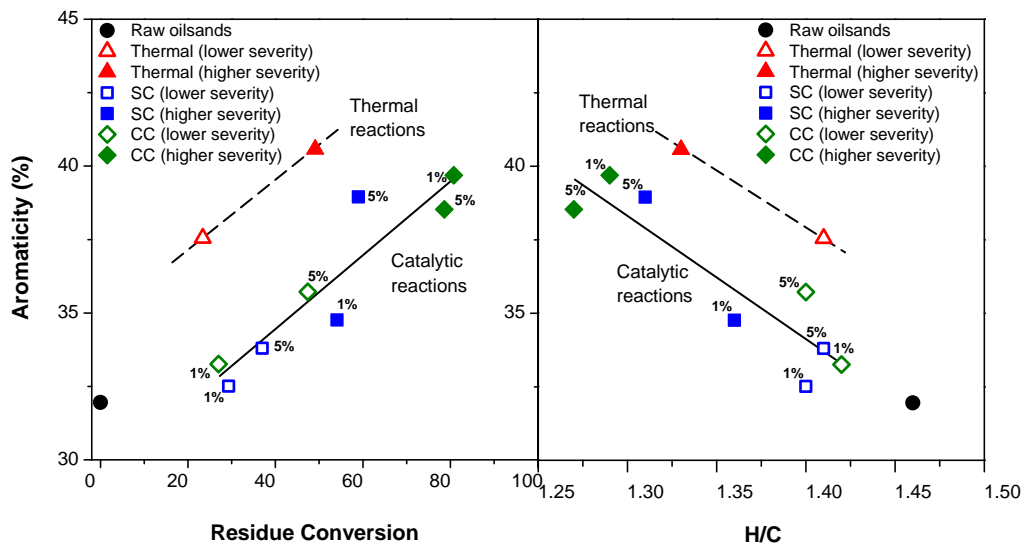


Figure 5-13: Aromaticity of liquid products from thermal and NZ catalyzed reactions as a function of residue conversion (left) and H/C ratio (right).

The strong adsorptive and acidic properties of NZs were expected to result in significant removal of heteroatoms and metals by adsorption during cracking reactions. NZ addition removed a substantial fraction of the constituent sulfur from bitumen, particularly at higher loading and reaction severity, reducing the sulfur concentration in the liquid products (Figure 5-14). Based on the typical amounts of thiophenic and non-thiophenic sulfur fractions in Athabasca bitumen (~62% and ~38% respectively) [33], most of these are expected to be easy-to-remove non-thiophenic organic sulfides and thioethers.

While some reduction in nitrogen concentration (as low as 0.40 wt.%) was observed in the liquid products, particularly at high NZ loadings (Figure 5-15), no clear trend was observed. The only discernible pattern seen was that the high loading NZ added reactions generally produced lower nitrogen concentration of liquid products compared to the thermal or lower loading reactions. This is possibly due to the availability of higher numbers of adsorptive sites for nitrogen with increased loading.

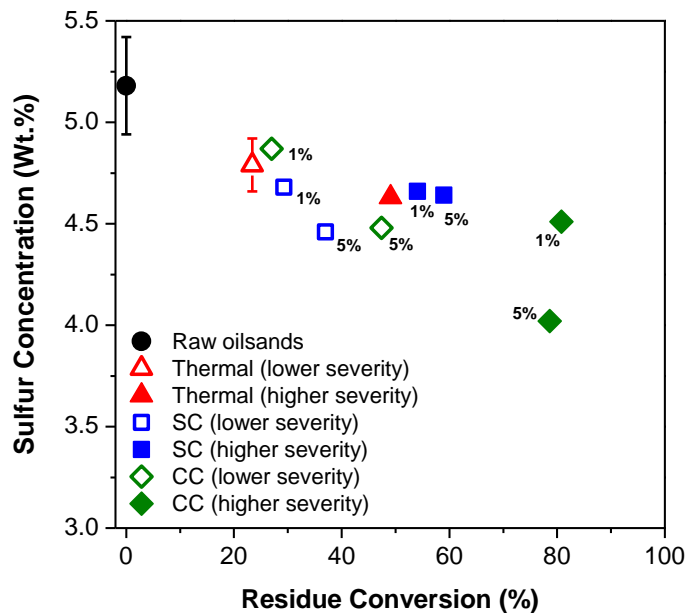


Figure 5-14: Sulfur concentration in liquid products from thermal and NZ catalyzed reactions. Error bars are for one standard deviation based on three repeated experiments conducted on each sample.

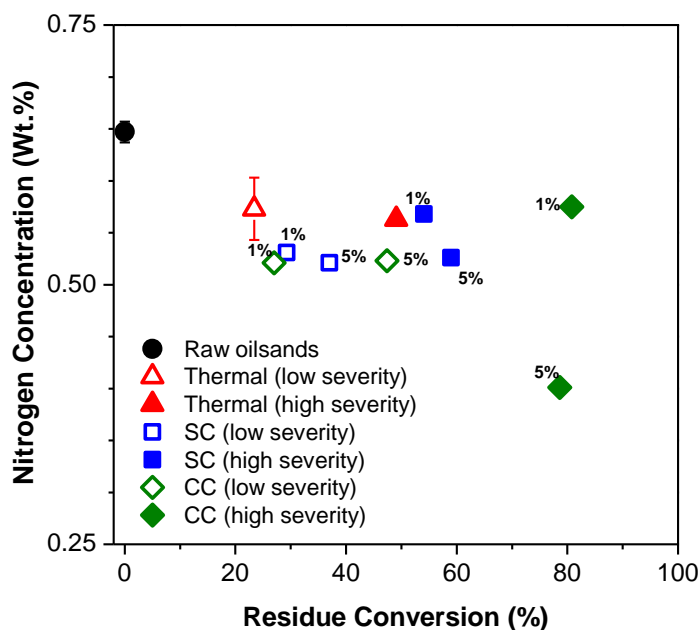


Figure 5-15: Nitrogen concentration in liquid products from thermal and NZ catalyzed reactions. Error bars are for one standard deviation based on three repeated experiments conducted on each sample.

Nitrogen and vanadium are also present as coordinated heteroatoms located within vanadyl porphyrin macrocycles [34], and removing one from the cycle is typically expected to facilitate the removal of the other. However, a separate model compound-based study done in these labs showed that vanadium can be selectively removed from the porphyrin rings without impacting the nitrogen concentration and, hence, the concentration of these two elements in bitumen can demonstrate different trends (G. Rocha, personal communication).

In agreement with this observation, significant vanadium removal was achieved by NZ addition and cracking despite limited nitrogen removal. Figure 5-16 shows that the vanadium concentration in liquid products from NZ-added reactions can be as low as 74 ppm compared to the 228 ppm in raw oilsands bitumen, as determined by INAA. The majority of the vanadium in Athabasca bitumen is present in the heavy asphaltene fraction [35], and therefore the concentration is a function of the residue conversion. At higher severity, the vanadium concentration in bitumen was significantly reduced due to high residue conversion. Higher NZ loading also invariably produced bitumen with lower concentrations of vanadium than in samples with lower NZ loading. These two observations combined indicate that NZ act as strong adsorbents for vanadium-containing complex aromatic structures, such as vanadyl porphyrins [36], which, following adsorption, are cracked into smaller vanadium-free fractions recoverable by extraction. INAA analysis also found that the vanadium-containing fragments concentrated on the NZ-waste sand mixture. The vanadium concentration in the waste sands increased from 3.2 ppm to 22.8 ppm between the raw unreacted sample, which has the highest vanadium concentration in liquid, and the higher severity 5% CC catalyzed sample, which has the lowest vanadium concentration in the liquid product (Figure 5-16).

ICP-MS analysis reconfirmed the INAA results on heavy metals removal. It was found that the vanadium concentrations of the toluene-extracted liquid products determined by ICP-MS analysis were in good agreement with those determined by INAA, and followed the same general trend (Figure 5-17). The sample preparation method for the ICP-MS analysis is rigorous and cumbersome, and involves several possible sources of error. Therefore, the ICP-MS data are compared with those obtained by INAA for validation. The data for 1% SC added higher severity reaction, however, is unavailable due to an accidental loss during conducting experiments.

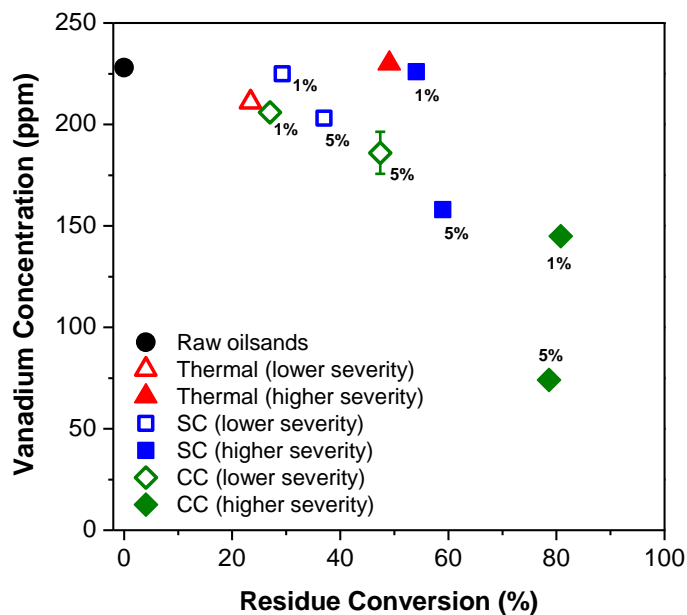


Figure 5-16: Vanadium concentration in liquid products from thermal and NZ catalyzed reactions as determined by INAA. The error bar is for one standard deviation based on four repeated experiments conducted on the sample.

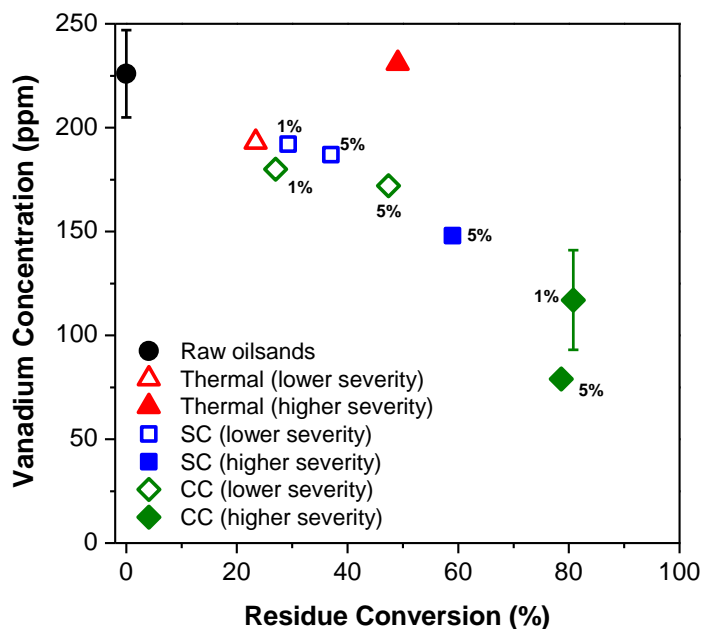


Figure 5-17: Vanadium concentration in liquid products from thermal and NZ catalyzed reactions as determined by ICP-MS analysis. The error bar is for one standard deviation based on multiple repeated experiments conducted on each sample.

ICP-MS analysis however, has one advantage over INAA: it can measure the concentration of nickel, another metal present in bitumen in significant quantity, more reliably than INAA. Because of the long decay time of nickel, it is difficult to determine the concentration using INAA. It was found that the concentration of nickel in liquids generated from the high loading higher severity reactions are much lower compared to those from the thermal reactions or low loading or lower severity catalyzed reactions (Figure 5-18). Interestingly the concentration goes up in the liquid products from thermally cracked or lower severity catalyzed reactions compared to the concentration in raw bitumen. This is due to the fact that little or no nickel removal occurs at these reaction conditions, and with some conversion of the liquids into gas and coke, the nickel content was concentrated in the remaining liquid. At higher severity and cracking, especially with catalyst addition, large compounds were reduced to smaller nickel-free fragments that were recovered by extraction, while the nickel were adsorbed by these catalysts. The lowest concentration of nickel (~80 ppm) was found in the liquid produced from the 5% CC loaded higher severity reaction.

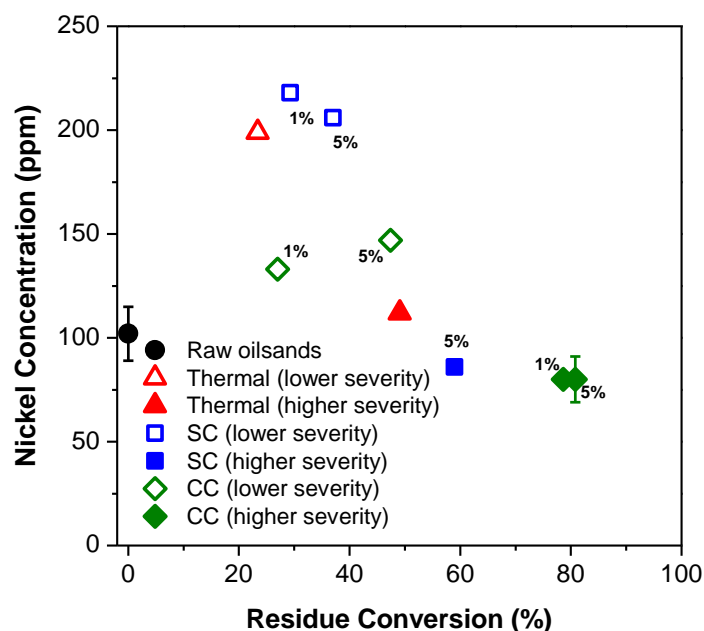


Figure 5-18: Nickel concentration in liquid products from thermal and NZ catalyzed reactions as determined by ICP-MS analysis. The error bar is for one standard deviation based on multiple repeated experiments conducted on each sample.

5.3.4 Summary of results

To summarize, NZ-added reactions demonstrated very high residue conversion by catalytic cracking and high liquid yields under low severity reaction conditions. Residue conversion increased with higher catalyst loading, reaction severity, and amounts of acid sites available for cracking. Undesirable products such as gas and coke, however, were low compared to typical industrial primary upgrading operations. NZ reduced the heavier fractions in raw bitumen into lighter components, lowering the viscosity, boiling point distribution and average molecular weight of products compared to analogous thermal reactions. In addition, NZ-catalyzed reactions reduced the heteroatoms and heavy metals concentrations in liquid products significantly while maintaining lower aromaticity and higher H/C ratios compared to analogous thermal reactions. A contrasting situation was observed for total liquid yield vs. quality, as the highest quality products are generated by higher severity reactions at the expense of total liquid yield. However, lower severity NZ-catalyzed reactions still provide high quality liquid products while achieving substantial residue conversion and high total yield. This represents a substantial net gain in the quality and quantity of crude oil available for additional secondary upgrading.

5.4 CONCLUSION

The water-activated natural zeolites are very effective catalysts for oilsands bitumen upgrading at low severity reaction conditions, well below typical thermal processing temperatures. These catalysts offer significant economical and operational advantages over the conventional thermal upgrading techniques. Based on the findings of this study, conducted in a scaled-up engineered system, it is possible to envision an integrated alternative approach to traditional extraction and upgrading of bitumen using water-enhanced natural zeolites to improve the transportability and quality of the bitumen and reduce processing steps. However, the economic feasibility of such process has to be evaluated in terms of energy, mass and utility requirements juxtaposed to its environmental benefits.

(A version of this chapter has been submitted for publication, and currently under review. Junaid ASM, Street C, Wang W, Rahman MM, An W, McCaffrey WC et al. *Integrated extraction and low severity upgrading of oilsands bitumen by activated natural zeolite catalysts*. *Fuel*. Submission: JFUE-D-11-00663, 17 May 2011. Used with permission from Elsevier.)

BIBLIOGRAPHY

- [1] Yufeng Y, Shuyuan L, Fuchen D, Hang Y. Change of asphaltene and resin properties after catalytic aquathermolysis. *Pet Sci* 2009; 6: 194-200.
- [2] Shen Z, Cao Z, Zhu X, Li X. Visbreaking of Chinese oilsands bitumen. *Pet Sci Technol* 2008; 26: 1676-83.
- [3] Ha HZ, Koppel P. Accurately predict viscosity of syncrude blends: An evaluation for mixing rules uncovers potential errors in fluid transportation of bitumen-based feeds. *Hydrocarb Process* 2008; 87: 87-92.
- [4] Chrones J, Germain RR. Bitumen and heavy oil upgrading in Canada. *Pet Sci Technol* 1989; 7: 783-821.
- [5] Strausz OP. Specific problems in the upgrading of Alberta oilsands bitumen. *J. Japan Petrol. Inst.* 1984; 27: 89-100.
- [6] Patel S. Canadian oilsands: Opportunities, technologies and challenges. *Hydrocarb Process* 2007; 86: 65-74.
- [7] National Energy Board, Canada. Canada's oil sands-opportunities and challenges to 2015: An update [Internet]. Calgary: National Energy Board; 2006 [cited 2011 May 12]. Available from: <http://www.neb.gc.ca/clf-nsi/rnrgynfmtn/nrgyrprt/lsnd/lsnd-eng.html>.
- [8] Hatch LF. A chemical view of refining. *Hydrocarb Process* 1969; 48: 77-88.
- [9] Cartlidge CR, Dukhedin-Lalla L, Rahimi P, Shaw JM. Preliminary phase diagrams for ABVB+n-dodecane+hydrogen. *Fluid Phase Equilib* 1996; 117: 257-264.
- [10] Casalini A, Mascherpa A, Vecchi C. Modifications induced by visbreaking on composition and structure of atmospheric residues. *Fuel Sci Technol Inter* 1990; 8: 427-45.
- [11] Ding F, Ng SH, Xu C, Yui S. Reduction of light oil catalytic cracking of bitumen-derived crude HGOs through catalytic selection. *Fuel Process Technol* 2007; 88: 833-45.
- [12] Ng S, Zhu Y, Humphries A, Zheng L, Ding F, Gentzis T, et al. FCC study of Canadian oil-sands derived vacuum gas oils: 1. Feed and catalyst effects on yield structure. *Energy Fuels* 2002; 16: 1196-1208.
- [13] Agarwala M, Yarranton W. An asphaltene association model analogous to linear polymerization. *Ind Eng Chem Res* 2001; 40: 4664-72.
- [14] Peramanu S, Pruden B, Rahimi P. Molecular Weight and Specific Gravity Distributions for Athabasca and Cold Lake Bitumens and Their Saturate, Aromatic, Resin, and Asphaltene Fractions. *Ind Eng Chem Res* 1999; 38: 3121-30.

- [15] Strong D, Filby RH. Vandyl porphyrin distribution in the Alberta oil-sand bitumens. In: Filby RH, Branthaver JF, editors. Metal complexes in fossil fuels, ACS Symposium Series, vol. 344. Washington: American Chemical Society; 1987. p. 154-72.
- [16] Villalanti DC, Raia JC, Maynard JB. High-temperature simulated distillation applications in petroleum characterization. In: Meyers RA, editors. Encyclopedia of analytical chemistry. Chichester: John Wiley & Sons Ltd; 2000. p. 1-15.
- [17] Standard test method for determination of boiling range distribution of crude petroleum by gas chromatography, ASTM D 5307-97 (Reapproved 2007). Philadelphia: American Society for Testing and Materials; 2007. p. 1-7.
- [18] Giles HN. Analysis of crude oils. In: Drews AW, editor. ASTM manual on hydrocarbon analysis, ASTM Manual Series, MNL 3. 4th ed. Philadelphia: American Society for Testing and Materials; 1989. p. 20-7.
- [19] Standard test method for viscosity-temperature charts for liquid petroleum products, ASTM D341-03. Philadelphia: American Society for Testing and Materials; 2003. p. 4-5.
- [20] Standard test method for low temperature, low shear rate, viscosity/temperature dependence of lubricating oils using a temperature-scanning technique, ASTM D 5133-05. Philadelphia: American Society for Testing and Materials; 2005. p. 1-12.
- [21] Seyer FA, Gyte CW. Viscosity. In: Loren G, Hsi C, editors. AOSTRA technical handbook on oilsands, bitumen and heavy oil. Edmonton: Alberta Oilsands Technology and Research Authority; 1989, p. 153-84.
- [22] Standard test method for relative molecular mass (molecular weight) of hydrocarbons by thermoelectric measurement of vapor pressure, ASTM D 2503-92 (Reapproved 2007). Philadelphia: American Society for Testing and Materials; 2007. p. 1-3.
- [23] Díaz C, Blanco CG. NMR: A powerful tool in the characterization of coal tar pitch. *Energy Fuels* 2003; 17: 907-13.
- [24] Savage PE, Klein MT. Asphaltene reaction pathways: 3. Effect of reaction environment. *Energy Fuels* 1988; 2: 619-28.
- [25] Soundararajan S. Determination of thermal cracking kinetics of Athabasca bitumen vacuum residue [dissertation]. Edmonton (AB): University of Alberta; 2001.
- [26] Khorasheh F, Gray MR. High-pressure thermal cracking of n-hexadecane. *Ind Eng Chem Res* 1993; 32: 1853-63.
- [27] Khorasheh F, Gray MR. High-pressure thermal cracking of n-hexadecane in aromatic solvents. *Ind Eng Chem Res* 1993; 32: 1864-76.

- [28] Khorasheh F, Gray MR. High-pressure thermal cracking of n-hexadecane in tetralin. *Energy Fuels* 1993; 7: 960-7.
- [29] Raseev S. Thermal and catalytic processes in petroleum refining. New York: Marcel Dekkar, Inc.; 2003.
- [30] Junaid ASM, Rahman M, Yin H, McCaffrey WC, Kuznicki SM. Natural zeolites for oilsands bitumen cracking: Structure and acidity. *Micropor Mesopor Mater* 2011; 144: 148-57.
- [31] Junaid ASM, Wang W, Street C, Rahman M, Gersbach M, Zhou S, et al. Viscosity reduction and upgrading of Athabasca oilsands bitumen by natural zeolite cracking. In: Ardil C, editor. *Proceedings of the International Conference on Chemical Engineering*; 2010 Sep 28-30; Amsterdam, the Netherlands. Amsterdam: World Academy of Science, Engineering and Tehnology; 2010 Sep. 485 p.
- [32] Peter CS, Robert LL. An experimental investigation of viscous heating in some simple shear flows. *AIChE Journal* 1974; 20: 474-84.
- [33] Brons G, Yu JM. Solvent deasphalting effects on whole Cold Lake Bitumen. *ACS Prepr. Petrol. Chem. Div.* 40: 785-793.
- [34] Czernuszewicz RS, Maes EM, Rankin JG. Resonance Raman spectroscopy of petroporphyrins. In: Kadish KM, Smith KM, Guillard R, editors. *Theoretical and physical characterization, The porphyrin handbook*, vol. 7. San Diego: Academic Press; 2000. p. 293-335.
- [35] Filby RH, Strong D. Nickel (II) and vanadium (IV) complexes in Alberta oil-sand bitumens. In: Oballa CM, Shih SS, editors. *Tar Sand and Oil Upgrading Technology*, AIChE Symposium Series, vol. 282. New York: American Institute of Chemical Engineers; 1991, p. 1-9.
- [36] Yen TF. Chemical aspects of metals in native petroleum. In: Yen TF, editor. *The role of trace metals in petroleum*. Ann Arbor: Ann Arbor Science Publishers Inc.; 1975, p. 1-30.

Energy Requirements

6.1 INTRODUCTION

NZ-based low temperature cracking has the potential to be developed to an effective oilsands bitumen extraction and integrated upgrading process. However, for practical reasons the process needs to be energy efficient as well as effective. In this chapter the energy requirement calculations for the process is presented and compared to that of a typical industrial process.

6.2 METHODS

The industrial process chosen for the comparative calculations consists of a typical Clark hot water extraction (CHWE), gravity separation with primary separation vessels (PSV) and floatation cells (FC), paraffinic froth treatment (PFT) and a primary upgrading (PU) unit. The flow diagram is presented in Figure 6-1. Process conditions and compositions are based on literature data [1,2], and presented in Table 6-1. The proposed NZ-based process has a low temperature reactor and a pentane-extraction unit. The flow diagram is presented in Figure 6-2. Conditions and compositions are based on the results presented in the previous chapter, and also

Energy Requirements

enlisted in Table 6-1. For brevity, a representative reaction conducted at 300 °C with 5% CC and 3% water addition has been chosen. All calculations are conducted based on 1 kg of product bitumen.

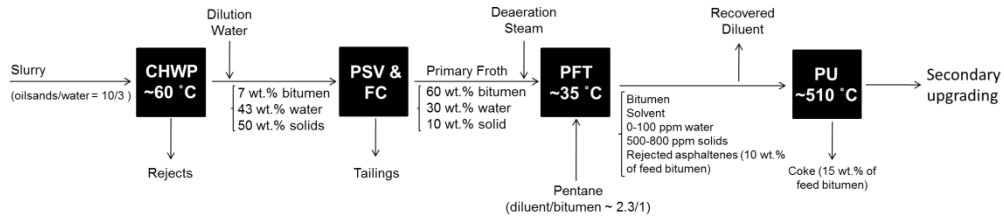


Figure 6-1: Process flow diagram for the typical industrial process used for the energy balance calculations. The process consists of a Clark hot water extraction (CHWE), paraffinic froth treatment (PFT) and primary upgrading (PU) unit. Conditions and compositions are based on literature data [1,2].

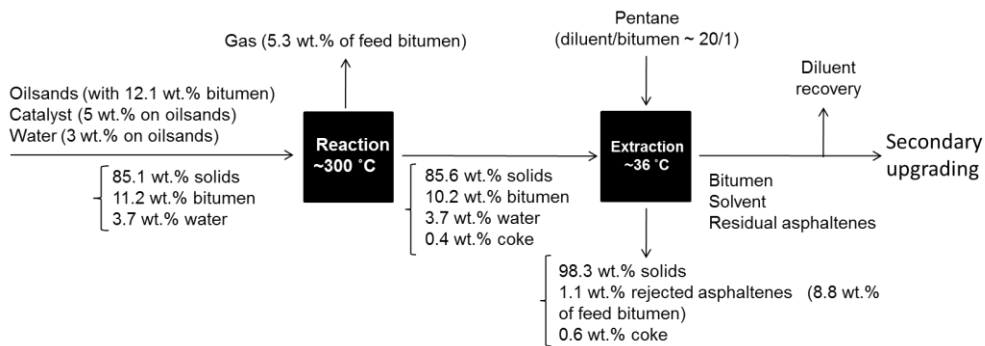


Figure 6-2: The flow diagram for the proposed NZ-based integrated extraction-upgrading process for oilsands bitumen. Conditions and compositions are based on the results of this study.

Table 6-1: Industrial and proposed process conditions for oilsands bitumen extraction and upgrading mass and energy balance calculations.

Process Conditions	
Industrial ^a	Proposed
<p><i>CHWE</i> Temperature: 60 °C</p>	<p><i>Reaction</i> Temperature: 300 °C</p>
<p><i>Froth treatment</i> Temperature: 35 °C Solvent/bitumen: 2.3 mL g⁻¹</p>	<p><i>Pentane extraction</i> Temperature: boiling point Solvent/bitumen: 20 mL g⁻¹</p>
<p><i>Upgrading</i> Temperature: 510 °C Coke: 15 wt.% of feed bitumen</p>	

a From references [1,2]

6.2.1 Assumptions

The main assumptions for the calculations are:

- i) The energy requirements are for heating only; no heat losses occur.
- ii) Energy required for pumping, electrical and mechanical work, and transportation are negligible.
- iii) The solvent to bitumen ratio required for the extraction is linearly dependent on the content of the solids entering the extraction unit.
- iv) Maintaining a proportional solvent to bitumen ratio will cause precipitation of ~50% of the asphaltenes fed to the extraction unit. This is analogous to the industrial PFT process which precipitates ~50% of the asphaltenic content in the feed.

6.2.2 Energy calculations

Energy requirements for heating and phase change are calculated using simple heat balances (Equations 6-1 and 6-2 respectively):

$$E = mC_p(T_2 - T_1) \quad (6-1)$$

$$E = mH_v \quad (6-2)$$

where E, m, C_p, H_v, denote Energy, mass, specific heat capacity at constant pressure, and heat of vaporization respectively; T₁ and T₂ denote temperature levels.

6.2.3 Physical and thermochemical properties

The properties are evaluated using the relations/values enlisted in Table 6-2.

Table 6-2: Physical and thermochemical properties used for energy balance calculations for industrial and proposed oilsands bitumen extraction and upgrading processes.

Parameter	Quantity or relation	Reference
<i>Density (ρ)</i>		
Pentane	8.57 (mol L ⁻¹ ; 301 K)	[3]
<i>BP temperatures (T_b)</i>		
Pentane	309.2 K	[3]
Water	373.2 K	[3]
<i>Heat capacities (C_p)</i>		
Solid fraction in oilsands (>325 mesh)	$914+331\times 10^{-3}T-2415\times 10^{-4}T^2$ (J kg ⁻¹ K ⁻¹ ; for 300 K<T<700 K)	[1]
Bitumen	$55+6818\times 10^{-3}T-4464\times 10^{-6}T^2$ (J kg ⁻¹ K ⁻¹ ; for 300 K<T<600 K)	[1]
Water	$-203.60+1.52T-3.20\times 10^{-3}T^2+2.47\times 10^{-6}T^3$ $+3.85\times 10^6T^{-2}$ (J mol ⁻¹ K ⁻¹ ; for 298 K≤T≤500 K)	[3]
Steam	$30.09+6.83\times 10^{-3}T+6.79\times 10^{-6}T^2-2.53\times 10^{-9}T^3+8.21\times 10^4T^{-2}$ (J mol ⁻¹ K ⁻¹ ; for 500 K≤T≤1700 K)	[3]
Sand (for NZ)	$-6.08+2.52\times 10^{-1}T+3.25\times 10^{-4}T^2-1.69\times 10^{-7}T^3+2.55\times 10^4T^{-2}$ (J mol ⁻¹ K ⁻¹ ; for 298 K≤T≤847 K)	[3]
Pentane	168.6 (J mol ⁻¹ K ⁻¹ ; for 300 K≤T≤463 K)	[3]
<i>Specific enthalpies of vaporization (H_v)</i>		
Pentane	25.79 (kJ mol ⁻¹ ; at $T_b=309.2$ K)	[3]
Water	40.65 (kJ mol ⁻¹ ; at $T_b=373.2$ K)	[4]

6.3 ENERGY REQUIREMENTS

The energy requirement calculations for the industrial and proposed process are presented in Table 6-3. Based on the calculations it is evident that the proposed process requires significantly higher energy (~10.0 MJ) to produce 1 kg of bitumen compared to the industrial process (~3.7 MJ). Interestingly, the difference in the energy requirements between the industrial and the proposed process is mostly contributed by the pentane-extraction and the reaction steps in the proposed process. The reaction is conducted at 300 °C and using a large amount of solids. The analogous PU step in the industrial process, although at a higher temperature of 510 °C, uses bitumen, a much smaller quantity, and hence requires substantially less energy. A previous calculation done in our lab had drawn similar general conclusion [5]. However, the energy requirements estimated from these two separate sets of calculations vary significantly. Part of this discrepancy is possibly due to neglecting the effects of temperature on solvent properties in the previous calculation.

Table 6-3: Mass and energy requirements for the industrial and proposed processes for oilsands bitumen extraction and upgrading, based on 1 kg of liquid product.

	Industrial Process	Proposed Process
<i>Mass (g)</i>		
Oilsands (12 wt.% bitumen)	12505	10145
Water	3751	304
Catalyst	-	507
<i>Energy (kJ)</i>		
Heating		
Oilsands	444.6	3060.7
Water	627.0	907.3
Catalyst	-	131.7
Total energy for heating	1071.5	4099.7
Froth treatment	842.8	-
Upgrading	1787.5	-
Pentane extraction	-	5945.9
Total energy requirement	3701.9	10045.6

The biggest contribution to the energy requirement, however, is the regeneration of the large amount of pentane employed for liquid products extraction. A solvent:bitumen ratio of 20:1 was used for the calculations based on the solids content of the stream entering the extraction process. A typical industrial PFT process employs a ratio of ~2.1-2.5 for a solids content of ~10 wt.%. For a solids content of ~86 wt.% in the proposed process, this ratio is scaled-up to 20:1. This high ratio was to ensure that a sufficient amount of solvent is in contact with the liquid products contained within a large sand matrix.

It is important to note that despite the significantly higher energy requirement, there are additional benefits associated with the proposed NZ-based process. It requires only 1/10th the amount of water compared to a CHWE-based industrial process, therefore is much more environmentally friendly in terms of fresh water requirement. Additionally it will almost eliminate the need to create and maintain chemical containing massive tailings ponds. The process will not require a PU unit, which will reduce the capital and operating costs as well as eliminate operational problems associated with primary upgraders. It also has some secondary upgrading effects which will reduce operational loads on further upgrading and impart positive effects such as increasing downstream catalyst life. Substantial reduction in bitumen viscosity at the first step of the process, i.e. reaction, facilitates the intermediate handling and transportation of liquid products without the need for addition and energy intensive regeneration of expensive solvents. Whether these additional benefits are sufficient to offset the higher energy requirements of the proposed process is dependent on a complete comparative economic analysis, which is beyond the scope of this study. Besides, as in most industrial processes, it is also possible to recover and reuse a substantial fraction of the energy input.

While a more energy efficient way of implementing the NZ-based proposed process demands further study, a different avenue worth exploring is to use the catalysts on extracted bitumen for upgrading purposes only. An additional comparative energy balance calculation was conducted for a proposed bitumen upgrading reaction using 10 wt.% catalyst and 10 wt.% water addition at 300 °C, resulting in a ~93 wt.% recovery of liquid products (typical recovery based on experimental results). The base case for primary upgrading was selected as the current industrial fluidized coking process, operating at 510 °C. The results,

presented in Table 6-4 based per kg of liquid product, showed that the proposed process is much less energy intensive (~1.6 MJ) than the current industrial process (~1.0 MJ). This is readily understandable due to the large difference in operating temperature (>200 °C) of these processes. Considering the fact that the proposed process will impart additional secondary upgrading effects, this can indeed be a viable alternative demanding further attention. A detailed study on the effects of NZ-catalyzed cracking on industrially extracted bitumen is presented in the next chapter.

Table 6-4: Mass and energy requirements for the industrial and proposed processes for extracted bitumen upgrading based on 1 kg of liquid product.

	Industrial Process	Proposed Process
<i>Mass (g)</i>		
Bitumen	1315.8	1075.3
Water	-	107.5
Catalyst	-	107.5
<i>Energy (kJ)</i>		
Heating		
Bitumen	1567.4	653.4
Water	-	320.4
Catalyst	-	27.9
Total energy requirement	1567.4	1001.7

6.4 CONCLUSION

Clearly, both the proposed NZ-based integrated extraction-upgrading and extracted bitumen upgrading are interesting. However, the integrated process requires a complete economic analysis to establish its cost-effectiveness. Further study is required to improve the energy efficiency of the process. For example, a properly engineered system can be designed to efficiently extract from large amounts of solids with relatively smaller quantities of solvent. The system can employ recycling of solvents without regeneration until saturation, proper distribution system to reduce solvent quantities, and heat recovery. On the other hand, the extracted bitumen upgrading is clearly energy efficient compared to an industrial upgrading unit.

BIBLIOGRAPHY

- [1] Masliyah J. Fundamentals of oilsands extraction. ChE 534 Course Materials. Edmonton: University of Alberta; 2011.
- [2] Gray MR. Hydrocarbon fluid properties & processing. ChE 522 Course Materials. Edmonton: University of Alberta; 2008.
- [3] NIST Chemistry Webbook [Internet]. Gaithersburg (MD): National Institute of Standards and Technology. c2011 - [cited 2011 Jul 15]. Available from: <http://webbook.nist.gov/chemistry>
- [4] Wikipedia: Enthalpy of vaporization [Internet]. San Francisco (CA): Wikimedia Foundation. c2001 - [cited 2011 Jul 15]. Available from: http://en.wikipedia.org/wiki/Enthalpy_of_vaporization
- [5] Street CA. Catalytic Cracking and Upgrading of Oilsands Bitumen Using Natural Calcium Chabazite [dissertation]. Edmonton (AB): University of Alberta; 2011.

Upgrading of Extracted Bitumen and *in situ* Application of Natural Zeolites

7.1 INTRODUCTION

The energy requirement calculations (Chapter 6) demonstrated that using NZs for upgrading extracted bitumen can be an interesting and energy efficient aspect. An interesting feature of this is that when the catalysts are used in liquid bitumen phase, they are potentially recoverable and reusable, provided they are still active following the reactions and the process is economically feasible.

Another important avenue is to use the NZ-catalysts for *in situ* upgrading of bitumen. Processes such as SAGD or VAPEX use prolonged low temperature heating to reduce the viscosity of bitumen *in situ*. Because the NZ-based upgrading operates at or near the temperature regime of these processes, it will be interesting to observe the effects of using these catalysts with such upgrading processes. If the catalysts can be effectively delivered to the bitumen combined with a downhole processing, a potential environmentally friendly and highly energy efficient upgrading method can be developed with reduced production time. Downhole delivery of ultra-dispersed catalysts for bitumen upgrading is a developing field [1,2].

This chapter presents the studies on the upgrading effects of NZ-catalysts on extracted bitumen. The impacts of catalyst loading and reaction time on extracted bitumen are evaluated with respect to the viscosity reduction of liquid products. Another aspect of this study is to demonstrate the reusability of these catalysts without significant additional treatment.

7.2 MATERIALS AND METHODS

7.2.1 Materials

The industrially produced partially deasphalted Athabasca bitumen and raw oilsands used for this study was obtained from the Syncrude facility at Mildred Lake near Fort McMurray, Alberta, Canada.

Clinoptilolite (SC) and sedimentary Ca-chabazite (CC) were obtained from Saint Clouds, New Mexico and Bowie, Arizona respectively. Silica dried from a Ludox HS Colloidal 40 wt% silica-water solution was used as a control material for the reusability experiments for the catalysts. All samples were ground to <44 μm particles.

7.2.2 Cracking reactions and extraction

To test the effect of NZ-cracking on industrially extracted partially deasphalted bitumen, stainless steel Swagelok micro-batch reactors (~14 cm^3 capacity) were used. Reactors were loaded with approximately 3 g of bitumen and specified amounts of NZ, purged and leak tested in a similar manner, and then subjected to a mild cracking temperature in a fluidized sand bath maintained at 400 $^{\circ}\text{C}$. The levels of catalyst used were 0 (thermal reaction), 10, 25, 50, and 100 wt. % of the bitumen. The reactor was quenched in cold water to stop the reaction 40 min after reaching thermal equilibrium. The liquid products were separated from the solid catalyst by repeated centrifuge separation and toluene extraction, and then dried under vacuum at a temperature slightly higher than the equivalent atmospheric boiling point of toluene (~115 $^{\circ}\text{C}$).

Another series of experiments were designed to test the reusability of the catalysts. The experiments were performed on toluene-extracted bitumen at 300 $^{\circ}\text{C}$ with 10 wt.% water and 10 wt.% catalyst or control material (powdered silica gel) for

24 h. The liquid products were toluene-extracted by Soxhlet apparatus following each reaction, and the catalysts were recovered by drying the remaining solids on the filter paper at 115 °C. The recovered catalysts were reused in a second cycle with fresh bitumen without further treatment.

The final set of reactions was designed to test the effects of reaction time on cracking reactions. These reactions were conducted with 10 wt.% water and 10 wt.% catalyst on toluene-extracted bitumen obtained from raw oilsands. Thermal reactions were conducted as control experiments. The reaction times were 1, 4, 16 and 48 h. A lower temperature of 300 °C was selected to prevent overcracking and to test the possibility of prolonged low temperature upgrading of bitumen using NZs. The liquid products were toluene-extracted from the reacted mixture using a Soxhlet apparatus and then dried at 115 °C prior to re-adding the condensate fractions.

7.2.3 Viscosity measurements

Viscosity of the liquid products was measured by a Brookfield DV-E chamber and spindle viscometer at least at three different temperatures. The procedure has been described in details in Section 5.2.8. The two parameters of Equation (5-4) [3-6] were determined from experimental data fitting (Appendix B), and the resulting viscosity values were converted to an equivalent 50 °C value (if no reading were found at this temperature).

7.3 RESULTS AND DISCUSSION

7.3.1 NZ-cracking for extracted bitumen upgrading

NZ-catalyzed cracking of the industrially extracted partially deasphalted Athabasca bitumen reduced the viscosity of the liquid products significantly. Reactions using 10 wt.% loading of the catalysts (based on bitumen weight) reduced the viscosity of bitumen to approximately 14-16% (using CC) and 16-20% (using SC) of the viscosity of the raw feed (Figure 7-1) [7]. These measured viscosities are also significantly lower ($\leq 55\%$) than those of thermally cracked bitumen. For both catalysts, increasing the loading beyond 10 wt.% does not substantially impact the viscosity reduction. Despite the measures to ensure mixing, i.e., shaker sand-bath and thermal equilibrium, this could be due to the clumping of the catalysts in the reactor

that may have resulted in inadequate mixing of the additional amounts. However, because of the low energy requirement (Section 6.3), the NZ-based process appears to be a viable alternative over the conventional bitumen upgrading operations.

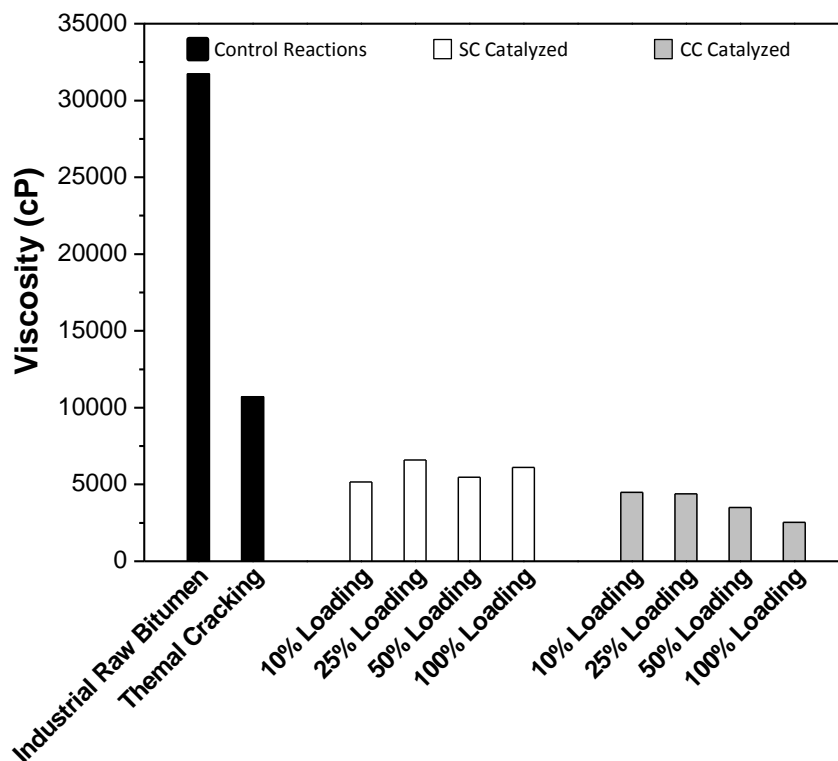


Figure 7-1: Viscosity of liquid products following thermal or NZ catalyzed cracking of industrially-extracted partially deasphalted Athabasca bitumen; values reported at 50 °C [7]. Reused with permission from the World Academy of Science, Engineering and Technology.

7.3.2 Reusability of the catalysts

To determine the reusability of the catalysts two sets of reactions were conducted with each catalyst and the control material (powdered silica). After each reaction for the first set (Cycle 1), the recovered catalysts/control materials were reused for the next set (Cycle 2). The results are presented in Figure 7-2.

For the first cycle of reaction with SC, it was found that the viscosity decreased from 144,900 cP (toluene-extracted feed bitumen) to 51,600 cP, a decrease of ~64%. In the second cycle of cracking with recycled SC, the viscosity of bitumen decreased to 100,000 cP, showing a ~31% reduction [8]. Visually, it was observed

that the SC was covered with a carbonaceous material after the first reaction. The viscosity of the product from silica added reaction in the first cycle was much higher compared to the catalyzed reactions, which also increased in the second cycle. With CC as the catalyst, somewhat similar effect was observed; in the first cycle of cracking the viscosity was reduced to 119,500 cP. In the second cycle, in contrast to SC, the viscosity was even lower at 52,000 cP despite coke formation. This may be due to suppression of secondary cracking of the medium fractions to gaseous lighter fraction by coke deposition on the active sites [9]. This is also supported by the fact that the CC catalyst has a much higher site density (Table 2-6), a substantial fraction of which is located within the larger micropore area (Table 2-3) available for secondary cracking of smaller fragments, as compared to the SC catalyst [10].

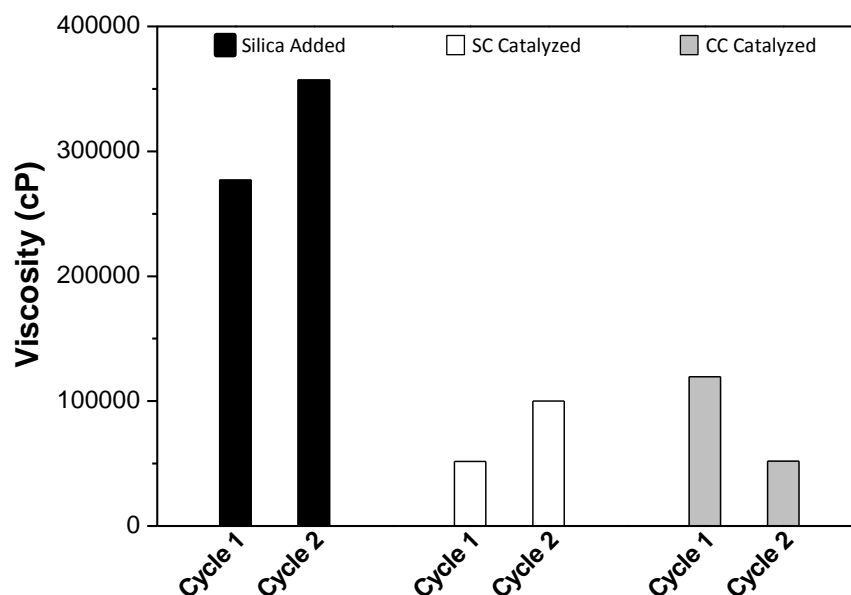


Figure 7-2: Reusability of NZ catalysts measured with respect to viscosity reduction of the liquid products. The recovered catalysts from the first cycle were reused in the second cycle of cracking reactions.

Based on the fact that clays, sands and minerals adsorb heavy hydrocarbons [11-13], some level of fouling or deactivation of the NZ was expected [8]. However, these experiments confirm that, despite the carbonaceous deposits, the NZs retained some activity after the long (24 h) first catalytic cycle. Based on such observation, it is logical to conclude that the catalysts can be reused for cracking without additional treatment. However, the total number of cycles that the catalysts could undergo

without complete deactivation could not be determined. Due to the small amounts of catalysts used for these reactions, catalyst loss was high. Multiple reactions in the first cycle were required to recover adequate amounts of catalysts for the next cycle of reactions. Because of the insufficient amounts of catalysts recovered from the second cycle, the experiments could not be continued for subsequent cycles.

7.3.3 NZ-cracking for prolonged low temperature bitumen upgrading

It was generally observed that NZ catalyzed reactions reduce the viscosity of the liquid products as a function of reaction time, and outperforms the analogous thermal runs (Figure 7-3). At 48 h, the products of the catalyzed reactions have viscosities of ~34000-69000 cP, which is ~15-25% of their corresponding values for the 1 h reactions, and 30-60% of those of the equivalent thermal run. The SC catalyzed reactions generally performed better than the CC catalyzed reactions. An anomaly for the SC catalyzed 4 h run exists, where the viscosity of the liquid product remains unchanged from 1 to 4 h. The results demonstrate that the NZs are also effective to reduce the viscosity of bitumen by prolonged low temperature upgrading. This can be extended for potential *in situ* applications as SAGD, particularly considering the long heating periods and operating temperatures of such applications.

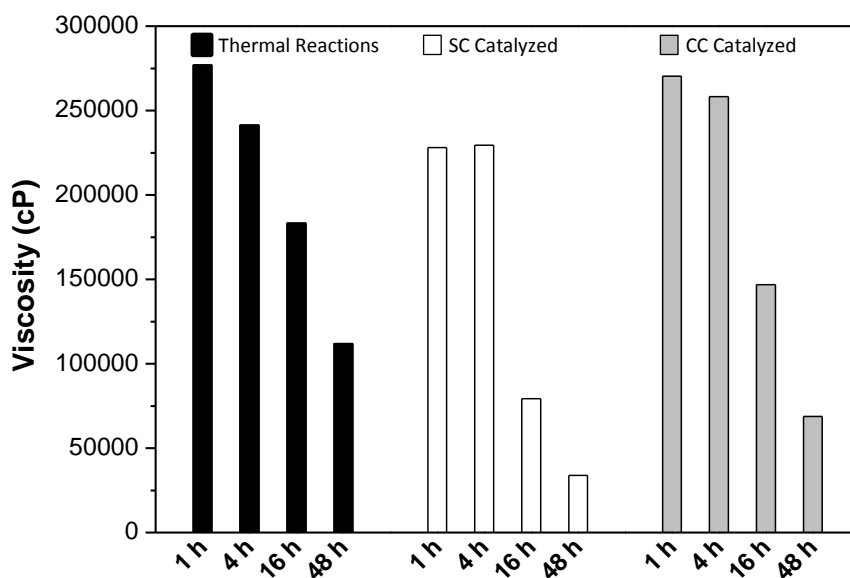


Figure 7-3: Viscosity reduction of liquid products by low temperature prolonged catalytic cracking of toluene-extracted Athabasca bitumen; values reported at 50 °C.

The standard deviation (SD) of the experimental results was 3.0% from the average viscosity values (cP) reported at 50 °C. This was determined based on five experiments conducted on a single representative sample.

7.4 CONCLUSION

NZ-cracking can be an energy efficient method for extracted bitumen upgrading. This is more appealing since the catalysts have long activity and reusability under processing conditions. NZs also demonstrate high activity in low temperature prolonged upgrading of bitumen, which has potential *in situ* application. However, practical *in situ* application of NZs will require successful delivery of the catalysts downhole for processing, which remains a very challenging aspect.

BIBLIOGRAPHY

- [1] Zamani A, Maini B, Pereira-Almao P. Experimental study on transport of ultra-dispersed catalyst particles in porous media. *Energy Fuels* 2010; 24: 4980–8.
- [2] Hassanzadeh H, Abedi J. Modelling and parameter estimation of ultra-dispersed *in situ* catalytic upgrading experiments in a batch reactor. *Fuel* 2010; 89: 2822–8.
- [3] Ha HZ, Koppel P. Accurately predict viscosity of syncrude blends: An evaluation for mixing rules uncovers potential errors in fluid transportation of bitumen-based feeds. *Hydrocarb Process* 2008; 87: 87-92.
- [4] Seyer FA, Gyte CW. Viscosity. In: Loren G, Hsi C, editors. *AOSTRA technical handbook on oilsands, bitumen and heavy oil*. Edmonton: Alberta Oilsands Technology and Research Authority; 1989, p. 153-84.
- [5] Standard test method for viscosity-temperature charts for liquid petroleum products, ASTM D341-03. Philadelphia: American Society for Testing and Materials; 2003. p. 4-5.
- [6] Standard test method for low temperature, low shear rate, viscosity/temperature dependence of lubricating oils using a temperature-scanning technique, ASTM D 5133-05. Philadelphia: American Society for Testing and Materials; 2005. p. 1-12.
- [7] Junaid ASM, Wang W, Street C, Rahman M, Gersbach M, Zhou S, et al. Viscosity reduction and upgrading of Athabasca oilsands bitumen by natural zeolite cracking. In: Ardil C, editor. *Proceedings of the International Conference on Chemical Engineering*; 2010 Sep 28-30; Amsterdam, the Netherlands. Amsterdam: World Academy of Science, Engineering and Tehnology; 2010 Sep. 485 p.
- [8] Junaid ASM, Street C, Wang W, Rahman MM, An W, McCaffrey WC, Kuznicki S.M. Integrated extraction and low severity upgrading of oilsands bitumen by activated natural zeolite catalysts. 2011. 30 p. Manuscript in submission as a journal article (JFUE-D-11-00663) with *Fuel* as of 17 May 2011, currently under review.
- [9] Street C. *Catalytic cracking and upgrading of oilsands bitumen using natural calcium chabazite [dissertation]*. Edmonton (AB): University of Alberta; 2011.
- [10] Junaid ASM, Rahman M, Yin H, McCaffrey WC, Kuznicki SM. Natural zeolites for oilsands bitumen cracking: Structure and acidity. *Micropor Mesopor Mater* 2011; 144: 148-57.
- [11] Santi CA, Cortes S, D’Acqui LP, Sparvoli E, Pushparaj B. Reduction of organic pollutants in olive mill wastewater by using different mineral substrates as adsorbents. *Bioresource Technology* 2008; 99: 1945–51.

- [12] Yuan G. Natural and modified nanomaterials as sorbents of environmental contaminants. *Journal of Environmental Science and Health*. 2004; A39: 2661-70.
- [13] Clonfero E, Schieppati R. Reduction of polycyclic aromatic hydrocarbons from thermal clay recycled oils using technical adsorbents. *Polycyclic Aromatic Compounds* 1999; 16: 41-50.

Conclusions

8.1 CONCLUSIONS FROM THE CURRENT STUDY

The objective of this study was to investigate the potential of economical and abundant natural zeolites (NZ) for single-pass catalytic cracking, waterless extraction and integrated low temperature upgrading of oilsands bitumen. Conventional bitumen extraction and upgrading processes have environmental, operational and quality-related issues. The extraction processes consume large volumes of fresh water and generate chemically polluted, high volume tailings ponds. The upgrading processes require hydrogen and expensive catalysts and deal with complex operational issues. The bitumen products are highly viscous, contain high concentrations of heteroatoms and metals, and require the use and regeneration of expensive diluents for transportation and recovery. This study was intended to provide insight into an alternative, more environmentally friendly and integrated method for oilsands bitumen processing.

A series of analytical and surface sensitive techniques were applied to understand the structural and compositional features of the raw and ion-exchanged

NZs feasible for acid cracking of heavy oil. A pioneering proof-of-concept study was conducted to establish the activity of acidified NZs for solid-phase oilsands bitumen cracking. An exploratory study was then conducted on a novel method to further enhance the activity of these minerals through self-acidification by simple water addition. Next, the core of the study focused on evaluating the performance of this self-acidified, NZ-based, integrated waterless extraction and low temperature upgrading processes in a scaled-up, engineered system. Finally, energy balance calculations were conducted to determine the feasibility of this novel process. A complementary study also investigated the potential of using NZs for energy efficient upgrading of pre-extracted bitumen. The important conclusions from the findings of this study are summarized below:

8.1.1 Unique structural and compositional properties of NZs for oilsands bitumen cracking

NZs have surface and acidic properties favorable for heavy oil cracking [1]. With platy morphologies and external surface areas comparable to the commercial cracking catalyst zeolite Y (ZY), NZs are able to accommodate large petroleum molecules such as asphaltenes. Both raw and ammonium-exchanged forms of these minerals have large numbers of acid sites that are as strong or stronger than those of ZY. These unique properties, in addition to their abundance and low cost, make these minerals very attractive for bitumen cracking applications [1].

8.1.2 Waterless (light hydrocarbon) extraction of bitumen assisted by NZ-catalyzed cracking

NZ-catalyzed cracking at temperatures well below those required for thermal cracking or visbreaking can reduce the heavy fractions in bitumen into smaller, lighter components that are almost entirely extractable with light hydrocarbons such as pentane or hexane [2]. This can potentially eliminate/reduce the use of water for extraction of the oil from the sand.

8.1.3 Enhanced activity of NZs in the presence of water

The addition of small amounts of water (~3 wt.% of the feed oilsands) can generate hydroxyl groups on raw NZ surfaces by self-acidification through

hydrolysis [3]. These acid groups actively participate in catalytic cracking reactions and significantly increase the efficiency of NZ-catalyzed cracking. The resultant liquid products are lighter and less viscous compared to those generated by cracking with the dry catalysts [3]. The protons generated through hydrolysis are found to be distributed within the liquid fractions generated through catalytic cracking of bitumen.

8.1.4 Potential integrated extraction and low temperature upgrading process using NZ catalysts

In an engineered system that enhances the contact between the feedstock and the NZ catalysts through continuous mixing, substantial cracking can be achieved at very low catalyst loadings (~1-5 wt.% based on feed) and temperatures (~300 °C) [4]. Heavy molecules such as asphaltenes can be converted to light hydrocarbon extractable, lower molecular weight fractions, while maintaining high overall recovery of the oil (>90%). Residue conversion from these reactions was found to be dependent on the large number of acid sites, and also possibly on the high external surface area of the catalysts. The resultant liquid products are much less viscous, with lower boiling point distributions and molecular weights. With proper mixing, NZs remove the majority of the vanadium, and significant amounts of nickel and heteroatoms (nitrogen and sulfur), from the liquid products [4]. Liquids produced from thermal reactions are also more aromatic compared to the products from NZ-cracking [4]. Analogous thermal treatment, without the catalysts, does not result in comparable extractability and upgrading. The thermal conditions used in this NZ-based treatment are significantly milder than those of industrial upgrading operations.

8.1.5 NZ-based cracking is an energy-intensive process

The proposed NZ-based catalytic cracking and solvent extraction is expected to be more energy intensive than a typical industrial process consisting of hot water extraction, paraffinic froth treatment and primary upgrading operations. The majority of the projected energy requirements relate to the regeneration of the large amounts of solvents used for extraction. However, since the NZ-based process has additional secondary upgrading effects and environmental benefits, any complete economic

analysis considering the feasibility of the process should take these factors into account.

8.1.6 Energy efficient upgrading of extracted bitumen and potential *in situ* application

NZ-based upgrading of extracted bitumen, in contrast, was found to be much less energy intensive than both NZ-based oilsands cracking and industrial upgrading processes. Prolonged (~48 h), low temperature (~300 °C) reactions or short (<1 h) reactions at moderate temperatures (~400 °C) [5] effectively reduce the viscosity of extracted bitumen and increase its transportability. These results show promise for an interesting alternative application of NZs. Particularly, the concept of low temperature prolonged upgrading can be extended for a potential *in situ* application of these catalysts.

8.1.7 Reusability and catalyst life

Although the objective of this study was to develop NZs as economic single-pass, disposable cracking agents for heavy oil, an exploratory investigation conducted on pre-extracted bitumen discovered that these minerals remain active beyond a single cycle of prolonged (24 h) operation at 300 °C. Despite significant coke deposition on the surface over the long reaction time, the NZs remained active when reused in a subsequent cycle.

8.2 RECOMMENDATIONS AND FUTURE WORK

Several interesting avenues for future investigation have arisen from this project.

8.2.1 Reduction of energy requirements for solid oilsands cracking

In order to develop an economically feasible NZ-based process for solid oilsands cracking, energy consumption needs to be reduced. The bulk of the energy required for the proposed NZ-based process is dedicated to the regeneration of the extraction solvent. Development of an energy efficient solvent-based extraction unit could address this challenge, possibly through reducing solvent amounts by recycling and/or more efficient distribution.

8.2.2 Increasing the residue-free liquid yields

NZ-catalyzed cracking results in an ~15% increase in residue-free liquid yields compared to raw bitumen, however, it may be possible to increase this yield even further. In general, higher conversion of residue by thermal or catalytic cracking will lead to higher gas and coke make, eventually resulting in only incremental gains in residue-free liquid products. The use of hydrogen in limited amounts, in combination with the catalytic cracking, might suppress coke and gas formation and enhance the secondary upgrading effects of the NZ-based process. Additionally, the acid sites responsible for undesired reactions such as secondary cracking of light hydrocarbons can be attempted to be poisoned selectively. Future work will be required to establish the feasibility of these approaches, and to understand the economics of such processes.

8.2.3 Product homogeneity and process robustness

NZs are naturally available minerals with impure phases [1] and non-homogeneous composition within deposits. Use of these minerals in “as-mined” form may result in non-uniform product distributions from catalytic reactions. Work needs to be done to design a process robust enough to handle these variations, in addition to the varying composition of the feed oilsands.

8.2.4 Prolonged low temperature *in situ* application

The NZs remain active for prolonged reaction times while in contact with the feedstock at a reaction temperature (~300 °C) that is reasonably close to the operating temperatures of *in situ* oilsands extraction processes including steam-assisted gravity drainage (SAGD). One potential application would be to use these minerals as ultra-dispersed catalysts for *in situ* upgrading of bitumen. If the NZs can be successfully distributed within the formation by the SAGD process steam such that they are in contact with the bitumen, it may be possible to reduce the viscosity and the production time by orders of magnitudes. However, devising an effective method of delivery remains a challenge.

8.2.5 NZ applications in the extraction of other unconventional resources

In light of the interesting effects of NZs on Albertan oilsands bitumen, similar studies could be conducted to determine their catalytic value in the extraction of other unconventional resources such as shale oil, extra-heavy oil and oilsands from other geographic locations.

8.3 CONCLUDING REMARKS

Natural zeolite-assisted cracking has significant potential as an alternative integrated approach to the extraction and upgrading of oilsands bitumen. These extraordinary minerals are found to increase both the total and residue-free liquid yields of cracking, reduce the asphaltene, heteroatom and heavy metal content in the liquid products, and eliminate and/or reduce the need for water in processing. These observations suggest the possibility of an economical, waterless and more environmentally-friendly integrated extraction-upgrading process for oilsands with fewer operational steps. However, the current projected energy requirements for a natural zeolite-based extraction-upgrading process are high, and further research and development are required to increase the efficiency of the process. *In situ* application of these minerals is an alternative option, worthy of future exploration.

BIBLIOGRAPHY

- [1] Junaid ASM, Rahman M, Yin H, McCaffrey WC, Kuznicki SM. Natural zeolites for oilsands bitumen cracking: Structure and acidity. *Micropor Mesopor Mater* 2011; 144: 148-57.
- [2] Junaid ASM, Yin H, Koenig A, Swenson P, Chowdhury J, Burland G et al. Natural zeolite catalyzed cracking-assisted light hydrocarbon extraction of bitumen from Athabasca oilsands. *Appl Catal A* 2009; 354: 44-9.
- [3] Junaid ASM, Rahman MM, Wang W, Street C, McCaffrey WC, Kuznicki SM. On the role of water in natural zeolite catalyzed cracking of oilsand bitumen: method and mechanism. 2011. 40 p. Unpublished manuscript currently in preparation for submission to *Energy Fuels* as a journal article; expected submission: October, 2011.
- [4] Junaid ASM, Street C, Wang W, Rahman MM, An W, McCaffrey WC, Kuznicki S.M. Integrated extraction and low severity upgrading of oilsands bitumen by activated natural zeolite catalysts. 2011. 30 p. Manuscript in submission as a journal article (JFUE-D-11-00663) with *Fuel* as of 17 May 2011, currently under review.
- [5] Junaid ASM, Wang W, Street C, Rahman M, Gersbach M, Zhou S, et al. Viscosity reduction and upgrading of Athabasca oilsands bitumen by natural zeolite cracking. In: Ardil C, editor. *Proceedings of the International Conference on Chemical Engineering*; 2010 Sep 28-30; Amsterdam, the Netherlands. Amsterdam: World Academy of Science, Engineering and Tehnology; 2010 Sep. 485 p.

Vapor Pressure Osmometer Calibration and Average Molecular Weight Measurement

The Knauer K-7000 vapor pressure osmometer (VPO) can be calibrated with a standard material whose molecular mass is within the range of the expected values of samples under study (in this case $\geq 500 \text{ g mol}^{-1}$). Several solutions of different concentration are prepared by dissolving the standard material in a suitable solvent, and maintaining a temperature that prevents molecular association. These solutions are injected as separate runs, and a linear regression plot of $\text{MV C}^{-1} (\text{kg mol}^{-1})$ vs. $\text{C} (\text{mol kg}^{-1})$ is prepared from the data, where MV and C are measurement value and concentration of solution respectively. The calibration constant, K_C is determined as $[\text{MV C}^{-1}]_{\text{C}=0}$ by extrapolating the curve to $\text{C}=0$.

Similarly, values of the measurement constant K_M for samples of unknown average molecular weights (AMW) are determined by preparing individual $\text{MV C}^{-1} (\text{kg g}^{-1})$ vs. $\text{C} (\text{g kg}^{-1})$ plots, and measuring $[\text{MV C}^{-1}]_{\text{C}=0}$ by extrapolating the curve to $\text{C}=0$. Finally, the AMW of a sample is calculated as a ratio of K_C to K_M (Equation 4.4). The procedure is illustrated by Figures A-1 and A-2.

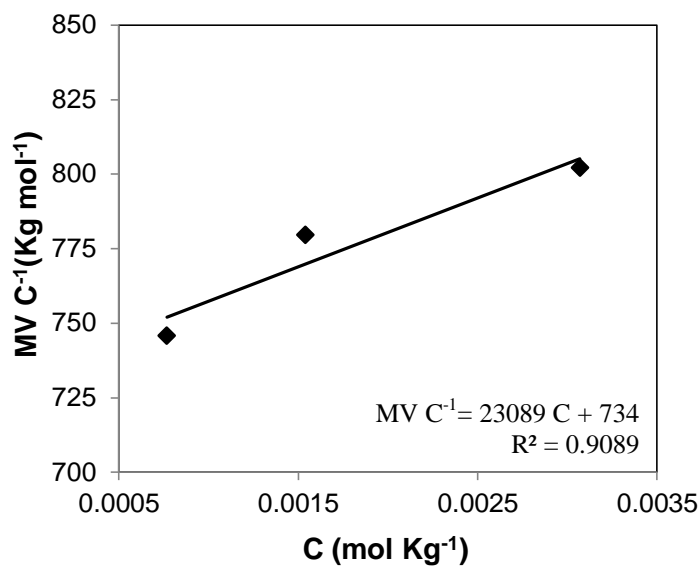


Figure A-1: Calibration of Knauer K-7000 vapor pressure osmometer and determination of the calibration constant, K_C .

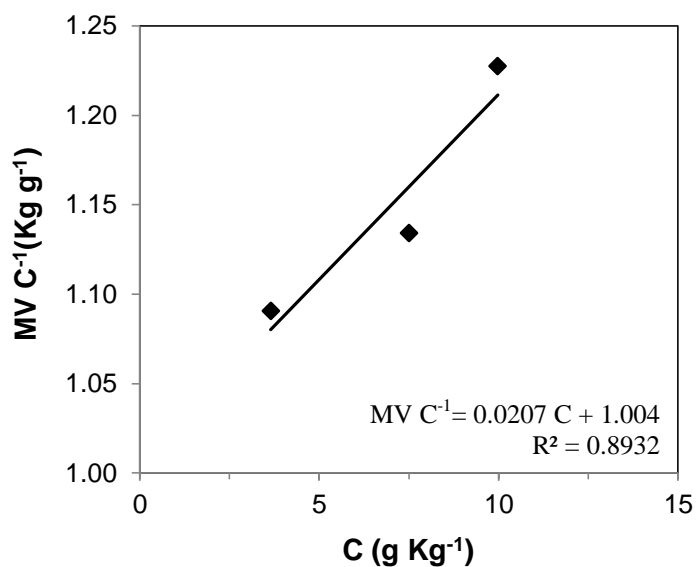


Figure A-2: Determination of the measurement constant, K_M , for a sample of unknown AMW.

The calibration constant ($K_C = 734 \text{ Kg mol}^{-1}$) for the osmometer and the measurement constant for this particular sample of unknown AMW ($K_M = 1.004 \text{ Kg g}^{-1}$) are the intercepts of the linear regression plots in Figures A-1 and A-2 respectively. Therefore, the AMW of the sample is determined using Equation 4.4 as:

$$\text{AMW} = K_C / K_M = 734/1.004 = 731 \text{ (g mol}^{-1}\text{)}$$

ASTM Equation Parameters Estimated by Data Fitting

The two parameters (a_1 and a_2) of ASTM equation (Equation 5.4) were estimated for each toluene-extracted liquid product by linear data fitting using Polymath version 6.1 software. The estimated values are presented in Tables C-1-C3:

Table B-1: ASTM equation parameters estimated for toluene-extracted liquid products from 3 wt.% water-added 1 h oilsands reactions.

Reaction		ASTM Equation parameters		R ² value for fitting
Temperature (°C)	Catalyst	a ₁	a ₂	
300	None	22.31061	-3.447098	0.9999981
	1% SC	22.45977	-3.469964	0.9999905
	1% CC	22.28952	-3.443303	0.9999999
	5% SC	22.78488	-3.555917	0.9997826
	5% CC	24.79169	-3.917677	0.9999913
350	None	24.27993	-3.810743	0.9999988
	1% SC	23.53371	-3.687778	0.9999603
	1% CC	17.10714	-2.623443	0.9997136
	5% SC	30.72386	-4.969767	0.9919285
	5% CC	24.21783	-3.923410	0.9901297

ASTM Equation Parameters Estimated by Data Fitting

Table B-2: ASTM equation parameters estimated for liquid products from 10 wt.% water-added 300 °C toluene-extracted bitumen reactions.

Reaction		ASTM Equation parameters		R ² value for fitting
Time (h)	Catalyst	a ₁	a ₂	
1	None	23.31212	-3.59690	0.9996889
	10% SC	22.19274	-3.40635	0.9944558
	10% CC	23.21064	-3.57970	0.9998127
4	None	23.47091	-3.62640	0.9999927
	10% SC	20.52447	-3.11754	0.9935885
	10% CC	22.51388	-3.45997	0.9992224
16	None	24.10426	-3.73725	0.8206399
	10% SC	23.19253	-3.59453	0.9999611
	10% CC	23.26466	-3.59776	0.9999945
48	None	23.82244	-3.69823	0.9999864
	10% SC	23.65698	-3.68829	0.9999283
	10% CC	--	--	--

Table B-3: ASTM equation parameters estimated for liquid products from 10 wt.% water-added 300 °C toluene-extracted bitumen reactions for 24 h, conducted to test the reusability of the catalysts.

Reaction		ASTM Equation parameters		R ² value for fitting
Cycle	Catalyst	a ₁	a ₂	
1	10% Silica	22.57803	-3.48230	0.9996884
	10% SC	16.00846	-2.35930	0.962124
	10% CC	15.71167	-2.29613	0.8834316
2	10% Silica	22.51147	-3.45611	0.9996207
	10% SC	16.34331	-2.40686	0.9706371
	10% CC	14.98415	-2.18204	0.9471056

Estimation of Relative Thermal Reaction Severity by Literature Data Fitting

The relative reaction severity (RSS) values of thermal reactions were estimated by fitting literature data [C1] on reaction severity (RS) of similar feed material as a function of residue conversion (Figure C1).

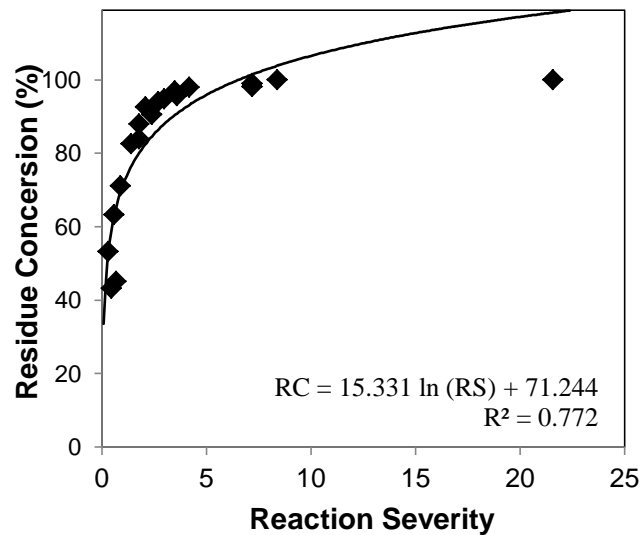


Figure C-1: Fitting of literature data on thermal reaction severity as a function of residue conversion (Athabasca residue feed).

Estimation of Relative Thermal Reaction Severity by Literature Data Fitting

The fitted residue conversion data were interpolated to determine RS values for the thermal reactions conducted in this study. The calculated RS values were then normalized by the highest value to estimate the RSS values for the thermal reactions (Table C-1).

Table C-1: Estimation of relative reaction severity from literature data [C1] fitting.

Centerline temperature of thermal reaction (°C)	Reaction severity	Relative reaction severity
300	0.044	1.00
350	0.236	5.35

Bibliography

[C1] Soundararajan S. Determination of thermal cracking kinetics of Athabasca bitumen vacuum residue [dissertation]. Edmonton (AB): University of Alberta; 2001.